AN APPLICATION OF THE FINITE ELEMENT METHOD FOR ROCK SLOPE STABILITY ANALYSIS

by

David John Hammel

A Dissertation Submitted to the Faculty of the

DEPARTMENT OF MINING AND GEOLOGICAL ENGINEERING

In Partial Fulfillment of the Requirements
for the Degree of

DOCTOR OF PHILOSOPHY
WITH A MAJOR IN GEOLOGICAL ENGINEERING

In the Graduate College

THE UNIVERSITY OF ARIZONA

1971

THE UNIVERSITY OF ARIZONA

GRADUATE COLLEGE

I hereby recommend that this dissertation prepared under my direction by **David John Hammel**

entitled **An Application of the Finite Element Method for Rock Slope Stability Analysis**

be accepted as fulfilling the dissertation requirement of the degree of **Doctor of Philosophy**

J. L. Abel, Jr. — Dissertation Director — 12/5/70 — Date

After inspection of the final copy of the dissertation, the following members of the Final Examination Committee concur in its approval and recommend its acceptance:*

J. L. Abel, Jr.	12/5/70
W. C. Dotson	12/5/70
L. C. Dotson	12/7/70
E. E. Tracy	12/5/70
[illegible]	12-7-70

*This approval and acceptance is contingent on the candidate's adequate performance and defense of this dissertation at the final oral examination. The inclusion of this sheet bound into the library copy of the dissertation is evidence of satisfactory performance at the final examination.

STATEMENT BY AUTHOR

This dissertation has been submitted in partial fulfillment of requirements for an advanced degree at The University of Arizona and is deposited in the University Library to be made available to borrowers under rules of the Library.

Brief quotations from this dissertation are allowable without special permission, provided that accurate acknowledgment of source is made. Requests for permission for extended quotation from or reproduction of this manuscript in whole or in part may be granted by the head of the major department or the Dean of the Graduate College when in his judgment the proposed use of the material is in the interests of scholarship. In all other instances, however, permission must be obtained from the author.

SIGNED: David F. Hammel

ACKNOWLEDGMENTS

The author wishes to express his sincere gratitude to Dr. John F. Abel, the dissertation director, for continued guidance and constructive criticism during the course of the study. Review of the manuscript and encouragement from members of the examination committee, Dr. W. C. Lacy, Dr. W. C. Peters, Professor J. C. Dotson, and Dr. J. S. Sumner, proved to be invaluable.

Appreciation is extended to Compañia Minera de Cananea, S. A. de C. V., for the availability of facilities, data and assistance. Grateful acknowledgment is extended to: R. C. Weed, General Manager; W. C. Pill, Mine Engineer; C. C. Brown, Chief Geologist; A. Bustamonte, Geologist.

Acknowledgment is due also to the United States Bureau of Mines, Denver, Colorado, for providing, on a special loan basis, a basic finite element computer program.

TABLE OF CONTENTS

TABLE OF CONTENTS--Continued

TABLE OF CONTENTS--Continued

LIST OF ILLUSTRATIONS

LIST OF ILLUSTRATIONS--Continued

LIST OF TABLES

ABSTRACT

The stability of a 70^{o} open-pit mine slope was investigated by analyzing two-dimensional plane-strain finite element models of the slope.

In the course of the study, laboratory-determined physical properties of the rock substance were progressively modified in order to more closely approximate the in-place rock mass of the open-pit slope. Residual stresses were investigated in the laboratory so that the in situ pre-mining stress distribution could be more closely approximated in the model analysis. Critical geologic structure (joint) attitudes were determined from field information and, then, were modeled.

The pit slope was evaluated by utilizing five different finite element models. The possible slope conditions modeled covered a range of conditions from homogeneous, isotropic, linearly elastic and gravity loaded to non-homogeneous, anisotropic, tectonic and gravity loaded, with non-linearly deforming modeled joints. Several failure criteria were applied to each model in order to determine the probable stability conditions of the slope models.

Results of the finite element analyses indicate the following: (1) slope models that contained modeled joints and that were

subjected to high loading (tectonic + gravity loads) conditions were subject to localized failure in zones within and adjacent to joint elements in proximity to the open-pit wall, (2) gravity loaded slope models which did not contain modeled joints were stable in every respect, (3) tensile stress zones developed in regions where joint elements were adjacent to the pit wall, (4) non-linear deformation (yielding) and sliding occurred in nearly all of the joint elements, and (5) resultant excavation-induced vertical displacement on the floor of the pit was twice as great for the combination of tectonic and gravity loading (11" to 12") as was the excavation-induced vertical displacement which resulted from gravity loading conditions (5" to $5\frac{1}{2}$") only.

CHAPTER 1

INTRODUCTION

A complete rational analysis for the design of rock slopes is a desirable but probably unattainable goal. Poor understanding of failure criteria for large rock masses, unknown boundary conditions, internal rock defects that can not be readily sampled, and lack of information on in situ stress conditions emphasize the importance of experience in designing stable rock slopes. Much effort has been expended recently to complement professional experience with computer related mathematical techniques. One such technique is the finite element method of stress analysis.

The finite element method is a mathematical modeling technique based on elastic theory which is used for calculating displacements and stresses in continuous media. This method, when applied to the stability analysis of slopes in rock, has the following advantages over many other slope analysis techniques:

1. Non-homogeneous materials and anisotropic material properties can be modeled.
2. Non-linear elastic and time-dependent relationships can be analyzed.

3. The method is completely general in that any geometry can be examined and small scale detail can be included.
4. Geologic structure (joints and faults) can be modeled.
5. Virtually any loading situation can be examined.

The finite element method for rock slope stability analysis is limited primarily by the adequacy of the input data. Specifically, some of these limitations are as follows:

1. Physical properties of the in-place rock mass must be estimated from testing of small scale specimens of the rock substance.
2. Sufficiently detailed geologic information is not economically obtainable.

Statement of the Problem

The purpose of the study was two-fold. First, the finite element method was used to aid in determining potential stability conditions in a 70^{o} slope in a proposed open-pit mine, the 755 Area pit at Cananea, Sonora, Mexico. Second, this method of analysis was examined for its applicability in predicting stability and for its ability to provide useful information to aid in open-pit mine slope design.

Scope of the Study

A two-dimensional, plane-strain analysis was utilized for the Cananea analysis. Five different slope models were designed and

then tested with the finite element method. Model conditions vary from simple to complex. The simplest model was homogeneous, isotropic, gravity loaded and linearly elastic. The most complex model tested was non-homogeneous and anisotropic, was loaded with a combination of gravity and tectonic boundary loads, and had model joints which were permitted to deform non-linearly. The other three models lie between these two extremes in degree of complexity.

Actual geologic conditions present in the 755 Area were modeled in detail. Variations in rock properties and elastic parameters were introduced into the model to match in situ conditions. The role of geologic discontinuities (joints, faults, seams, bedding) in the behavior of rock masses has been recognized for a long time by engineers who design excavations within and upon rock. These discontinuities may completely dominate stability conditions in most rock slopes. Therefore, considerable emphasis was placed on modeling geologic structure in a portion of this study. Residual stress measurements were performed and the results were incorporated into one of the models as boundary forces.

Variations in calculated stress and displacement were examined to determine what effect model variation would have on these analyses. Several failure criteria have been applied to estimate potential stability conditions of the slope.

Previous Development

The finite element method of stress analysis was used initially in the analysis of stresses in aircraft structures (Turner et al. 1956). The application of this technique to obtain solutions to boundary value problems in rock structure analysis became popular shortly thereafter, and today it is a much-used tool.

Extensive research has been performed in the past five years (1965-1970) in the application of the finite element method to problems in the applied engineering fields of soil and rock mechanics. Several notable effects have been observed which would appear to influence the analysis of rock slopes:

1. Effect of Varying the Angle of the Slope: Yu and Coates (1968) compared differences in stress distribution in homogeneous and isotropic model slopes of 45° and 60°. Results indicated that stress distributions did not differ significantly for the two slopes except that stress increased near the boundary of the openings (pit wall), particularly at the toe of the slope. Blake (1967 and 1968) modeled an actual open-pit mine slope which was being modified by increasing the pit slope angle. Results indicated that steepening the pit slope angle increased the maximum principal stresses surrounding the pit significantly only in the vicinity of the toe of the slope. Only a slight increase in stress occurred near the pit wall. Duncan and Dunlop (1969) examined slope stability problems in stiff-fissured clays and

shales. Their model analysis results indicated that normalized shear stresses (τ/σ_n) increase as slope angle increases.

2. Effect of Horizontal Stress (Non-Gravity Loading): Analyses of stress conditions around excavated slopes indicate that the initial horizontal stress has a considerable influence on the magnitudes of stresses following excavation. Yu and Coates (1968) and Duncan and Dunlop (1969) determined that under high horizontal stress, the stresses in the vicinity of the excavation are altered considerably and are approximately proportional to the ratio of horizontal stress to vertical stress. Blake (1967 and 1968) discovered that stress magnitudes and concentrations at the bottom of the pit are significantly increased with the addition of a small horizontal stress field. These experimental results point out the need to know pre-excavation in situ stress conditions for reasonable analysis of pit slopes with the finite element method.

Another item which influences stability analysis of rock slopes is the geologic discontinuity (joints, faults, bedding, seams). Generally, a rock mass is not a simple continuum, because it contains numerous discontinuities. These discontinuities appear to significantly influence, if not control, the stability of rock slopes in most situations. Therefore, any rational finite element analysis used for the design of slopes in rock should account for discontinuities which are present in the rock. Goodman, Taylor and Brekke (1968)

developed a method of incorporating the effect of joints into a finite element analysis. They represent a joint element as a two-dimensional tube of zero width, thus a one-dimensional element, which offers resistance to shear and compressive forces acting parallel to and normal to its axis. These axial and normal resistances are expressed as products of the axial and normal displacements and the unit stiffness of the joint in those two directions. Malina (1970) examined effects of discontinuities by assuming a joint system in a hypothetical rock and continuous footing model. The resultant deformation pattern and maximum principal stress direction were parallel to the jointing direction. Mahtab (1970) idealized a model rock slope as an aggregate of two distinct sets of elements: three-dimensional rock blocks and two-dimensional joint elements.

Non-brittle rock and most soils do not respond to external loading as linear elastic materials. Most often in these situations, the stress-strain relationship is non-linear, and in some materials, the deformation is also time-dependent. A popular means of modeling non-linearity has been to use a bi-linear analysis with assumed pseudo-elastic constants. Girijavallabhan (1967) analyzed several soil mechanics problems with this method. Woodward (1967) analyzed stresses and deformations in an earth embankment with a similar technique. Nair and Otus (1968) examined bi-linear deformation in the design of a large underground cavity in a salt dome and examined cavity closure with a linear analysis with superimposed creep.

The three-dimensional finite element method was developed during the 1960's. The first three-dimensional technique to be developed (Wilson 1965, Clough 1965b) was the axi-symmetric method. Girijavallabhan (1967) and Nair and Otus (1968) performed geo-mechanical analyses with this technique. A truly three-dimensional finite element method, almost completely general in nature, is described by Zienkiewicz and Cheung (1967). The stiffness derivations for some basic solid elements were given by Melosh (1962) and Rashid (1965). Zienkiewicz, et al. (1969) treats some recent innovations in the three-dimensional finite element method.

The error involved with the finite element method can be quite small. Clough (1965a) indicates that this technique can be very accurate, but that accuracy depends on the validity of the basic deformation patterns assumed within the elements. Yu, Gyenge and Coates (1968) discovered that small errors occurred at the bottom boundary of a finite element slope model: horizontal and vertical stress were, respectively, 6% and 7% less than calculated values.

CHAPTER 2

FINITE ELEMENT METHOD

The finite element method is essentially a generalization of structural analysis procedures which are used to calculate stresses and displacements (deflections) in two- and three-dimensional structures. Analyses can be performed for plane stress, plain strain, and three-dimensional axially symmetric or non-symmetric problems for continuous and discontinuous media.

The finite element method is based on the representation of a continuous medium by an assemblage of individual components, called elements. The elements are interconnected at a finite number of points, called nodal points. This finite element "model," then, approximates the original continuum. The material properties of the original system are retained in the individual elements of the finite element model.

It is the finite character of the structural nodal points which makes possible the analysis by means of simultaneous matrix equations. As for any structural analysis, the essential analysis problem is to satisfy the following three requirements simultaneously (Clough 1965a):

1. Equilibrium: the internal element forces acting at each nodal point must equilibrate the externally applied nodal force.

2. Compatibility: the element deformations must be such that they continue to meet at the nodal points in the loaded condition.

3. Force-Deflection Relationship: the internal forces and displacements within each element must be related to its individual geometric and material property characteristics.

A description of the finite element method, plane strain condition, follows. The basic information is adapted from Clough (1965a), Coates (1969b), and Girijavallabhan (1967). For a more complete discussion of the finite element method, see Clough (1960), Zienkiewicz and Cheung (1967), and Wilson (1963, 1965).

Basic Operations in Finite Element Analysis

The finite element analysis, displacement method, consists of the following basic operations:

1. Development of a stiffness matrix for each element with respect to a convenient local (element) coordinate system.

2. Transformation of the element stiffness matrix from the local coordinate system to a generalized coordinate system related to the complete structural assemblage.

3. Generation of the final stiffness matrix for the entire structural assemblage.

4. Formulation and solution of the system of simultaneous equilibrium equations expressing the relationship between the applied nodal forces and the resulting nodal displacements.

5. Determination of element strains from the computed nodal point displacements.

6. Determination of element stresses from element strains by means of the element stiffness matrices.

Stress-Strain Relations

In simple analyses, stress-strain relations are based on the assumption that uniform strain exists throughout each element. Consider an open-pit mine slope, infinitely long in the Y-direction as shown in the X, Y, Z coordinate system in Figure 1. Since plane strain conditions will be assumed, the displacement along the Y-axis is zero. The element thickness, d, in the Y-direction will be one unit. If a cubical element is considered, normal and shear stresses exist on each of the faces of the element as shown in Figure 1.

For plane strain,

$$\varepsilon_y = \gamma_{xy} = \gamma_{yz} = 0$$

If the material in the element is homogeneous, isotropic and elastic,

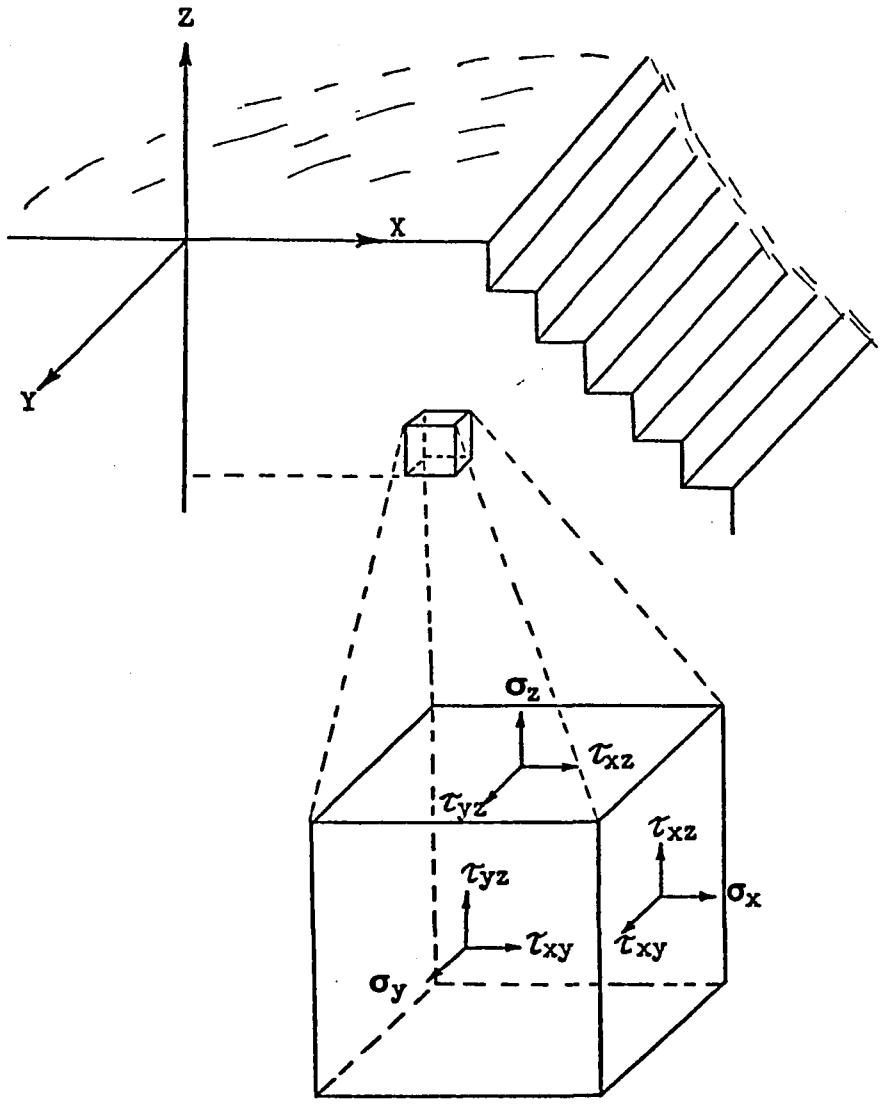

Figure 1. Stresses on a Cubical Element Within the Wall of an Open-Pit Mine Slope

$$\varepsilon_x = \frac{1}{E}\left(\sigma_x - \mu(\sigma_y + \sigma_z)\right)$$

$$\varepsilon_y = \frac{1}{E}\left(\sigma_y - \mu(\sigma_z + \sigma_x)\right)$$

$$\varepsilon_z = \frac{1}{E}\left(\sigma_z - \mu(\sigma_x + \sigma_y)\right)$$

$$\gamma_{xz} = \frac{2(1+\mu)}{E}\tau_{xy}$$

From the above, the following stress-strain relations are obtained for plane strain conditions:

$$\begin{bmatrix}\sigma_x\\ \sigma_z\\ \tau_{xz}\end{bmatrix} = E\lambda \begin{bmatrix}1 & \frac{\mu}{1-\mu} & 0\\ \frac{\mu}{1-\mu} & 1 & 0\\ 0 & 0 & \frac{1-2\mu}{2(1-\mu)}\end{bmatrix} \begin{bmatrix}\varepsilon_x\\ \varepsilon_z\\ \gamma_{xz}\end{bmatrix}$$

where

$$\lambda = \frac{1-\mu}{(1+\mu)(1-2\mu)}$$

and in matrix notation

$$(\sigma) = E\lambda[A]\,(\varepsilon) \qquad \text{Eq. 1}$$

Element Stiffness Matrix

A rectangular element is shown in Figure 2, together with assumed displacement functions. Displacements in the X and Z directions are shown by u and w, respectively. Nodal points are annotated as i, j, k, l. α_1 to α_8 are assumed displacement coefficients. The displacement functions represent linear displacement variations in the x and z directions. Therefore, each boundary remains a straight

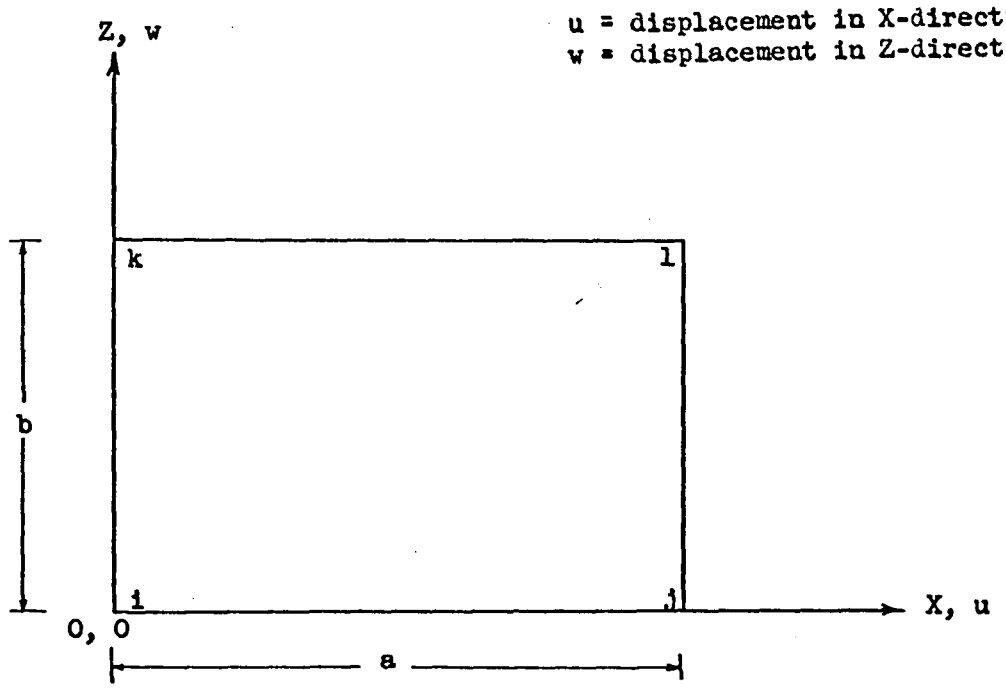

Assumed Displacement Functions:

$$\begin{pmatrix} u \\ w \end{pmatrix} = \begin{bmatrix} 1 & x & z & xz & 0 & 0 & 0 & 0 \\ 0 & 0 & 0 & 0 & 1 & x & z & xz \end{bmatrix} \begin{pmatrix} a_1 \\ a_2 \\ \cdot \\ \cdot \\ \cdot \\ a_8 \end{pmatrix}$$

Figure 2. Rectangular Element Stiffness

line during element deformation. Boundary and internal element compatibility are thus maintained during deformation. There are eight degrees of nodal point freedom (4 nodal points with x and z displacements at each one). Therefore, there are eight displacement functions provided, one for each degree of freedom. The stiffness matrix of this element is an eight-by-eight matrix.

A $[B]$ matrix is obtained for the element by introducing coordinates of the nodal points into the displacement functions:

$$\begin{bmatrix} u_i \\ u_j \\ u_k \\ u_l \\ w_i \\ w_j \\ w_k \\ w_l \end{bmatrix} = \begin{bmatrix} 1 & 0 & 0 & 0 & 0 & 0 & 0 & 0 \\ 1 & a & 0 & 0 & 0 & 0 & 0 & 0 \\ 1 & 0 & b & 0 & 0 & 0 & 0 & 0 \\ 1 & a & b & ab & 0 & 0 & 0 & 0 \\ 0 & 0 & 0 & 0 & 1 & 0 & 0 & 0 \\ 0 & 0 & 0 & 0 & 1 & a & 0 & 0 \\ 0 & 0 & 0 & 0 & 1 & 0 & b & 0 \\ 0 & 0 & 0 & 0 & 1 & a & b & ab \end{bmatrix} \begin{bmatrix} \alpha_1 \\ \alpha_2 \\ \alpha_3 \\ \alpha_4 \\ \alpha_5 \\ \alpha_6 \\ \alpha_7 \\ \alpha_8 \end{bmatrix}$$

and in matrix notation

$$(u) = [B]\,(\alpha) \qquad \text{Eq. 2}$$

A $[C]$ matrix, which represents internal strains, is obtained by differentiating the displacement functions:

$$\begin{pmatrix} \varepsilon_x \\ \varepsilon_z \\ \gamma_{xz} \end{pmatrix} = \begin{pmatrix} \frac{\partial u}{\partial x} \\ \frac{\partial w}{\partial z} \\ \frac{\partial u}{\partial z} + \frac{\partial w}{\partial x} \end{pmatrix} = \begin{bmatrix} 0 & 1 & 0 & z & 0 & 0 & 0 & 0 \\ 0 & 0 & 0 & 0 & 0 & 0 & 1 & x \\ 0 & 0 & 1 & x & 0 & 1 & 0 & z \end{bmatrix} \begin{pmatrix} a_1 \\ a_2 \\ \cdot \\ \cdot \\ \cdot \\ a_8 \end{pmatrix}$$

and in matrix notation

$$(\varepsilon) = [C](a) \qquad \text{Eq. 3}$$

The element material properties were previously defined by the stress-strain matrix $[A]$. Next, the matrix $[C^T A C]$, which is an eight-by-eight matrix for the rectangular element, is developed. Then each term of this matrix is integrated over the volume of the element. Utilizing the inverse of matrix $[B]$, this generalized coordinate stiffness is transformed to the coordinates of the respective nodal points. The resultant element stiffness matrix $[k]$ is an eight-by-eight matrix. If (s) and (u) are the force vector and nodal displacement vector, respectively, for the element,

$$[k](u) = (s) \qquad \text{Eq. 4}$$

Complete Assemblage Stiffness Matrix

The stiffness matrix for the complete assembly of elements is a block diagonal matrix. The diagonal elements in this matrix are the stiffness matrices for each of the individual elements:

$$\begin{bmatrix} k_{11} & & & & & & & \\ & k_{21} & & & & & & \\ & & \ddots & & & & & \\ & & & k_{12} & & & & \\ & & & & k_{22} & & & \\ & & & & & \ddots & & \\ & & & & & & k_{13} & \\ & & & & & & & k_{23} \\ & & & & & & & & \ddots \end{bmatrix} \begin{bmatrix} u_{11} \\ u_{21} \\ \vdots \\ u_{12} \\ u_{22} \\ \vdots \\ u_{13} \\ u_{23} \\ \vdots \end{bmatrix} = \begin{bmatrix} s_{11} \\ s_{21} \\ \vdots \\ s_{12} \\ s_{22} \\ \vdots \\ s_{13} \\ s_{23} \\ \vdots \end{bmatrix}$$

In matrix notation,

$$[K](U) = (S) \qquad \text{Eq. 5}$$

where $[K]$ is the composite stiffness matrix with respect to the local coordinates of all the element stiffness matrices, (U) and (S) are, respectively, the deflection vector and the force vector for the assemblage of all the elements.

The transformation matrix $[T]$ is developed next, to transfer the stiffness matrix with respect to the local coordinate system $[K]$ to the stiffness matrix in the generalized coordinate system $[\mathcal{K}]$.

$$[\mathcal{K}] = [T][K]^T[T] \qquad \text{Eq. 6}$$

Boundary Conditions

Boundary conditions are either in the form of restraint and movement (deflections) or forces. If an element is subjected to

external loading, the boundary forces (external loading) are included in the solution by incorporating the forces at nodal points which are affected. These forces then are introduced into the generalized force vector (F). An element may be restrained from moving or allowed to move (deflection). The stiffness matrix $[\mathcal{K}]$ is modified to include known deflections to maintain the boundary deflections which were specified. In matrix notation,

$$[\mathcal{K}](R) = (F) \qquad \text{Eq. 7}$$

where

(R) is the composite assemblage deflection vector.

Body forces of the material itself can be considered in a like manner. When the continuum is divided into a number of elements connected at nodal points, the weight of the material can be incorporated at appropriate nodal points. The body force, then, at a nodal point is the sum of the reactions of adjacent elements connected at that nodal point.

Solution of Equilibrium (Stiffness) Equations for Displacement

Displacements are solved for from equation 7. This equation represents 2N simultaneous equations, where N is the number of nodal points in the assemblage. Gaussian-elimination is used to perform the solution. Displacements, u, at each of the nodal points are obtained.

Determination of Strain and Calculation of Stress

Having solved the generalized stiffness equation for the displacements, stresses and strains can be determined. Strains are determined by combining equations 2 and 3,

$$(u) = [B]\,(\alpha) \qquad \text{Eq. 2}$$

$$(\varepsilon) = [C]\,(\alpha) \qquad \text{Eq. 3}$$

to form

$$(\varepsilon) = [C]\,[B]^{-1}\,(u) \qquad \text{Eq. 8}$$

The x and z components of the strain vector at the center of each element are determined with equation 8, where (u) are the displacements determined from the solution of the equilibrium (stiffness) equation in the previous section.

Next, stresses are calculated from equation 1,

$$(\sigma) = E\lambda[A]\,(\varepsilon) \qquad \text{Eq. 1}$$

The x and z components of the stress vector are calculated at the center of each of the elements. Principal stress values and orientation of principal axes can be determined with equation 1, also.

CHAPTER 3

DATA COMPILATION

It was necessary for model analysis to describe the rock in considerable detail, both in terms of the intact rock and the rock mass. Residual stress information, required in defining the stress distribution within the proposed open-pit mine area, was determined with an overcoring technique. Potentially hazardous geologic structure orientations were determined with geologic structural analyses.

Rock Substance

The term "rock substance" (Coates 1967) or "intact rock" (Deere 1969) refers to the rock material which can be sampled and tested in the laboratory, and which is free of the larger than sample size structural features such as joints, faults, seams, bedding planes and shear zones. The "rock mass" is composed of the rock substance plus these larger-scale structural features.

Physical Testing

Results of physical testing of the rock substance from Cananea were obtained from Zavodni (1969) and from work performed by students in the laboratory course in geomechanics at The University of Arizona. Zavodni's specimens were obtained from the existing Cananea Pit,

which is approximately 400 meters southeast of the proposed 755 Area pit. Figure 3 shows the location of the proposed 755 Area pit in relation to the Cananea pit and the Cananea district. Specimens tested by the geomechanics students were obtained from drill core taken from the 755 Area. There was good agreement between the two sets of results for like rock types.

The Cananea mine area is composed of volcanics intruded by several feldspathic quartz porphyry and quartz-free porphyry plugs; at least nine zones of strong brecciation are found within the main Cananea Pit area (Brown and Ayala 1966). These same rock units are found in the proposed 755 Area pit (Brown, personal communication). The volcanic (Mesa volcanic), quartz porphyry and breccia were the rock types that were sampled and tested in the laboratory.

Values of Young's modulus, E, Poisson's ratio, μ, and unconfined compressive strength, U_c, were obtained from the results of uniaxial compression tests. Young's modulus was determined as the tangent modulus. Values of Poisson's ratio and Young's modulus were selected from within the loading range which might be expected in the 755 Area pit, a range of 0-3000 psi. The lower values of unconfined compressive strength results were selected, because they will be more representative of the weaker rock mass strength.

Tensile strength values, T, were estimated from Brazilian tension, T_B, test results by the following approximate relationship:

$$T = 2/3 \times T_B$$

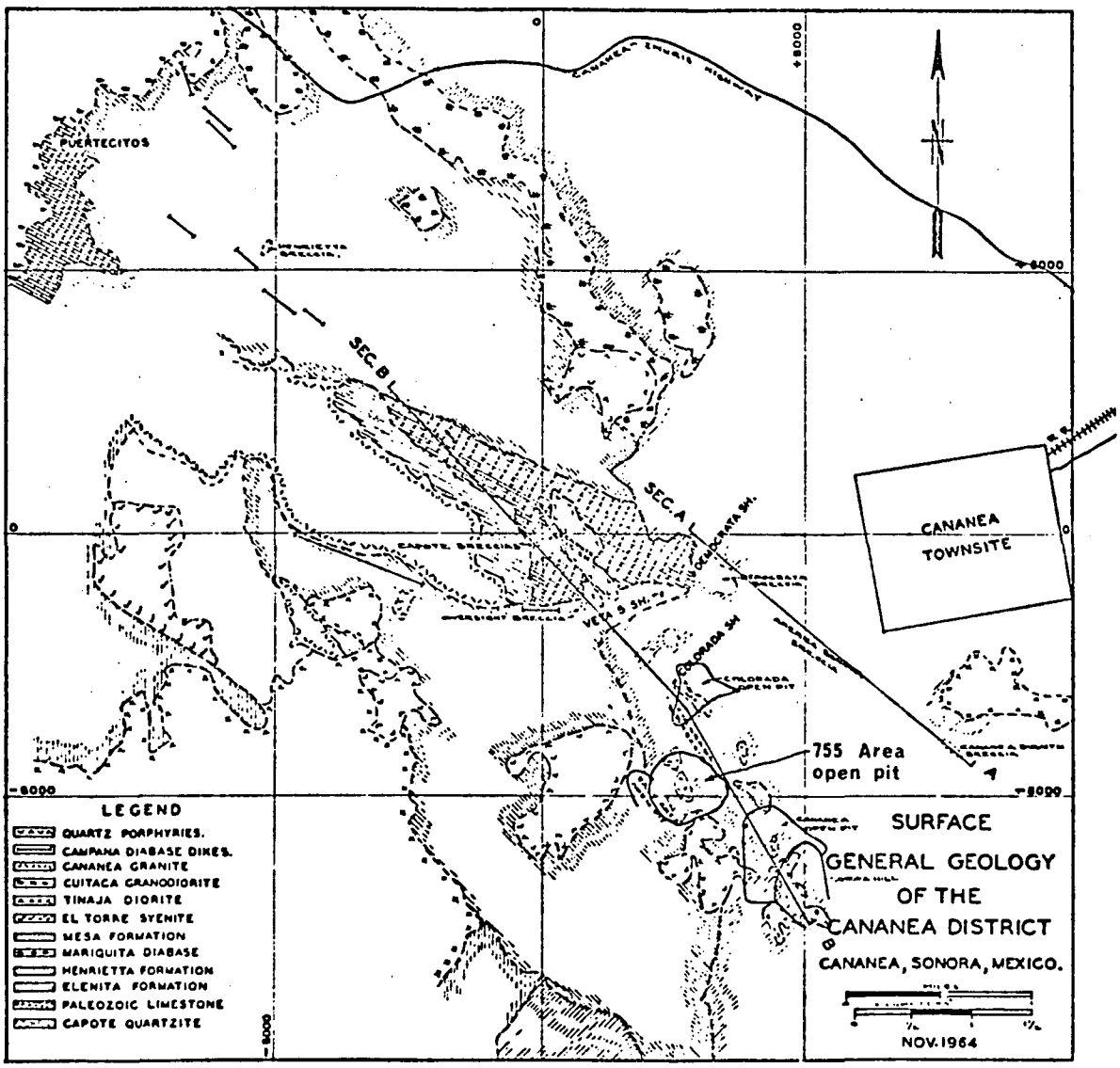

Figure 3. Location Map, 755 Area Open-Pit Mine. (After Velasco 1966)

Unit weights, γ, were determined for rock specimens from the leached (oxide) zone and sulphide zone for each rock type present in the proposed mine area. Densities for each specimen were determined by using a Jolly balance and applying Archimedes principle. Then, unit weights for each specimen were calculated.

Two additional rock units were defined and described. These are contact zones between the volcanic rock and the intrusive porphyry. One of these contact zones appears to be volcanic in nature, but contains porphyry fragments. The other contact zone appears to be a porphyry which contains fragments of volcanic material. These two zones were assigned values of E, μ, γ, U_c, and T based on the percentage of each of the two source materials (volcanic and porphyry) present. Table 1 lists selected values of Young's modulus, Poisson's ratio, unit weight, unconfined compressive strength and tensile strength for each of the five rock units. These values were selected on the basis outlined in this section.

Rock Substance Classification

Deere (1969) and Coates (1967) have developed classification systems which describe the intact rock (rock substance). Deere's classification is based on two important engineering properties of rock: the uniaxial compressive strength and modulus of elasticity. The first element of his classification is based on strength and the second element is based on modulus ratio. The rock being classified is put into one of six uniaxial compressive strength

Table 1. Selected Rock Substance Properties

Rock Type	E (10^6 psi)	μ	γ (pcf) oxide	γ (pcf) sulphide	U_c (psi)	T (psi)
Mesa volcanic	4.9	0.15	143	160	6500	720
Quartz porphyry	3.8	0.14	150	165	7900	580
Breccia	3.2	0.16	143	160	4500	440
Contact zone, volcanic with porphyry	4.5	0.145	143	160	7000	670
Contact zone, porphyry with volcanic	4.2	0.145	150	165	7400	630

categories. The upper portion of Table 2 lists the strength categories. The second element of the classification system is based on the modulus ratio. The modulus ratio is defined as the ratio of the modulus of elasticity to the uniaxial compressive strength. The lower portion of Table 2 lists the modulus ratio categories.

For the lower values of U_c selected from laboratory testing, Cananea mine rock has U_c values varying from 4500 to 7900 psi (Table 1). According to Deere's classification, this rock would be classified as low strength rock, Class D. The modulus ratio is 754 (high modulus ratio) for the volcanic rock, 481 (medium modulus ratio) for the quartz porphyry, and 712 (high modulus ratio) for the breccia. Therefore, these three rocks would be classified, respectively, as DH, DM and DH. They are, according to this classification, low strength rocks with medium to high modulus ratios.

Coates (1967) outlined a rock substance classification system in terms of strength and deformation characteristics. The system is as follows:

Geological Name
"Strong" or "Weak"
"Elastic" or "Yielding"

The rock substance strength is defined as "strong" when the uniaxial compression strength, U_c, is greater than 10,000 psi, and "weak" when the uniaxial compression strength is below this value. The term "yielding" would mean that the relative permanent strain upon loading is greater than 25% or the creep rate is greater than 2 microns/hour.

Table 2. Engineering Classification of Intact Rock. (After Deere 1969)

On Basis of Strength:

Class	Description	Uniaxial Compressive Strength (psi)
A	Very high strength	Over 32,000
B	High strength	16,000 - 32,000
C	Medium strength	8,000 - 16,000
D	Low strength	4,000 - 8,000
E	Very low strength	Less than 4,000

On Basis of Modulus Ratio:

Class	Description	Modulus Ratio
H	High modulus ratio	Over 500
M	Average (medium) ratio	200 - 500
L	Low modulus ratio	Less than 200

In successive loading-unloading cycles during the uniaxial compression testing of Cananea rock (Zavodni 1969), the following average permanent strain percentages in the loading direction were noted: porphyry = 12%, volcanics = 4%, and breccia = 2.7%. According to Coates' classification then, the Cananea mine rock which was tested is "weak" (less than 10,000 psi) and "elastic" (less than 25% permanent strain).

Zavodni (1969) determined from his testing that the porphyry behaved relatively elastically to 4700 psi, the volcanics to 4500 psi, and the breccia to 3300 psi. These loading ranges are all within the loading range expected in the 755 Area pit (0-3000 psi). Therefore, essentially elastic behavior could be expected in the rock substance in the 755 Area pit.

In summarizing the available information, the rock substance or intact rock in the 755 Area can be classified as "weak" or "low strength," having a medium to high modulus ratio, and exhibiting "elastic" behavior.

Rock Mass

The behavior of a rock mass subjected to a change in stress (excavation of an open-pit mine in this study) is governed both by the mechanical properties of the intact rock and by the number, attitude and nature of the geologic discontinuities in the rock mass. In some cases, the stability of a rock slope may be almost entirely controlled by these geologic discontinuities (joints, faults, seams). Large local variations in rock mass strength may

occur as a result of intense alteration (strong clay alteration or intense silicification). Similarly, the intensity of local shattering or fracturing on a small scale may result in large variations in rock mass strength. The properties of the rock substance must, therefore, be modified to account for these variations in the rock mass.

A better impression of the rock mass character for the 755 Area was obtained through the extensive examination of surface and underground maps and drill core logs and by field examination. Zones were located where the rock substance strength was to be reduced and subsequently introduced into the finite element models. This was accomplished by modifying the properties of each element so that the models closely approximated the in situ conditions from the 755 Area.

Reduced Parameters for the Rock Mass

Each element in the finite element models was modified in terms of Young's modulus, Poisson's ratio, unit weight, uniaxial compressive strength and tensile strength to take into account the local geologic conditions. These modifications were determined by examining all rock property information available for that element which could affect the rock properties for that elemental area. The specific geologic conditions taken into account were rock types, changes in degree and type of alteration, intensity of jointing, type and amount of mineralization that affected unit weight and core recovery. These variables were modeled by modifying laboratory

determined values of compressive and tensile strengths, unit weights, and elastic rock properties, where judged appropriate.

The following modifications were performed:

1. Any increase in the percentage of clay alteration was compensated for by a corresponding decrease in the "stiffness" and the strength of the model, i.e., E, Young's modulus, U_c, unconfined compressive strength, and T, tensile strength, would be decreased and μ, Poisson's ratio, would be increased for any element in the model which represented such an altered zone in the prototype.
2. Any increase in the percentage of silicification should increase the "stiffness" and strength of the model; therefore, E, U_c, and T would be increased and μ would be decreased for those elements which represented such zones.
3. Any decrease in the spacing of uncemented joints should decrease the strength and probably the element stiffness; thus, E, U_c and T would be decreased and μ increased for such elements.
4. Any increase in sulphide mineralization would increase the unit weight of the affected rock slightly. Material being used to model the leached or oxide zone would have to be represented by elements with a smaller unit weight. Conversely, the modeling of sulphide bearing rock would require a larger unit weight.
5. An increase in core recovery could feasibly be related to the overall quality of the rock (joint spacing, type and intensity of alteration). Therefore, an increase in core recovery

could be related to an increase in E, U_c, and T and a decrease in μ. Corresponding modifications were made to appropriate elements where core recoveries varied.

An attempt was made to use the rock quality designation, RQD, developed by Deere (1969) rather than percent core recovery. The RQD is based on a modified core recovery procedure. This indirect measure of fracture counting is obtained by adding up the total length of core recovered by counting only those pieces of core which are four or more inches in length. Deere (1969) believes that the RQD is a more sensitive and consistent indicator of general rock quality than is the gross core recovery percentage. The RQD could not be used to analyze core from the 755 Area, because nearly all of the core had been split and sampled previously. Therefore, gross percent core recovery was used.

Calculation of Reduced Parameter Values

A reduction number, corresponding to a percentage reduction, was assigned to each of the parameters being evaluated within model elements. Table 3 lists reduction numbers for each category of reduced parameters. A composite reduction number, which takes into account all of the reduced parameters, was calculated for each of the model elements. A sample calculation is performed for an element representing an in situ area of uniform geologic characteristics:

Table 3. Reduction Numbers for Reduced Parameters

Reduction Terms		Reduced Parameter Categories			
Reduction Number	Reduction Factor, %	Clay Alteration, % of total Specimen	Silicification, %	Spacing of Uncemented Joints, ft.	Core Recovery, %
-1	115	-	30-100	-	-
0	100	0	1-29	>50	100
1	85	1-20	-	21-50	93-99
2	70	21-40	-	10-20	83-92
3	55	41-60	-	3-9	68-82
4	40	61-80	-	1-2	50-67
5	25	81-100	-	0.2-0.9	30-49
6	10	Altered to soft or medium clay	-	<0.2	<30

Reduced Parameter		Reduction Number
30% clay alteration	=	2
10% silicification	=	0
1 ft. joint spacing	=	4
85% core recovery	=	2
Composite reduction number	=	8/N = 8/4 = 2

where

N = number of categories

The composite reduction number is equal to 2, which is equivalent to a reduction factor of 70% from Table 3. Then for values of U_c, T, and E for this element, reduced values are calculated:

Reduced Value = Rock Substance Value x Reduction Factor (%)

The U_c, T and E values assigned to this element are 70% of the laboratory determined values of U_c, T and E for the rock substance which is present in this element. The value of μ is increased for this element in a manner similar to the method used for decreasing the values of U_c, T and E.

Residual Stress Determination

Knowledge of the in situ state of stress is a necessary prerequisite for engineering design in rock. Stresses are quite often calculated by assuming that only gravity forces are present. It is well documented (Nichols, Lee and Abel 1969, Hooker and Johnson 1966,

Coates and Grant 1966) that forces other than gravity can contribute to the in situ state of stress. Voight (1966) considers "in situ stress" to be the result of force fields which he classifies as current gravitational forces and current and residual tectonic forces. Stresses due to current gravity loading can be calculated rather easily from elastic theory. Current tectonic stresses are probably not determinable. Residual tectonic stresses can generally be elastically released by strain relief and thus calculated (Voight 1966). Gravity loading and residual tectonic loading can be incorporated into the finite element analysis quite readily. As was indicated in Chapter 2, these two loads can be summed at appropriate nodal points to account for variations in any model loading situation.

There are several methods of determining the state of stress in rock. All of them involve measurement of deformation and then calculation of stress from the measured deformation. The principles underlying the design of rock stress measurement techniques and related instrumentation are reviewed by Leeman (1964). Most instruments provide purely biaxial information such as is provided by photoelastic strain gage techniques (Voight 1967) and strain gage overcoring (Merrill and Peterson 1961, Obert, Merrill and Morgan 1962). Operational techniques require diametral measurements in three separate boreholes drilled into the rock at suitable orientations to obtain sufficient information for the three dimensional stress ellipsoid (Gray and Toews 1967). The ideal

technique for determining the stress in rock would permit the determination of directions and magnitudes of principal stresses from strain measurements in a single borehole drilled in any desired direction into the rock. Methods developed by Leeman (1968), Rocha and Silvério (1969) and Nichols, Abel and Lee (1968) should accomplish that goal. These methods involve the use of strain gages glued on the walls of a borehole or a solid-inclusion borehole probe to determine three-dimensional stresses or stress changes in a rock mass caused by nearby excavation.

Voight (1968) has proposed a technique which requires no borehole instrumentation. By instrumenting drill cores on three planes of specified orientation soon after removal from the borehole, a portion of the total recoverable strain tensor is determined. There is empirical justification (Voight 1968, p. 205-208) for considering the recovered time-dependent strain to be proportional to the total recoverable strain and, thus, to the pre-existing state of stress. If strain gages are installed on drill core after the core has been removed from the borehole, only a partial component of strain can be determined. Voight's method is based on the premise that the partial recoverable strain at a point is proportional to the total recoverable strain.

Method of Stress Determination

The basic method as postulated by Voight (1968) has been modified by Gentry (1970a). Strain relief was measured as a result

of overcoring a strain gage on an oriented rock specimen with a diamond bit.

Two oriented samples were collected from the "Tunnel 1" level near the center of the 755 Area. One sample was taken from within a breccia pipe and the other from the surrounding volcanic rock. The sample from the breccia pipe was highly silicified and contained moderate clay (kaolinite) and sericite alteration. The volcanic specimen had undergone intense sericitization and kaolinitization. Both specimens had a volume of approximately 0.6 cubic foot.

The testing procedure proceeded as follows:

1. A horizontal and a vertical cut were made on each rock specimen with a diamond saw.
2. Strain gage rosettes with three equiangular 120° elements were mounted on these two faces with epoxy cement and then were monitored until the deformation (expansion) due to the saw cuts ceased. The rock effectively was stable, as indicated by the gages, after eight weeks for the breccia specimen and after five weeks for the volcanic specimen.
3. The strain gage rosettes were overcored to a depth of two inches with a 1 1/8" O. D. diamond bit around the 1" strain gage rosettes.
4. When the overcoring was completed, the specimens were again monitored. Monitoring continued until essentially all time-dependent deformation (expansion), as a result of overcoring the gages, was complete. Any change in strain readings

from pre-overcoring to post-overcoring should represent the measurement of residual strains released as the result of overcoring. The overcored breccia specimen was stable after five weeks and the overcored volcanic specimen stabilized after six weeks.

Data resulting from the overcoring, strains in each of the strain gage rosette elements, were then analyzed. Major and minor principal stress magnitudes and directions and maximum shear stress were calculated with a method described by Hetenyi (1954, p. 410-415). Strain gage rosette analysis requires the knowledge of E, Young's modulus, and μ, Poisson's ratio, because of the assumption of isotropy. Values of E and μ were selected for each of the two specimens according to the "Reduced Parameter Value" criterion as described previously in this chapter. The values used for the breccia specimen were $E = 3.2 \times 10^6$ psi and $\mu = 0.16$. The values used for the volcanic specimen were $E = 2.0 \times 10^6$ psi and $\mu = 0.32$.

Results

Only three of the four overcoring attempts were successful. In the unsuccessful attempt, several of the strain gage lead wires were cut off by the diamond bit during the overcoring step and had to be re-soldered to the gages. In the process, gage lead wire resistances changed and thus could not be compared accurately to original lead wire resistances for accurate determination of strain relief due to overcoring.

It was desirable to know the approximate vertical and horizontal stress magnitudes in the plane of a vertical section which would be analyzed by the finite element model. The section which was modeled had a bearing of N5W. The maximum principal stress in the horizontal plane of the breccia specimen was 585 psi and was oriented at N12E, only 17° to the east of the model section. Therefore, this value was used for the horizontal stress for the breccia specimen. The maximum principal stress in the vertical plane of the breccia specimen was 472 psi and was oriented at an inclination of only 7° 31' from the vertical. Therefore, this value was used for the vertical stress for the breccia specimen. Two of the three lead wires on the strain gage rosette on the horizontal plane of the volcanic specimen were cut off during overcoring. Results from analysis of strains in this strain gage were not used. The maximum principal stress in the vertical plane of the volcanic specimen was 832 psi and was oriented at an inclination of only 2° 51' from the vertical. Hence, this value was used for the vertical stress for the volcanic specimen. The minimum principal stress in the vertical plane is 515 psi and will be used for the horizontal stress in this specimen, because no stress values were available from the horizontal plane. The vertical plane in this specimen has a bearing of N65W; therefore the minimum principal stress (used for horizontal stress) is not in the same plane as the model section (N5W).

Applicability of Results

The directions of the principal stresses should be correct with this technique. In examining stress magnitudes, the ratio of

the vertical to the horizontal residual stresses should be the same as the ratio of the vertical to the horizontal in situ stresses according to Voight (1966 and 1968). The absolute magnitudes of residual stresses measured in this manner, however, are questionable, because they probably represent only a portion of the original in situ stresses.

Model Structure Determination

Planar geologic structure plays an important role in rock slope stability. Joints and faults associated with intrusive and extrusive rocks found in porphyry copper deposits, such as those at Cananea, can significantly affect the stability of open-pit mine slopes. In order to obtain geologic structure for a finite element model, actual in situ geologic structures were examined in the 755 Area. Only those geologic structures which are parallel to the infinite slope (parallel to the Y-direction in Figure 1) and also perpendicular to the model section are applicable for a two-dimensional, plane strain, finite element analysis. The model section was vertical and trended N5W-S5E. Therefore, structures selected for the analysis should have a strike of approximately N85E. The model open-pit mine slope dipped to the south; therefore southerly dipping geologic structure was examined most critically. Dip values that approximate critical sliding angles, 30°-65°, were sought. Subject to these restrictions, two types of geologic

structure information were examined to obtain model geologic structure for a finite element model:

1. Major joint sets
2. Intersections of major joint sets

Major Joint Sets

A joint set is defined as a group of more or less parallel joints. A major joint set, within the scope of this study, is a joint set which occurs throughout a significant portion of the mine area (755 Area). Zavodni (1970) plotted the attitudes of joints within the 755 Area using a Schmidt equal-area projection structural analysis. Data for the analysis came from maps of the surface and three development levels in the 755 Area.

The equal-area (Schmidt) projection provides a graphic method of presenting joint set orientations. Pincus (1951) discussed the application of equal-area and equal-angle projections in the analysis of rock fractures. The technique of applying a Schmidt equal-area, lower hemisphere, projection analysis to the design of open-pit mine slopes was further developed by Call (1967) and was utilized in previous Cananea geologic structural analysis by Zavodni (1969 and 1970).

Upon examination of the results determined from Zavodni's (1970) analysis of the 755 Area structural data, one major joint set, oriented at a critical attitude for model analysis, was discovered. This joint set strikes approximately N85E, perpendicular

to the model section, and dips to the south, into the pit, at 45°-55°.

Intersections of Major Joint Sets

Two nonparallel geologic discontinuities (faults, joints, seams) striking at an angle to the pit face and dipping in opposite directions form a tetrahedron that may be free to slide into the pit (Call 1967). The direction (bearing) and plunge of the line of intersection is the direction of motion. The plunge of the intersection is always less than the dip of the flatter of the two geologic structures.

Smith (1969) developed a computer program which computes the bearing and plunge of the intersection and the dihedral angle between the intersecting structure planes for all possible combinations in given joint set attitudes. This program was used to determine the intersections which were possible in the 755 Area. The results of Zavodni's (1970) Schmidt equal-area projection analysis of the 755 Area were analyzed and seven major joint sets were delineated for intersection determination. All possible intersection combinations were determined and examined for the critical range of values for bearing, plunge and dihedral angle. Only one intersection was found which satisfied all of these three criteria. This intersection has a bearing of N10W, which is approximately parallel to the model section; it has a plunge of 48° to the south, into the pit; and it has dihedral angles of 60° and 120°. This structure

intersection and the major joint set which was identified in the previous section were used to determine the attitude of the critical joints employed in two of the finite element models.

CHAPTER 4

METHOD OF ANALYSIS

Two-dimensional, plane-strain finite element analysis was utilized to estimate excavation (mining) induced displacement and stress changes in a particular open-pit mine slope. Five different finite element models were developed to model this 70^{o} pit slope. The effects of non-homogeneity and anisotropy were examined. Gravity and tectonic loads were modeled and their effects evaluated. The effects of geologic discontinuities (joints) were examined.

Approach Utilized

The finite element models of the 755 Area open-pit mine slope were evaluated in plane strain rather than plane stress. Tectonic loads, which were estimated from measurement of residual stresses, were introduced as boundary forces. Total displacements, which are a result of loading conditions plus excavation rebound, are not appropriate for determining stability conditions. Excavation displacements were utilized. They can be measured in the field and are critical for stability determination. Total stress, a result of loading and excavation, is applicable whereas excavation stress which is only part of the stress picture is not pertinent

to the evaluation of stability conditions. Figures 4 and 5 are, respectively, pre-excavation and post-excavation element meshes of the finite element models of the 755 Area pit. Individual elements are shown in the mesh. The models are vertical sections trending N5W to S5E, from left to right, through the north wall of the 755 Area pit. The right half of the models has been removed for ease of analysis and also due to approximate symmetry of the pit. The depression at the top left of the section models is an existing open-pit mine, the Colorada Pit.

Plane Strain

The plane strain condition, which considers adjacent restraint, more closely approximates in situ conditions for slopes of major size than does the plane stress condition. Therefore, plane strain is more appropriate for analysis of the 755 Area open-pit mine slope.

If plane stress conditions are assumed, all stresses acting upon the model would be parallel to one plane (the X-Z plane in Figure 1). The stress in the Y-direction, which is normal to the plane of the model, would then be zero. A plane stress model would be a thin plate of uniform, one-unit thickness.

All of these unrealistic assumptions can be negated in the plane strain condition. If a long body (the open-pit wall in Figure 1) is loaded by forces which are perpendicular to the Y-axis and which do not vary along the length of the body, the portion of

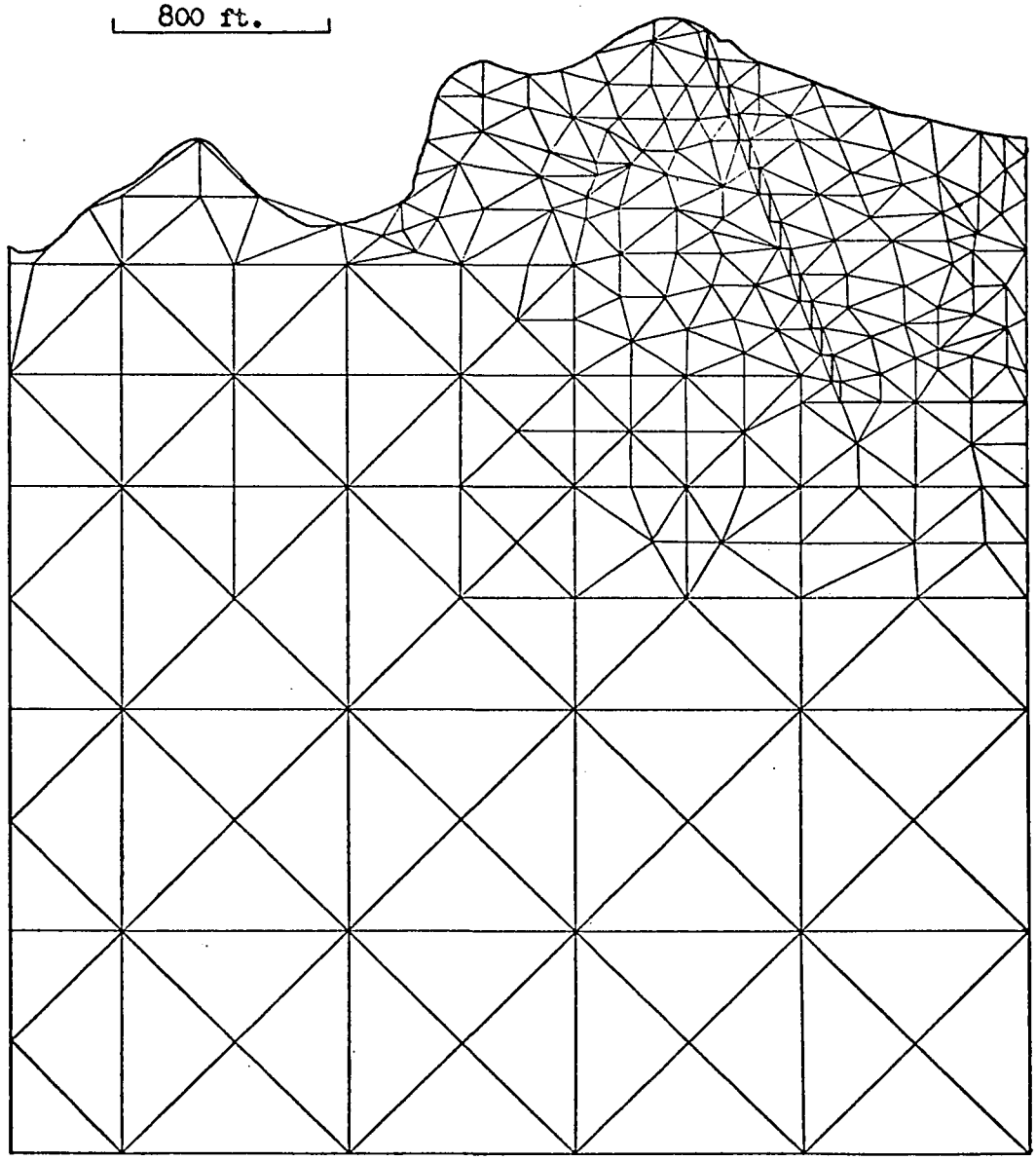

Figure 4. Pre-Excavation Finite Element Mesh, 755 Area Pit

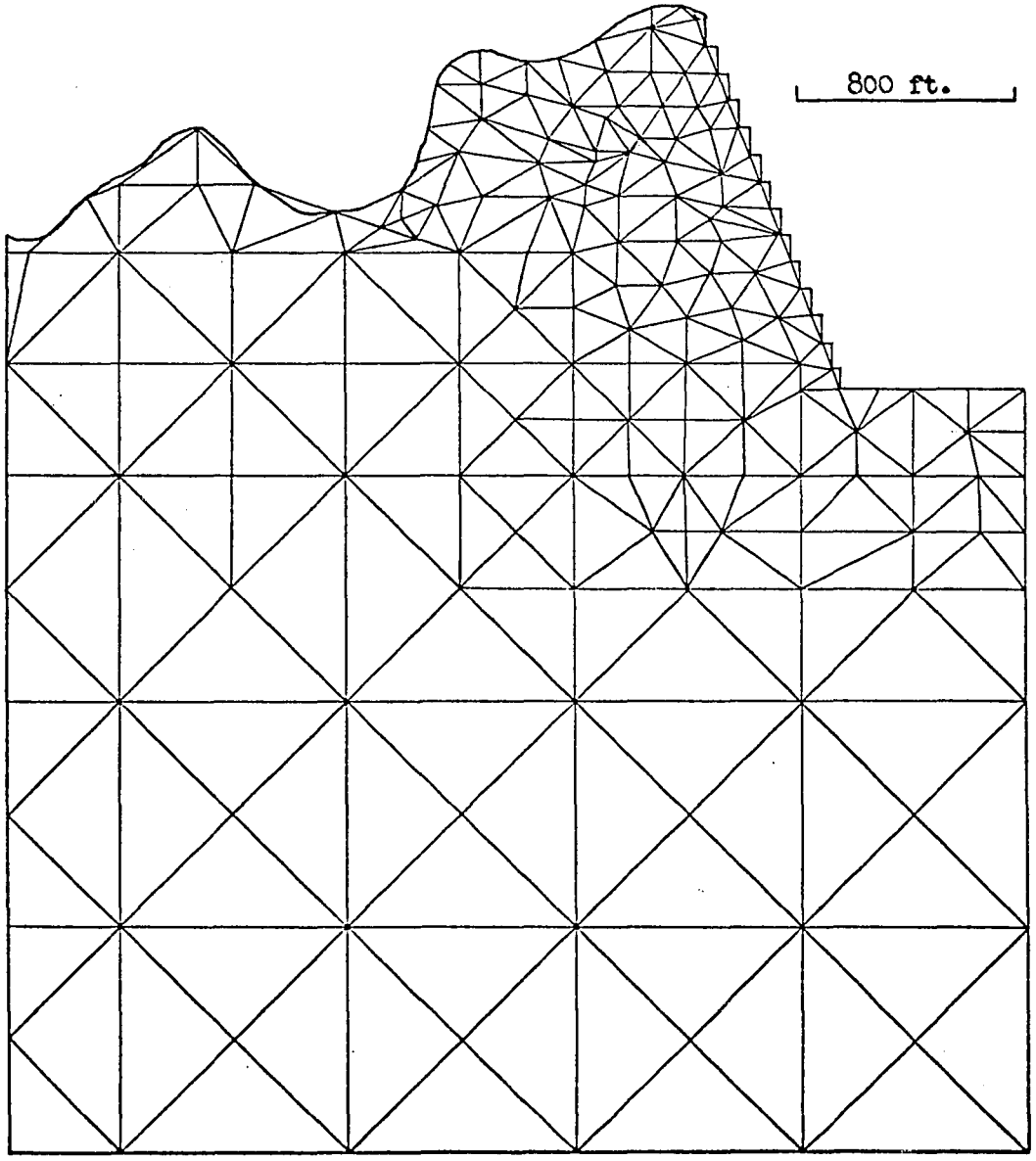

Figure 5. Post-Excavation Finite Element Mesh, 755 Area Pit

the body at a considerable distance from the ends has essentially a plane deformation and the displacements of all points of the deformed body are in planes perpendicular to the Y-axis (Timoshenko 1934). Because of the assumed infinite length of the open-pit wall, the deformation in the Y-direction, ε_y, is zero. Then it is sufficient to consider only one slice between two identical X-Z sections which are a unit distance apart along the Y-axis. Unlike plane stress, the plane strain condition does not require that the stress in the third dimension, σ_y, be equal to zero:

$$\sigma_y = \mu(\sigma_x + \sigma_z)$$

The X-Z plane is shown as the vertical section of the finite element model in Figures 4 and 5. Strain within each of the triangular elements is assumed to be uniform in the X-Z plane for analysis with the finite element method. Strain is prevented by σ_y in the Y-direction. The sizes and shapes of the elements in the finite element models were selected so that they would correspond to areas of approximately uniform rock mass conditions, e.g., the same type and intensity of alteration and same jointing intensity, in the 755 Area pit. Therefore, approximately uniform strain should occur within each of the in situ rock mass zones modeled by model elements.

Boundary Conditions

Boundary conditions were applied to the finite element models as end constraint and as external loading. Lateral boundaries of the models were permitted to displace vertically, but not horizontally. The procedure to prevent horizontal displacement (X-direction) was accomplished by assigning values of $u = 0$ at each nodal point on the lateral boundary for the displacement functions. Displacement functions for a rectangular-shaped element were described in Chapter 2 and were defined and illustrated in Figure 2. The bottoms of the models were allowed to displace horizontally, but not vertically. This was accomplished by assigning values of $w = 0$ at each nodal point on the horizontal or lower boundary for the displacement functions to achieve restraint in the Z-direction.

External loads were applied at the boundaries of the finite element models. Tectonic loads, which were approximated from residual stress measurements, were applied to the model boundaries as nodal point stresses.

Excavation Displacement

In order to examine potential stability conditions in an open-pit mine slope, the displacement of the slope is often monitored. The open-pit walls and floor should rebound, elastically, in response to excavation (mining). Since rebound is a normal response, elastically, and is readily determined, it can be used

as a standard for evaluating the stability of the slope. Slope displacement, which is measured during excavation (mining), can be compared with displacement calculated for elastic rebound. If the values are different, then displacement may be occurring as a result of non-elastic deformation or as a result of unstable slope conditions.

Displacements occur also in response to gravity and tectonic load application. These displacements must be removed from the total displacement in order to obtain the desired excavation displacement. This was accomplished in the modeling sequence with the following approach. The finite element model was loaded with gravity and/or tectonic loads for the pre-excavation condition. Resultant pre-excavation displacements were used as initial displacements for the next step. Next, excavation was modeled. Excavation displacements were determined by subtracting initial displacements from the total (resultant) displacements at each nodal point:

$$\delta_{excavation} = \delta_{resultant} - \delta_{initial}$$

Total Stress

The stability of an open-pit mine slope is affected by the total stress acting upon it, not just the excavation stress. Total stress would be comprised of stresses related to gravity and/or tectonic loading and stresses which arise due to the

creation of the excavation (the open-pit mine). Total stress for the finite element models of the 755 Area pit was determined in the following manner. Each model was loaded with gravity and/or tectonic loads prior to excavation. Excavation of the open-pit mine was modeled next. The resultant stress after excavation was the total stress which arises from both loading and excavation.

Model Descriptions

A vertical section trending N5W to S5E and intersecting the north wall of the proposed 755 Area pit was selected for model analysis with the finite element method. The section location and bearing were chosen so that the section would intersect the highest and, therefore, potentially the most critical wall of the proposed pit. The area through which this section was made was then modeled and analyzed for five different situations. Five open-pit slope models were designed and then tested with the finite element method. Model conditions varied from simple to complex. The simplest model, Model 1, was homogeneous, isotropic, linearly elastic and gravity loaded. The most complex model, Model 5, was non-homogeneous, anisotropic, loaded by gravity and tectonic loads, and had model joints which were permitted to deform non-linearly. The remaining three models lie between these two extremes in degree of complexity. The first model introduced one condition. Each succeeding model, from Model 2 to Model 5, introduced an additional major variation. Each variation was designed to model

an additional in situ condition. The effect was cumulative, such that Model 5 had all of the variations from Models 1 to 4 incorporated into it as well as an additional variation introduced for the fifth model. Model 5, then, had all of the (geologic) variations incorporated in it and, therefore, was designed to be most representative of actual in situ conditions of the north slope of the 755 Area pit.

Model 1

Model 1 was homogeneous, isotropic, linearly elastic and gravity loaded. It was composed of one homogeneous material with isotropic properties. Homogeneity was accomplished by averaging the values of the selected rock substance properties for the five rock types which are listed in Table 1. Weighted averages, weighted according to the number of elements of each rock type present, were determined. Then an average was calculated for the entire model. Figure 4 shows the pre-excavation element mesh. Of the 420 elements shown, 386 modeled volcanic rock, 8 modeled quartz porphyry, 22 modeled material from the contact zones, and 4 modeled material from a breccia pipe. Weighted averages were then calculated for E, Young's modulus, μ, Poisson's ratio and γ, unit weight, for the entire model. Weighted averages of rock substance properties which were utilized for analysis of Model 1 were

$$E = 4.85 \times 10^6 \text{ psi} \qquad \mu = 0.15 \qquad \gamma = 165 \text{ pcf}$$

An example of the pre-excavation state of stress for a simple gravity loaded model is illustrated in Figure 6. The pre-excavation state of stress is composed of S_v, the vertical stress, and S_h, the horizontal stress. The vertical stress is due to gravity, as related to the unit weight, γ, of the material. The horizontal stress is partially due to Poisson's effect, as related to Poisson's ratio, μ, and partially due to gravity loading which produced the vertical driving stress, S_v. Model 1 loading was due to gravity effects, also. The geometry of Model 1 is different than the simplified model shown in Figure 6, but the gravity loading mechanism is the same.

Model 2

Model 2 was homogeneous and isotropic within each of the five different rock type zones. The model as a whole was non-homogeneous and anisotropic. Loading was due to gravity effects only; no tectonic loads were introduced. Each of the five rock type zones were outlined. Within each of these zones, values of E, Young's modulus, μ, Poisson's ratio, and $\gamma_{sulphide}$, unit weight, were assigned which correspond to rock substance properties. Values of E, μ and $\gamma_{sulphide}$ were selected from Table 1 for each of the five rock type zones. Model 2, as in Model 1, had 386 volcanic, 8 porphyry, 22 contact zone material, and 4 breccia model elements.

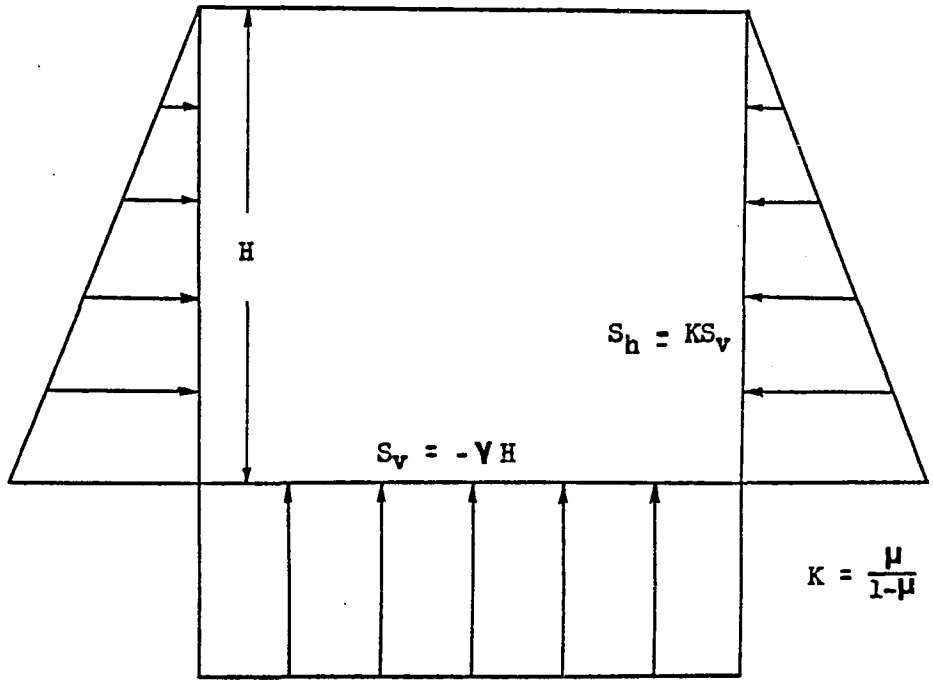

Figure 6. Pre-Excavation State of Stress, Simple Gravity-Loaded Model

The pre-excavation state of stress for Model 2 was determined in the same manner as for the pre-excavation state of stress for Model 1. Unit weight was different for each rock type in Model 2; whereas unit weights were averaged for the entire model in Model 1. Unit weights for the sulphide zone were used in Model 2.

Model 3

Model 3 was non-homogeneous and anisotropic within different rock type zones and for the model as a whole. This model was homogeneous and isotropic only within each finite element. Loading was due to gravity effects only. Individual elements were constructed to model the rock in detail. All determinable rock property differences which could affect rock strength locally were modeled. Differences in rock types, changes in type and degree of alteration, intensity of jointing, type and amount of mineralization that affected unit weight, and core recovery were all accounted for in Model 3. These variables were modeled by modifying laboratory determined values of compressive and tensile strengths, unit weights, and elastic rock properties of the rock substance where it was deemed appropriate. Modification of the rock substance values in an attempt to model the rock mass was discussed in detail in Chapter 3, p. 26-31. Table 4 lists the modified rock substance values for modeling the rock mass which were utilized in Model 3.

Table 4. Modified Rock Substance Values for Modeling the Rock Mass

Rock Type	Reduction Number	μ	E(10^6 psi)	γ (pcf) Oxide	γ (pcf) Sulphide
Mesa Volcanic	0	0.15	4.90	143	160
	1	0.19	4.16	"	"
	2	0.23	3.43	"	"
	3	0.28	2.69	"	"
	4	0.32	1.96	"	"
	5	0.36	1.22	"	"
	6	0.40	0.49	"	"
Quartz Porphyry	0	0.14	3.80	150	165
	1	0.18	3.23	"	"
	2	0.23	2.66	"	"
	3	0.27	2.09	"	"
	4	0.31	1.52	"	"
	5	0.36	0.95	"	"
	6	0.40	0.38	"	"
Contact Zone, (volcanic with porphyry)	0	0.145	4.50	143	160
	1	0.19	3.82	"	"
	2	0.23	3.15	"	"
	3	0.27	2.47	"	"
	4	0.32	1.80	"	"
	5	0.36	1.12	"	"
	6	0.40	0.45	"	"
Breccia	0	0.16	3.20	143	160
	1	0.20	2.72	"	"
	2	0.24	2.24	"	"
	3	0.28	1.76	"	"
	4	0.32	1.28	"	"
	5	0.36	0.80	"	"
	6	0.40	0.32	"	"
Contact Zone, (Porphyry with volcanic)	0	0.145	4.20	150	165
	1	0.19	3.57	"	"
	2	0.23	2.94	"	"
	3	0.27	2.31	"	"
	4	0.32	1.68	"	"
	5	0.36	1.05	"	"
	6	0.40	0.42	"	"

Model 3 was subjected to gravity loading only. The pre-excavation state of stress for Model 3 was determined in the same manner as for Models 1 and 2. Two unit weights were introduced for each rock type in Model 3: $\gamma_{sulphide}$ and γ_{oxide}.

Model 4

This model was essentially the same as Model 3, except that joints were incorporated. Model 4 was non-homogeneous and anisotropic within each rock type zone and also for the model in its entirety. The model was homogeneous and isotropic only within each finite element. Loading was due to gravity only. The same modified rock substance values were employed in this model as were used in Model 3.

Two joints, which were continuous from the crown of the slope all the way to the pit face, were modeled. The joints were modeled as one-half inch thick elements which were filled with clay gouge material. The thirteen joint elements were elongate triangular shaped elements. The location and attitude of the model joints were determined according to the methods outlined in detail in Chapter 3, p. 37-40. The model joints are perpendicular to the model section and dip southerly into the 755 Area pit at 45°. The attitude of the model joints was selected on the basis of the attitudes of the following: (1) a major joint set and (2) the intersection of two major joint sets. The clay gouge material was assigned the following

values: $\phi = 15^{o}$-20^{o}, c = 576 psf. The selection of continuous, clay gouge filled joints which dip into the pit at a critical sliding angle probably would lead to the worst (stability-wise) condition for joint modeling.

Model 4 was subjected to gravity loading only. The pre-excavation state of stress for Model 4 was ascertained in the same manner as for Models 1, 2 and 3. Values utilized for loading of Model 4 were the same as those used for Model 3.

Model 5

This model was essentially the same as Model 4, except that loading was a combination of gravity and tectonic loads. Model 5 was anisotropic and non-homogeneous for the model as a whole and within each rock type zone. The model was isotropic and homogeneous only within each finite element. The same modified rock substance values and two continuous model joints were employed in this model as were used in Model 4.

Residual tectonic stress was determined in a manner outlined in detail in Chapter 3, p. 33-37. Essentially, residual tectonic stress was determined by utilizing the results of the stress-relief overcoring technique. A modification of a method proposed by Voight (1968) was employed. Rock samples for overcoring were taken from within and adjacent to a breccia pipe in the 755 Area. Three of four overcoring attempts were successful. Results indicate that the vertical to horizontal stress ratio could be 5:6 in the breccia pipe and 8:5 just outside of the breccia pipe.

The pre-excavation state of stress was assumed to be a result of both gravity and tectonic loading for Model 5. The vertical to horizontal residual tectonic stress ratio of 5:6 was utilized in conjunction with gravity loading so that the worst (highest) possible horizontal loading condition could be modeled. The pre-excavation state of stress for Model 5 was

$$\text{Total Force Vector} = \Sigma(\text{Gravity}) + \Sigma(\text{Tectonic})$$

and in matrix notation

$$(F) = (G) + (T_r)$$

where

(G) is the matrix for the summation of gravity forces at all elements, (T_r) is the matrix for the summation of residual tectonic forces at all elements, and (F) is the force vector for the complete assemblage of finite elements in the model.

CHAPTER 5

ANALYSIS OF RESULTS

The five open-pit finite element models were analyzed for stress redistribution and for changes in displacement resulting from excavation (mining). The stability conditions for each of the model open-pit slopes were estimated by examining several critical failure criteria.

Mining-Induced Stress Redistribution

The pre-excavation state of stress, or virgin state of stress, in a rock mass is altered as a result of creating any excavation, in this case an open-pit mine. These excavation-induced stress alterations occur as local stress concentrations and reductions. Five finite element models of the 755 Area pit were described in detail in Chapter 4. Computer contour plots of the pre-excavation and post-excavation state of stress for these five models were examined for significant stress changes.

The principal stresses and the maximum shear stress are related to one another mathematically. Only the principal stress results from model analyses will be discussed, because a discussion of maximum shear stress results would follow similar lines. Maximum shear stress contour plots are presented in Appendix I.

Figures 7 to 16 are, respectively, computer-drawn plots of maximum principal stress contours for the pre-excavation and post-excavation conditions for Models 1-5. Tables 5 and 6 list the maximum principal stress changes due to excavation at selected nodal points along the pit wall for these five models. Two areas near the final pit wall were selected to examine stress changes: (1) at one-half the pit depth and (2) at the toe of the pit slope. Three nodal points were chosen from each of these areas so that results which were representative of each area could be obtained and then general conclusions made for the two areas. Nodal points 159, 156 and 148 (Table 5), at one-half the pit depth, are located at the 7th, 8th and 9th benches from the top of the pit, respectively, as illustrated in Figure 8. Nodal points 136, 134 and 132 (Table 6) are located near the toe of the pit at the 12th, 13th and 14th benches from the top of the pit, respectively.

Model 1: Homogeneous, Gravity Loading

At One-Half the Pit Depth. Model 1 (Figures 7 and 8) had a relatively small increase in stress due to excavation: 17%, 25% and 32% at nodal points 148, 156 and 159 (Table 5). The initial and final stress magnitudes, also, were small: 600-700 psi for pre-excavation and 700-800 psi for post-excavation conditions.

At the Toe of the Pit Slope. There was a smaller increase, percentage-wise, in stress due to excavation at the toe of the pit slope than at one-half the pit depth: 15%, 14% and 4% at the three nodal

Table 5. Maximum Principal Stress Changes in the Pit Wall at One-Half the Pit Depth, psi

Model	Pre-excavation			Post-excavation			Percent Increase		
	NP 148	NP 156	NP 159	NP 148	NP 156	NP 159	NP 148	NP 156	NP 159
1	731	622	545	857	776	718	17	25	32
2	734	625	548	862	779	720	17	25	31
3	688	588	509	807	748	692	17	27	36
4	1017	747	585	1961	1290	909	93	73	55
5	3898	3182	2666	7598	5571	4032	95	75	51

Table 6. Maximum Principal Stress Changes at the Toe of the Pit Slope, psi

Model	Pre-excavation			Post-excavation			Percent Increase		
	NP 132	NP 134	NP 136	NP 132	NP 134	NP 136	NP 132	NP 134	NP 136
1	1245	1133	1055	1434	1296	1096	15	14	4
2	1252	1139	1058	1447	1308	1103	16	15	4
3	1216	1094	1002	1389	1241	1042	14	13	4
4	1227	1114	968	1439	1323	1065	17	19	10
5	2720	2616	2185	3129	3072	2495	15	17	14

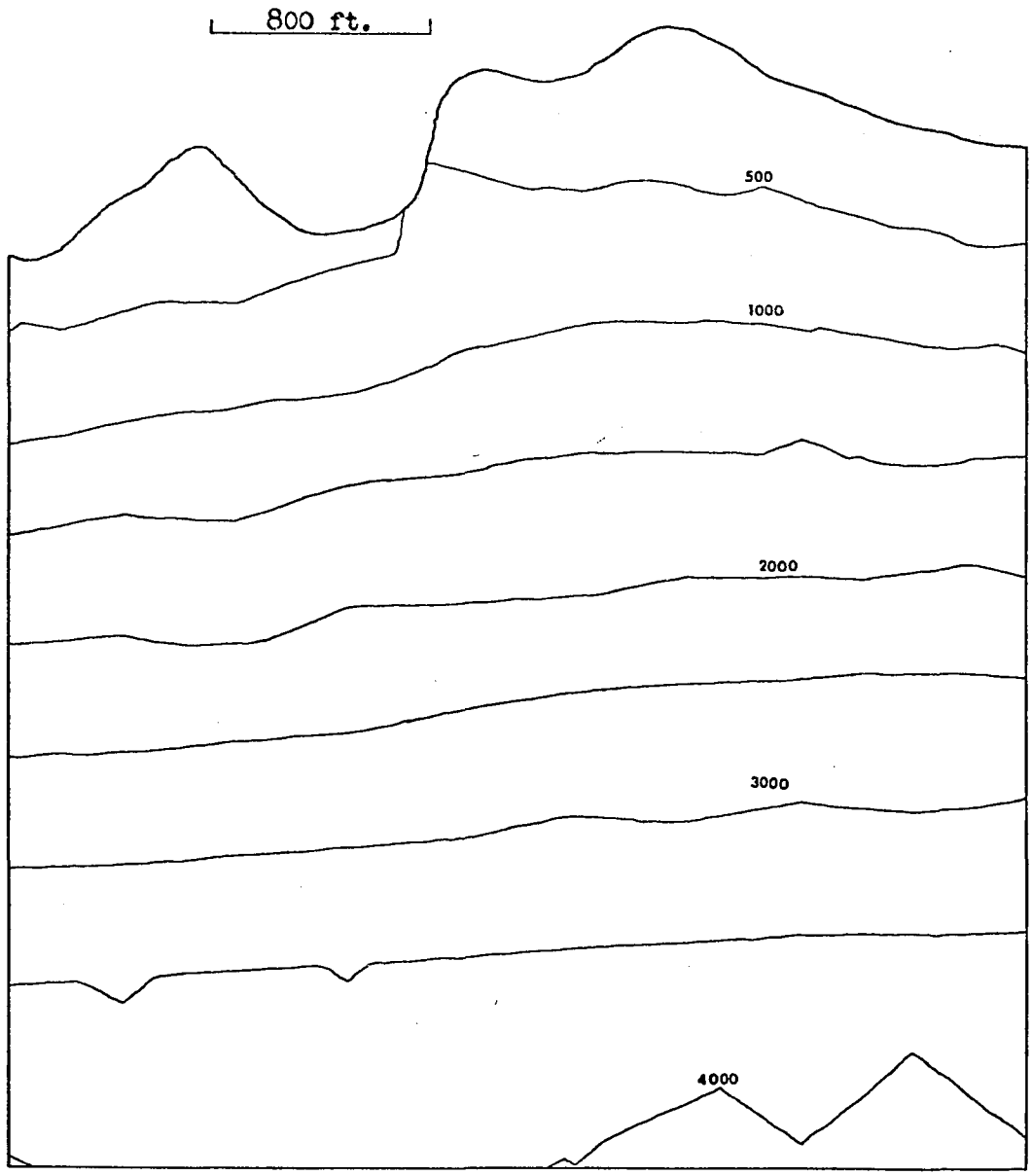

Figure 7. Model 1, Maximum Principal Stress Contours, Pre-Excavation

Contour Interval = 500 psi

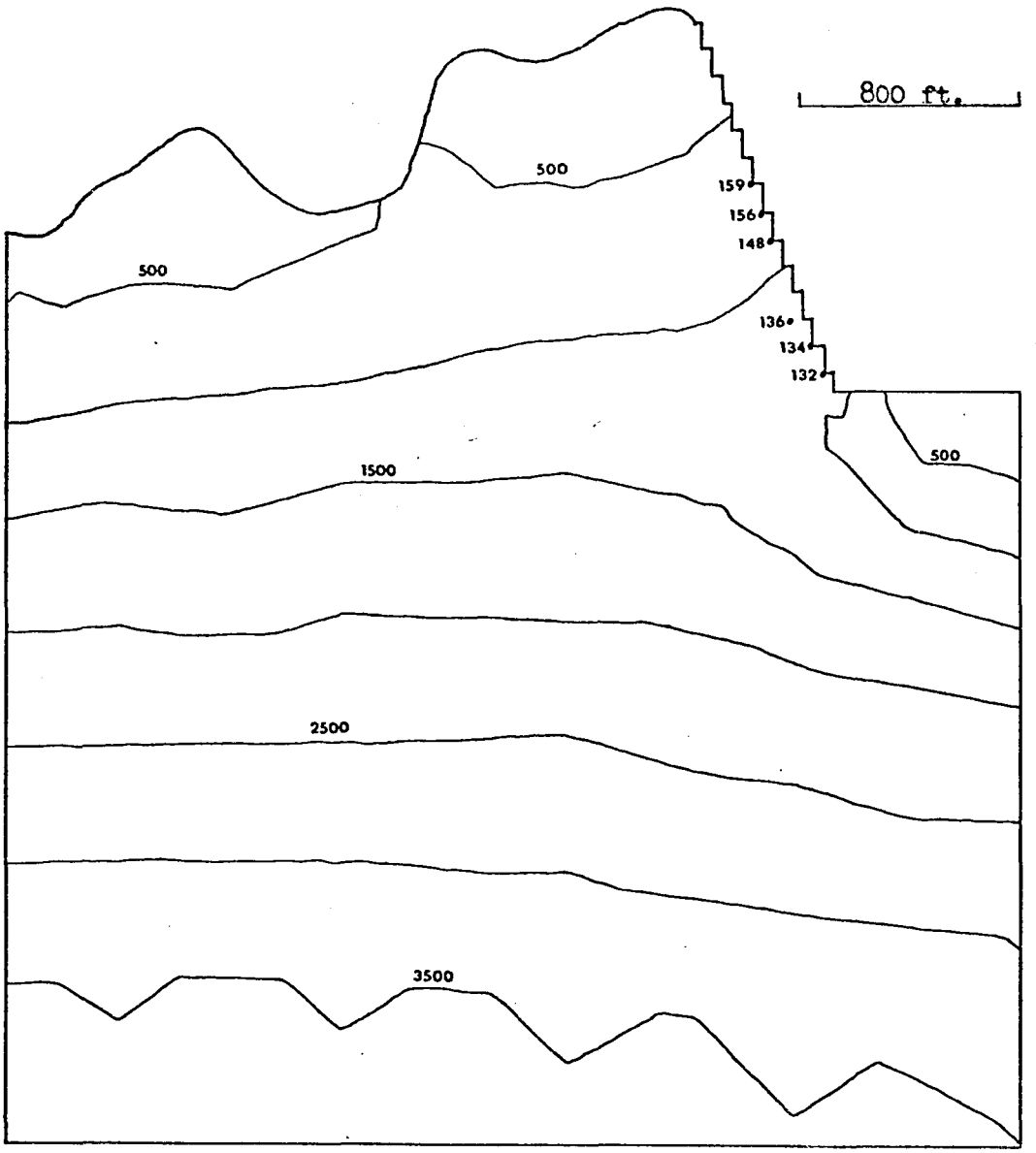

Figure 8. Model 1, Maximum Principal Stress Contours, Post-Excavation

Contour Interval = 500 psi

points (Table 6). However, the stress magnitudes, 1100-1400 psi, were higher at this greater depth. Higher stress magnitudes were expected, though, as a normal result of gravity loading.

Model 2: Rock Types Differentiated, Gravity Loading

At One-Half the Pit Depth. Model 2 (Figures 9 and 10) had a small increase in stress resulting from excavation. The percent increase was the same as for Model 1. Models 1 and 2 stress magnitudes for pre-excavation and post-excavation conditions were almost identical.

At the Toe of the Pit Slope. There was a smaller increase, percentage-wise, at the toe of the pit slope than at one-half the pit depth after excavation. Stress magnitudes for pre-excavation and post-excavation conditions and the percent increase after excavation were essentially identical for Models 1 and 2. Again, as in Model 1, stress magnitudes were higher at the toe than at one-half the pit depth in Model 2.

Observations. Models 1 and 2 had essentially the same stress distribution for both pre-excavation and post-excavation conditions. Very little difference was expected, because the techniques used for modeling the geologic conditions for both of these models were nearly identical as was previously described in Chapter 4.

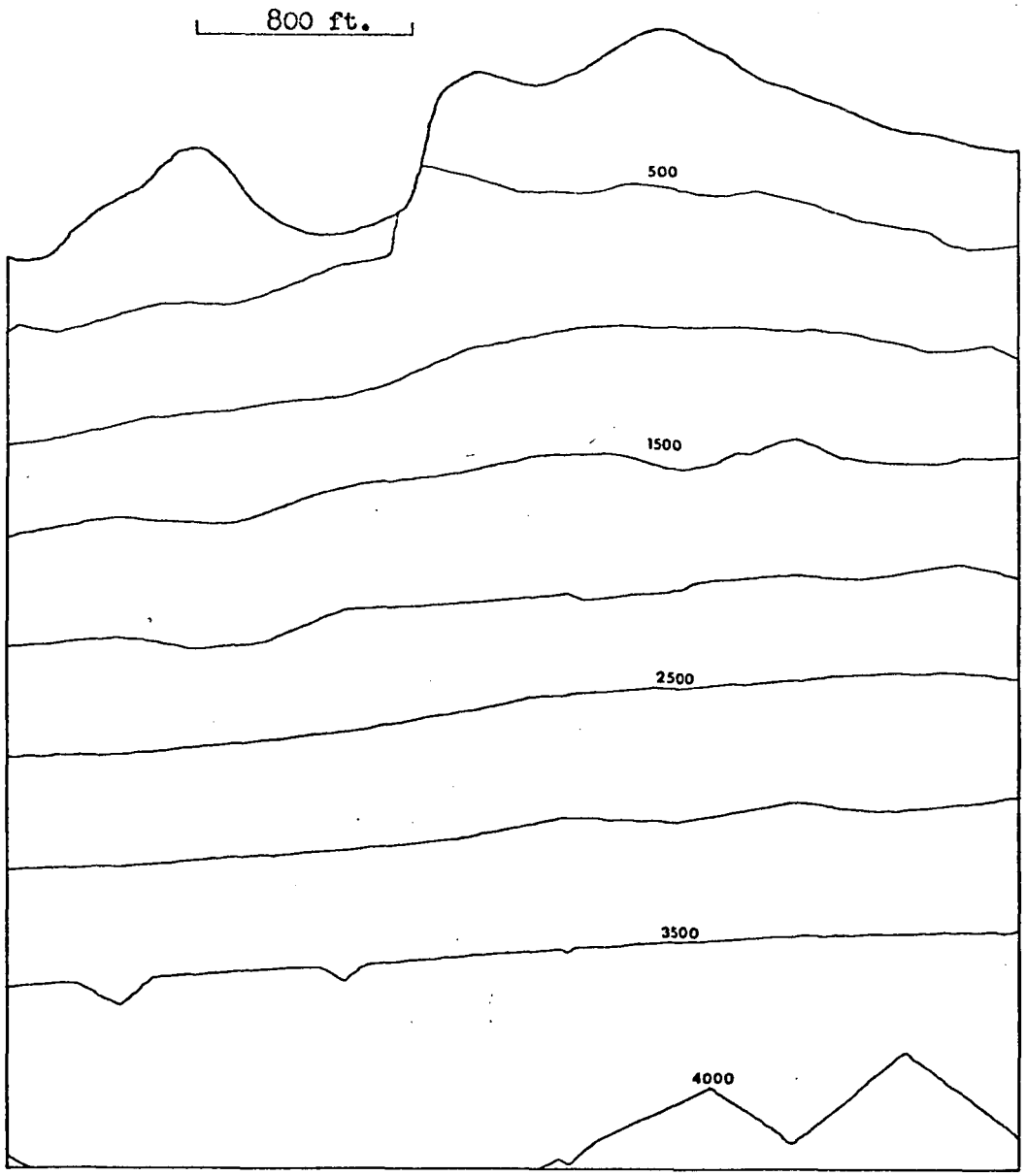

Figure 9. Model 2, Maximum Principal Stress Contours, Pre-Excavation

Contour Interval = 500 psi

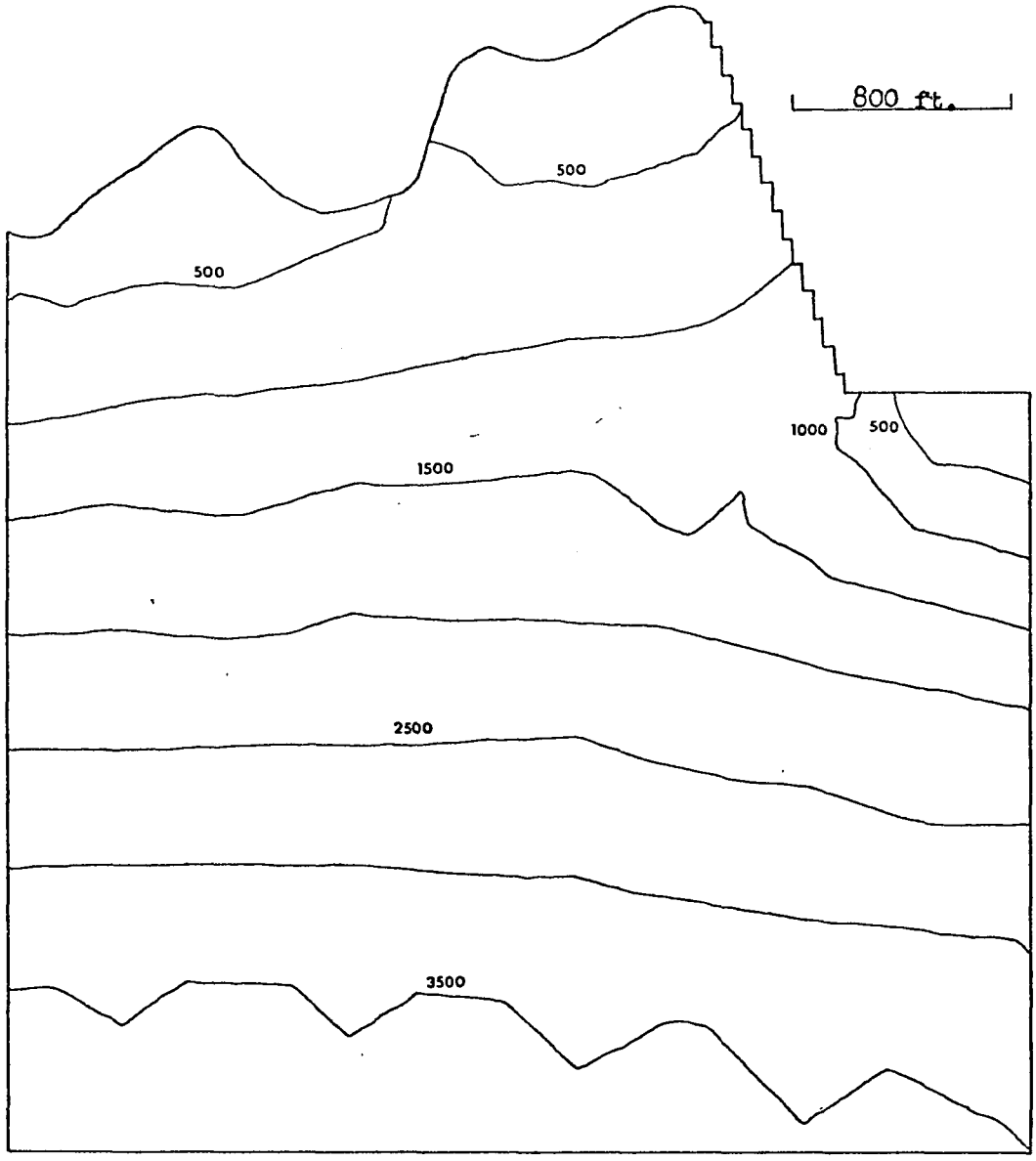

Figure 10. Model 2, Maximum Principal Stress Contours, Post-Excavation

Contour Interval = 500 psi

Model 3: Modified Element Parameters, Gravity Loading

At One-Half the Pit Depth. Model 3 (Figures 11 and 12) had a relatively small increase in stress due to excavation: 17%, 27% and 36% at nodal points 148, 156 and 159. The percent increase was only slightly higher for Model 3 than for Models 1 and 2 at nodal points 156 and 159. Stress magnitudes for Model 3 were slightly (4% to 8%) lower for both pre-excavation and post-excavation conditions than in the two previous models.

At the Toe of the Pit Slope. As in the two previous models, stress magnitudes were higher at the toe of the slope than at one-half the pit depth in Model 3. There was a smaller increase, percentage-wise, at the toe of the slope (14%, 13% and 4%) than at a point at one-half of the pit depth (17%, 27% and 36%). Stress magnitudes for this model were slightly lower for both pre-excavation and post-excavation conditions than in Models 1 and 2.

Observations. Model 3 had a slightly different stress distribution than Models 1 and 2. The smaller stress magnitudes in Model 3 were probably due to a combination of a slight decrease in loading and extensive modification of element elastic parameters as previously described in Chapter 4.

Model 4: Joint Elements, Gravity Loading

At One-Half the Pit Depth. Joint elements were added to Model 4. This model (Figures 13 and 14) had an appreciable increase

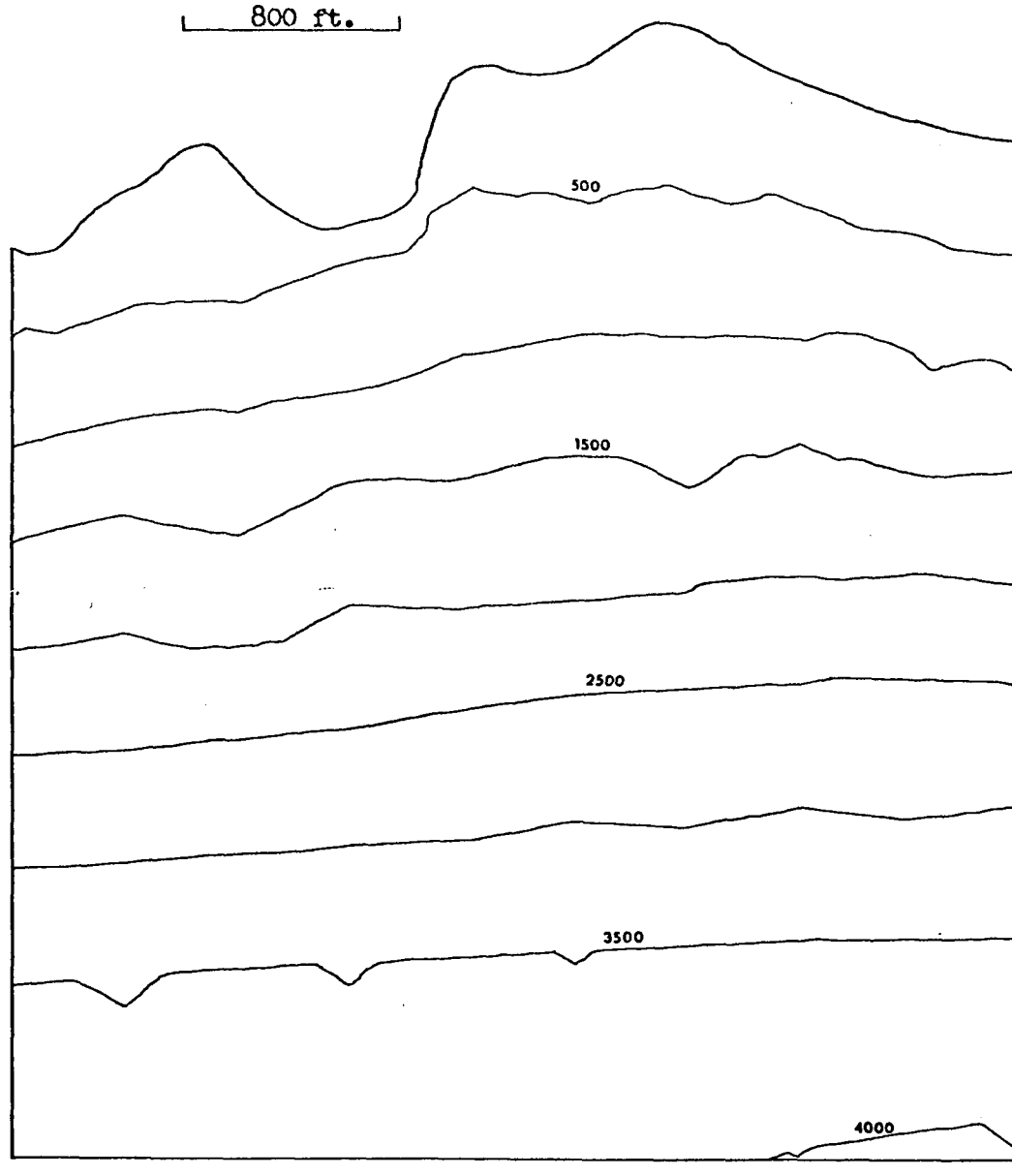

Figure 11. Model 3, Maximum Principal Stress Contours, Pre-Excavation

Contour Interval = 500 psi

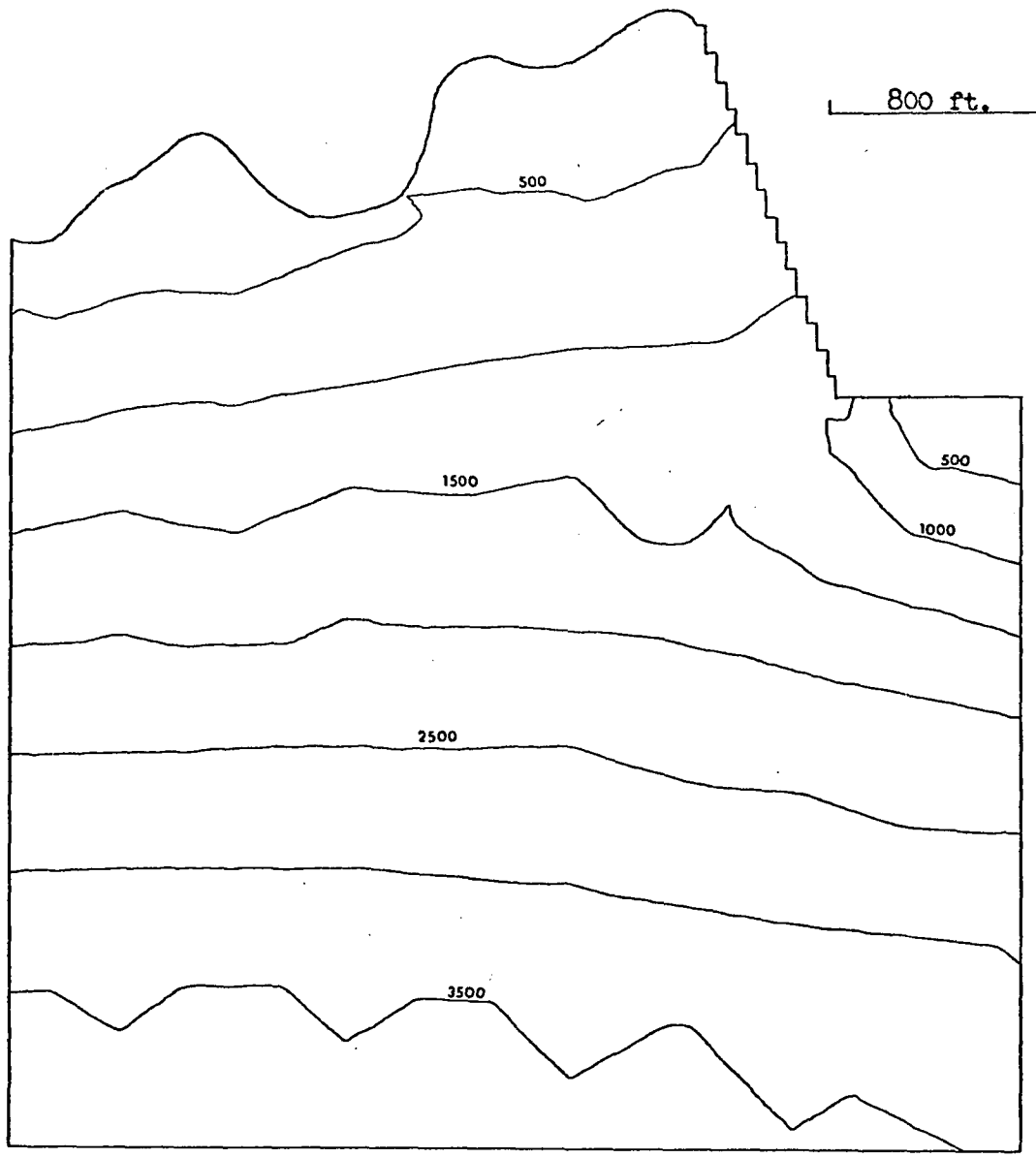

Figure 12. Model 3, Maximum Principal Stress Contours, Post-Excavation

Contour Interval = 500 psi

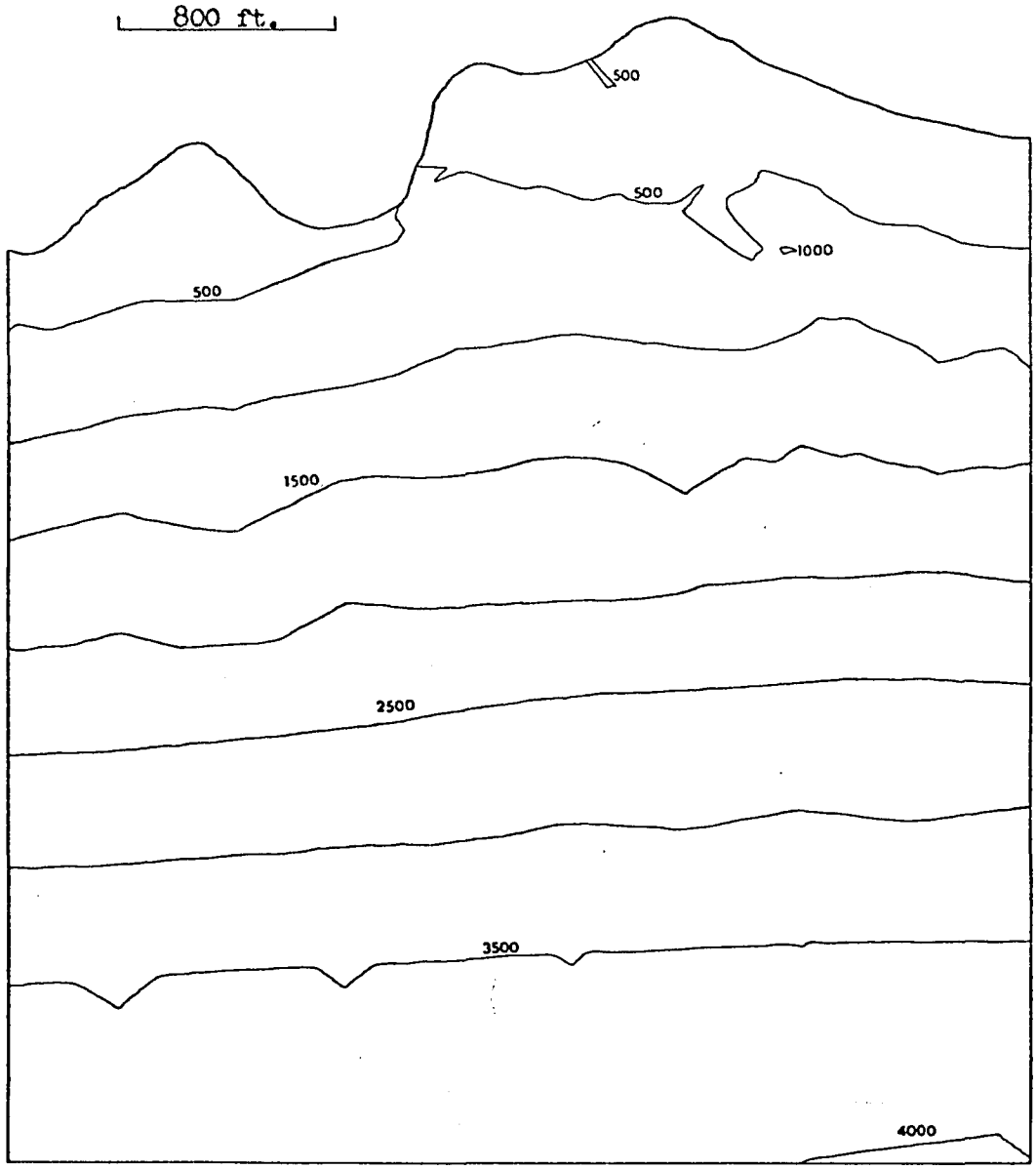

Figure 13. Model 4, Maximum Principal Stress Contours, Pre-Excavation

Contour Interval = 500 psi

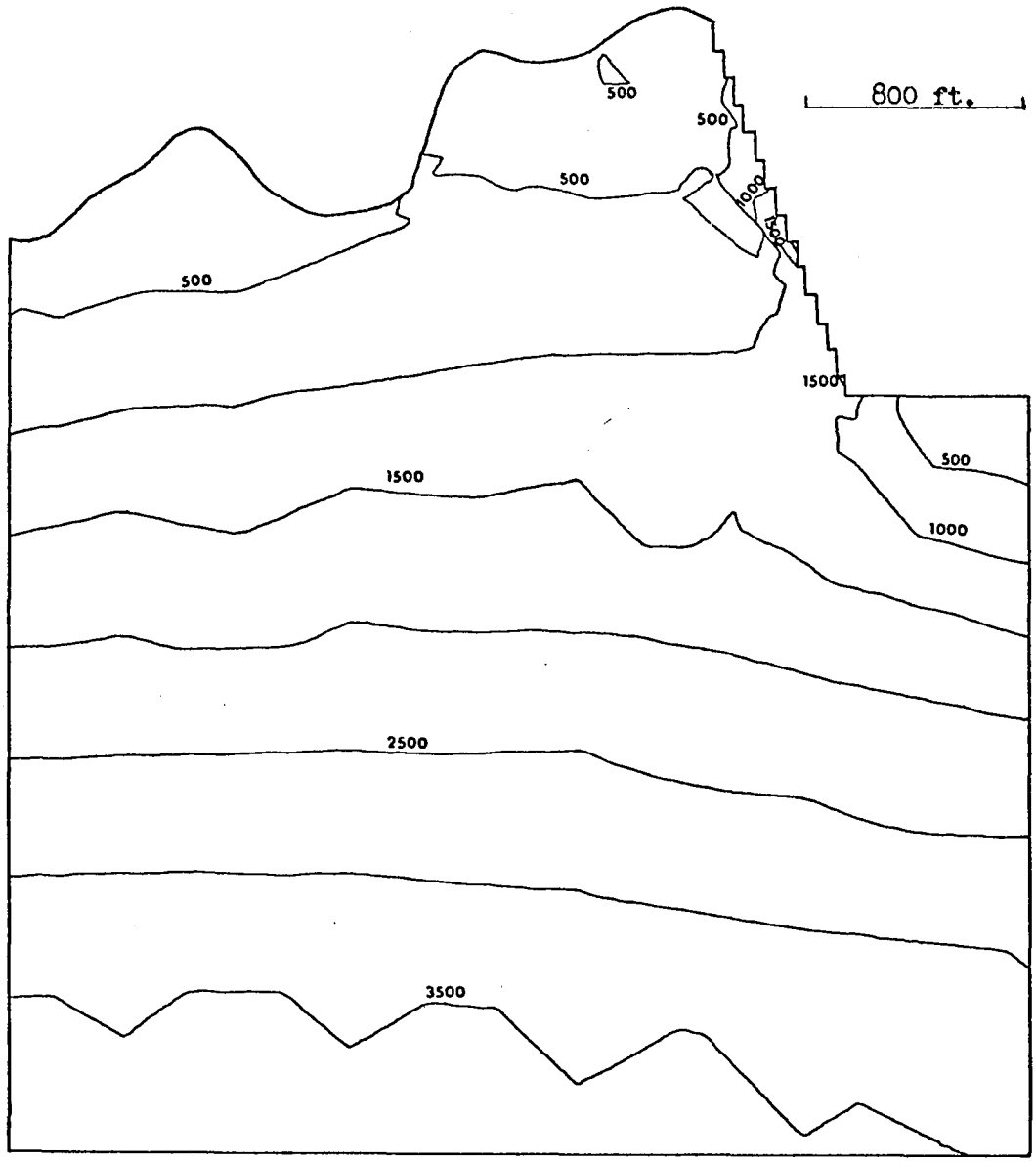

Figure 14. Model 4, Maximum Principal Stress Contours, Post-Excavation

Contour Interval = 500 psi

in stress due to excavation: 93%, 73% and 55%, respectively, at nodal points 148, 156 and 159. The increase in stress magnitudes from Models 1, 2 and 3 to Model 4 was approximately 30% to 100%. Also, there was a very large increase in the percent increase values, which were due to excavation, when comparing the three previous models with Model 4: from 17% to 93%, 26% to 73%, and 33% to 55% at the respective nodal points. Nodal points 148, 156 and 159 were located near the pit face in the vicinity of the joint elements. Therefore, these nodal points were probably undergoing additional stress build-up due to excavation and due to the relief of stress at the adjacent joint element nodal points.

At the Toe of the Pit Slope. There were relatively small stress increases due to excavation for Model 4 at the toe of the slope: 17%, 19% and 10%, respectively, at nodal points 132, 134 and 136. There was only a small change in the percent increase values (Table 5) from Models 1, 2 and 3 to Model 4: from 15% to 17%, 14% to 19%, and 4% to 10% at the respective nodal points. There was, essentially, no change in stress magnitudes at the toe of the slope from the three previous models to Model 4. The addition of joint elements did not appear to have much influence on increasing stress magnitudes prior to or after excavation or changing the percent increase values after excavation for the toe area. This was probably a result of the joint elements not being located near the toe of the slope and, therefore, not having much, if any, influence on stress changes at the toe.

Observations. As is illustrated by Figures 13 and 14, the stress distribution in Model 4 was modified considerably from the stress distribution in Models 1, 2 and 3 as a result of including modeled joints. Stress contour shapes tended to conform to the joint element outlines. Post-excavation stress magnitudes increased considerably in areas where modeled joints were in close proximity to the pit face.

Model 5: Joint Elements, Tectonic and Gravity Loading

At One-Half the Pit Depth. Residual tectonic stresses (higher horizontal than vertical stress) were added to gravity stresses in Model 5 (Figures 15 and 16). Pre-excavation and post-excavation stresses were increased by approximately 300% to 400% at a point at one-half the pit depth in this model over stresses that resulted in Model 4 at the same point. The percent increase in stress due to excavation in Model 5 was quite large: 95%, 75% and 51%, respectively, at nodal points 148, 156 and 159. However, there was not much of a difference in percent increase values, which are due to excavation, for Models 4 and 5: from 93% to 95%, 73% to 75%, and 55% to 51% at nodal points 148, 156 and 159. Therefore, it appears that at points at about one-half the pit depth, the addition of residual tectonic stresses to gravity stresses resulted primarily in an increase in stress magnitudes both prior to and after excavation.

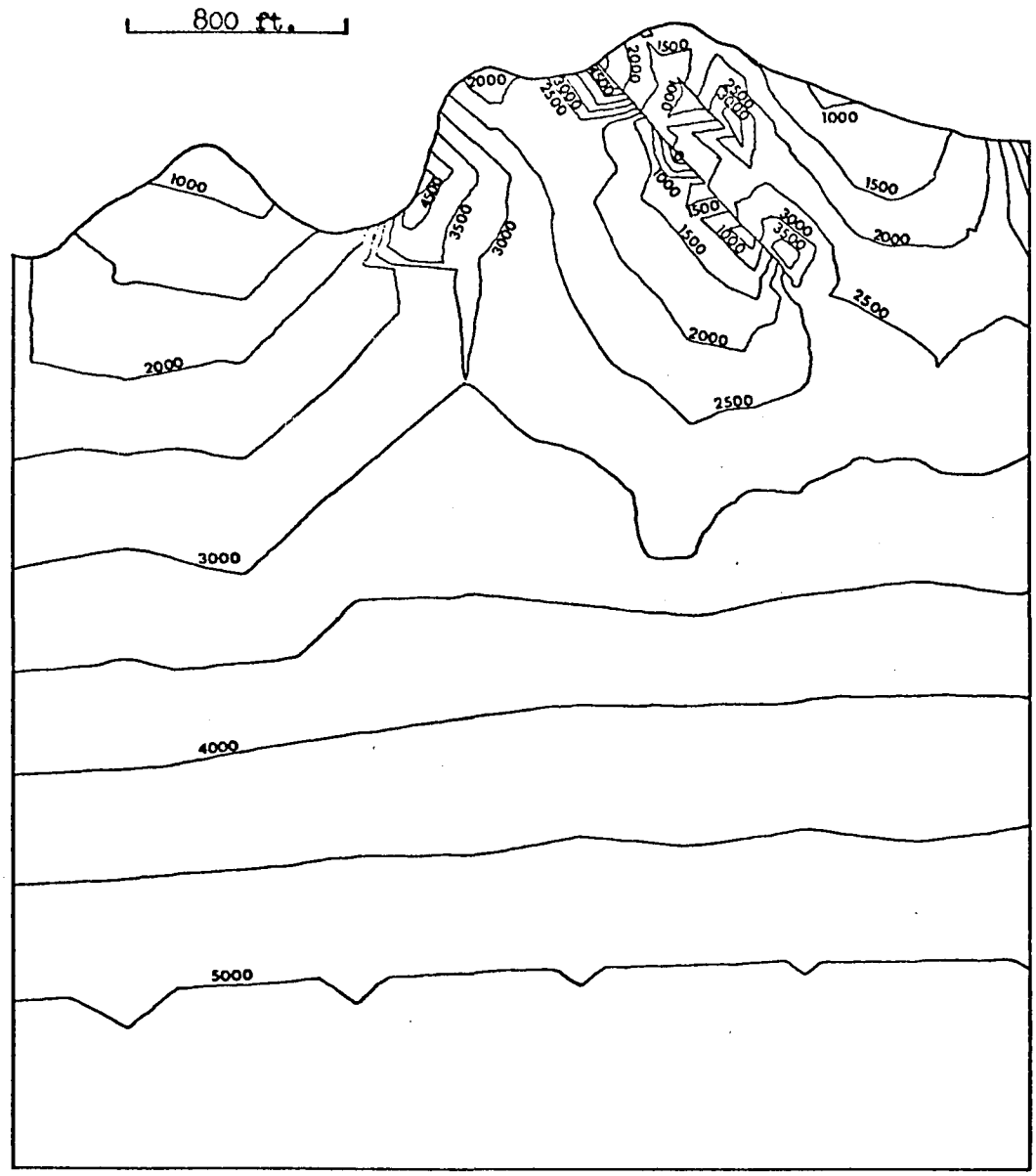

Figure 15. Model 5, Maximum Principal Stress Contours, Pre-Excavation

Contour Interval = 500 psi

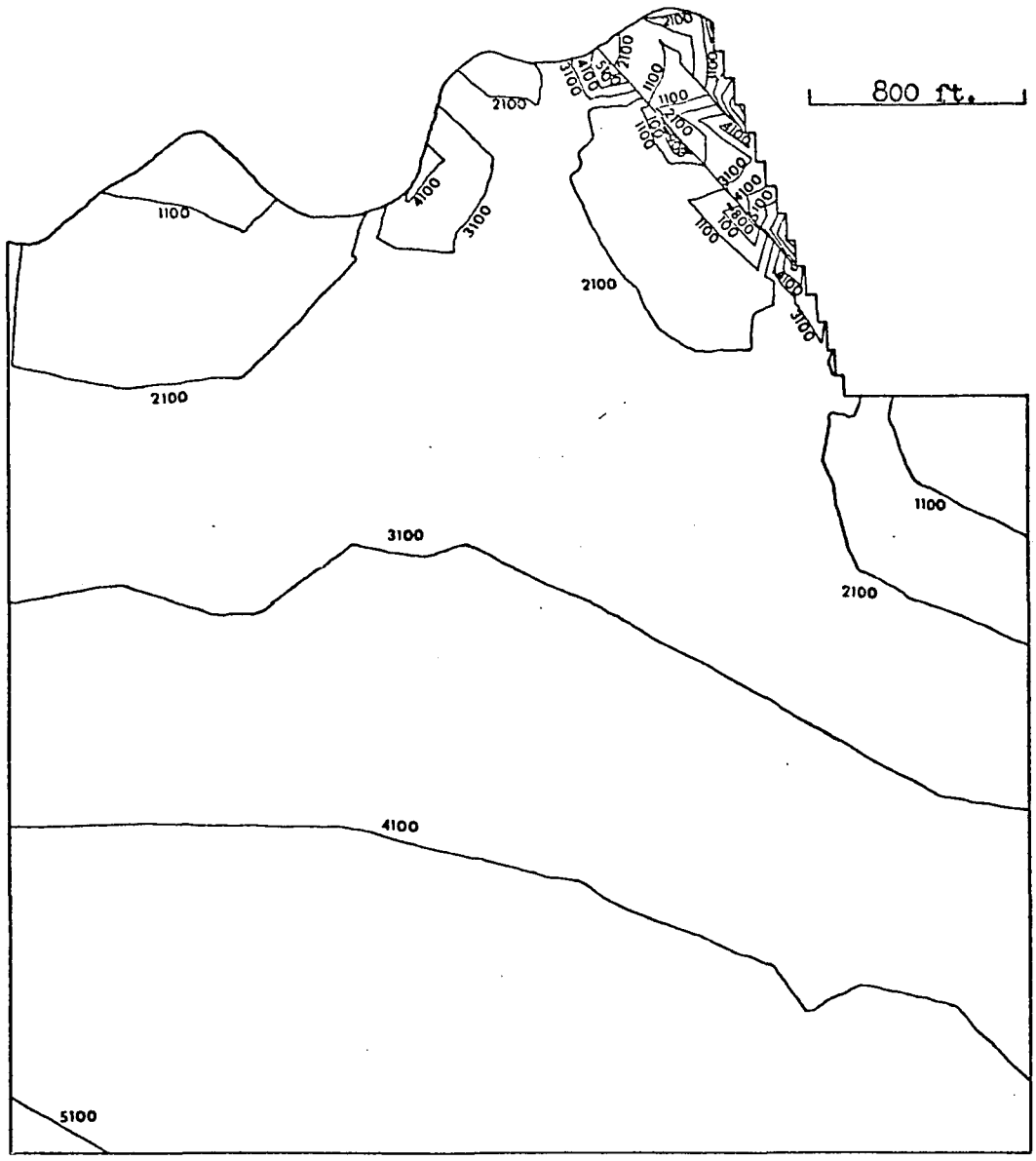

Figure 16. Model 5, Maximum Principal Stress Contours, Post-Excavation

Contour Interval = 1000 psi, negative stress equals tension

At the Toe of the Pit Slope. Pre-excavation and post-excavation stress magnitudes at the toe of the slope in Model 5 increased by approximately 200% over values from the previous four models. However, the percent increase after excavation was relatively small: 15%, 17% and 14%, respectively, at nodal points 132, 134 and 136. The percent change from the four previous models to Model 5 was small also: from 17% to 15%, 19% to 17%, and 10% to 14% at the respective nodal points. The same general effect was noted at the toe of the slope as at a point at one-half the pit depth: addition of residual tectonic stresses to gravity stresses resulted in an increase in stress magnitudes for pre-excavation and post-excavation conditions. A similar result was noted by Blake (1967 and 1968) and Duncan and Dunlop (1969). They discovered that the addition of an arbitrarily determined horizontal stress to gravity stresses resulted in larger stress magnitudes at the toe of a slope.

Observations. As is apparent in Figures 15 and 16, the stress distribution was quite different for Model 5 than for the previous four models. Pre-excavation and post-excavation stress magnitudes were appreciably increased as a result of including both tectonic loading and gravity loading. Stress magnitudes were particularly high near joint elements. It appears that joint elements, in conjunction with large loading magnitudes, tend to localize high stresses both before and after excavation.

Conclusions

There are approximately the same stress changes in Models 1, 2 and 3. The slightly smaller stress magnitudes in Model 3 are probably a result of a small decrease in model loading and modification of element elastic parameters. As a result of modeling joints, two effects are noted: (1) stress contours are modified extensively in the vicinity of joint elements to conform to the boundaries of the modeled joints and (2) post-excavation stress magnitudes increase considerably in areas where modeled joints were adjacent to the excavation. Two results are noted due to model loading with a combination of tectonic (higher horizontal than vertical stress) and gravity loads, both prior to and after excavation: (1) stress magnitudes are much larger than with only gravity loading and (2) stress magnitudes are very high near joint elements.

Excavation Displacement

The justification for the determination of displacement due to excavation was discussed in detail in Chapter 4. Excavation displacements are values which could be expected due to linear elastic rebound of the open-pit as a result of the act of excavation (mining).

Figures 17, 18, 19, 20 and 21 are, respectively, representations of resultant excavation displacements for Models 1, 2, 3, 4 and 5. The resultant vectors of excavation displacement are indicated by arrows at selected nodal points along the pit face and pit floor. These nodal points are numbered in the figures. The two continuous joints are shown in Figures 20 and 21 for Models 4 and 5.

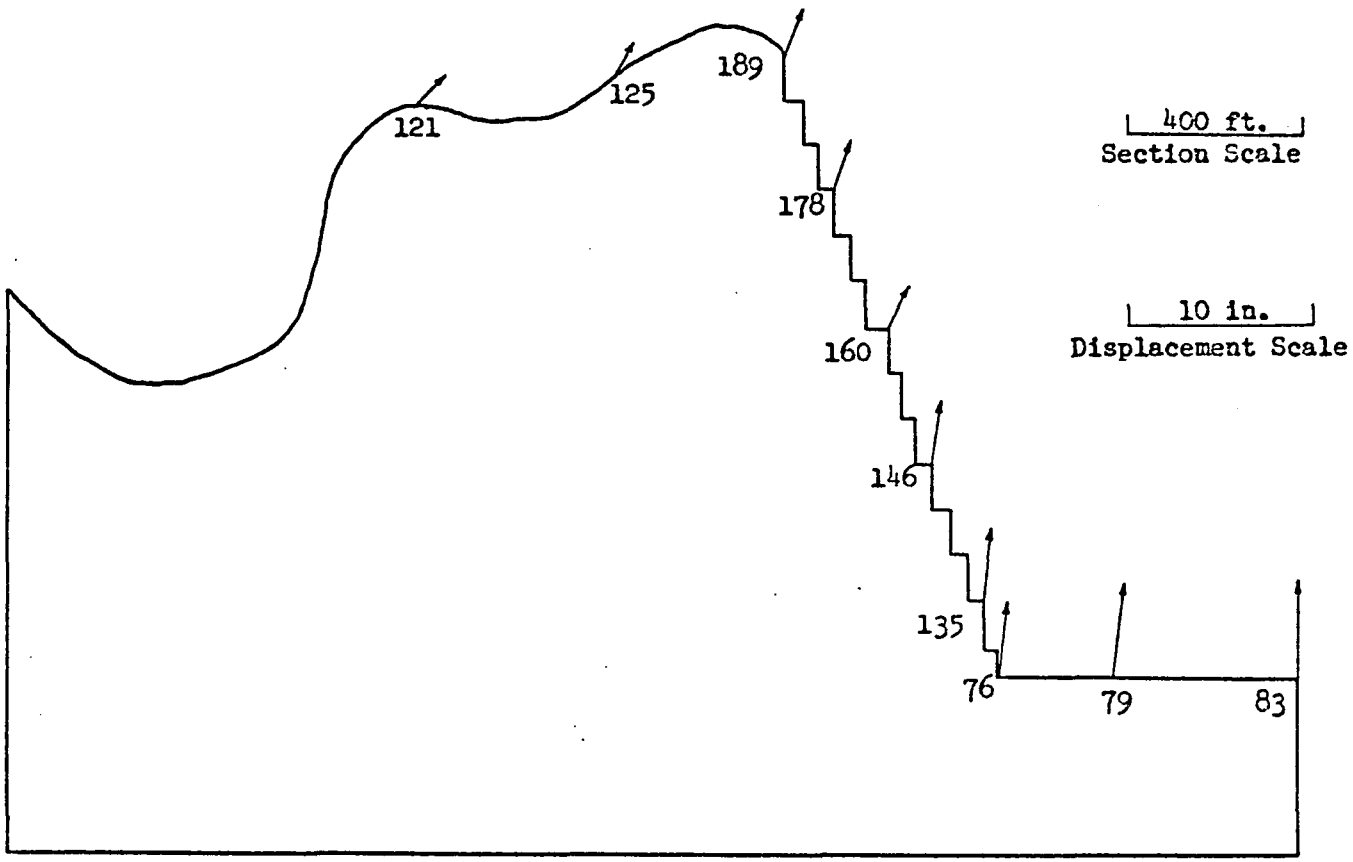

Figure 17. Model 1, Excavation Displacement

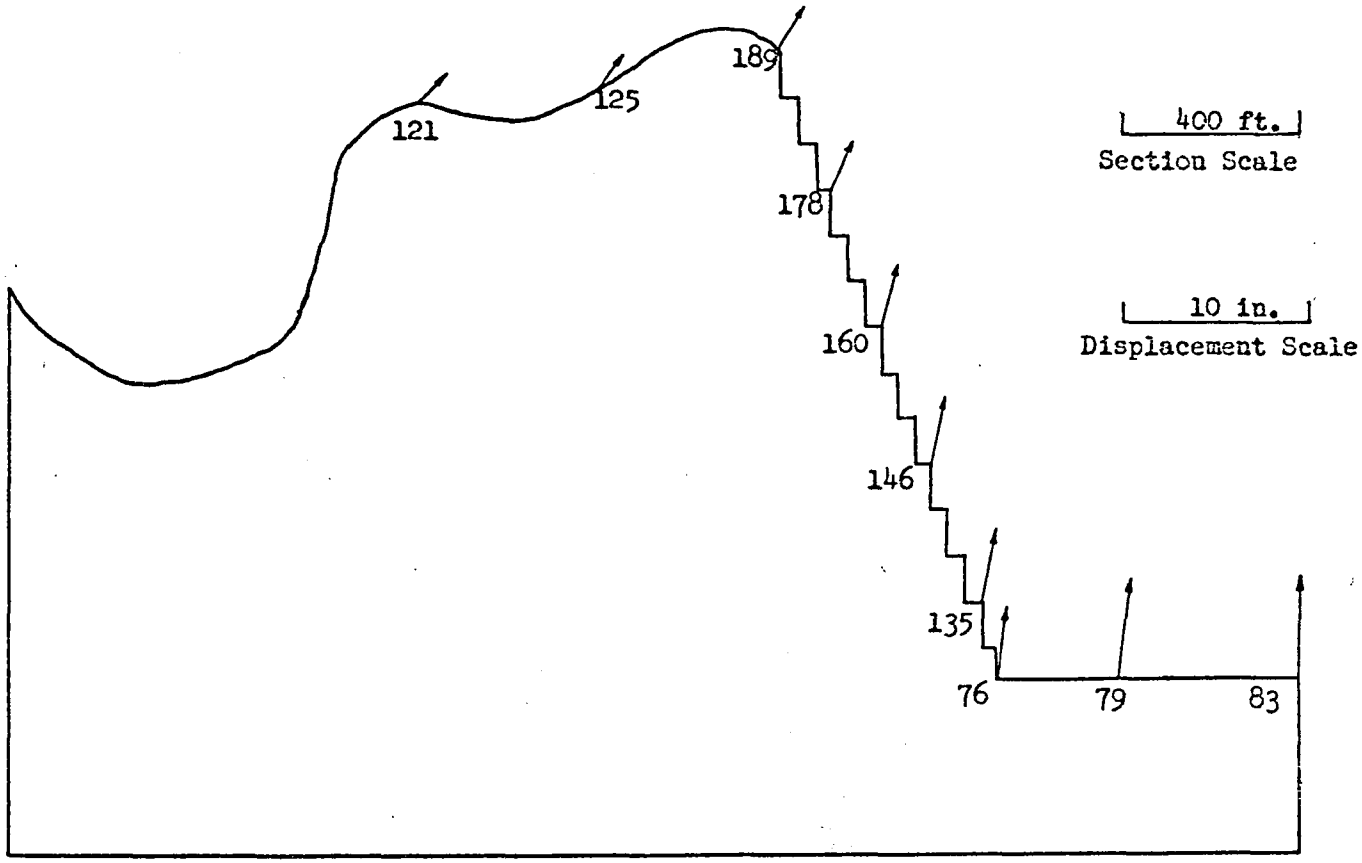

Figure 18. Model 2, Excavation Displacement

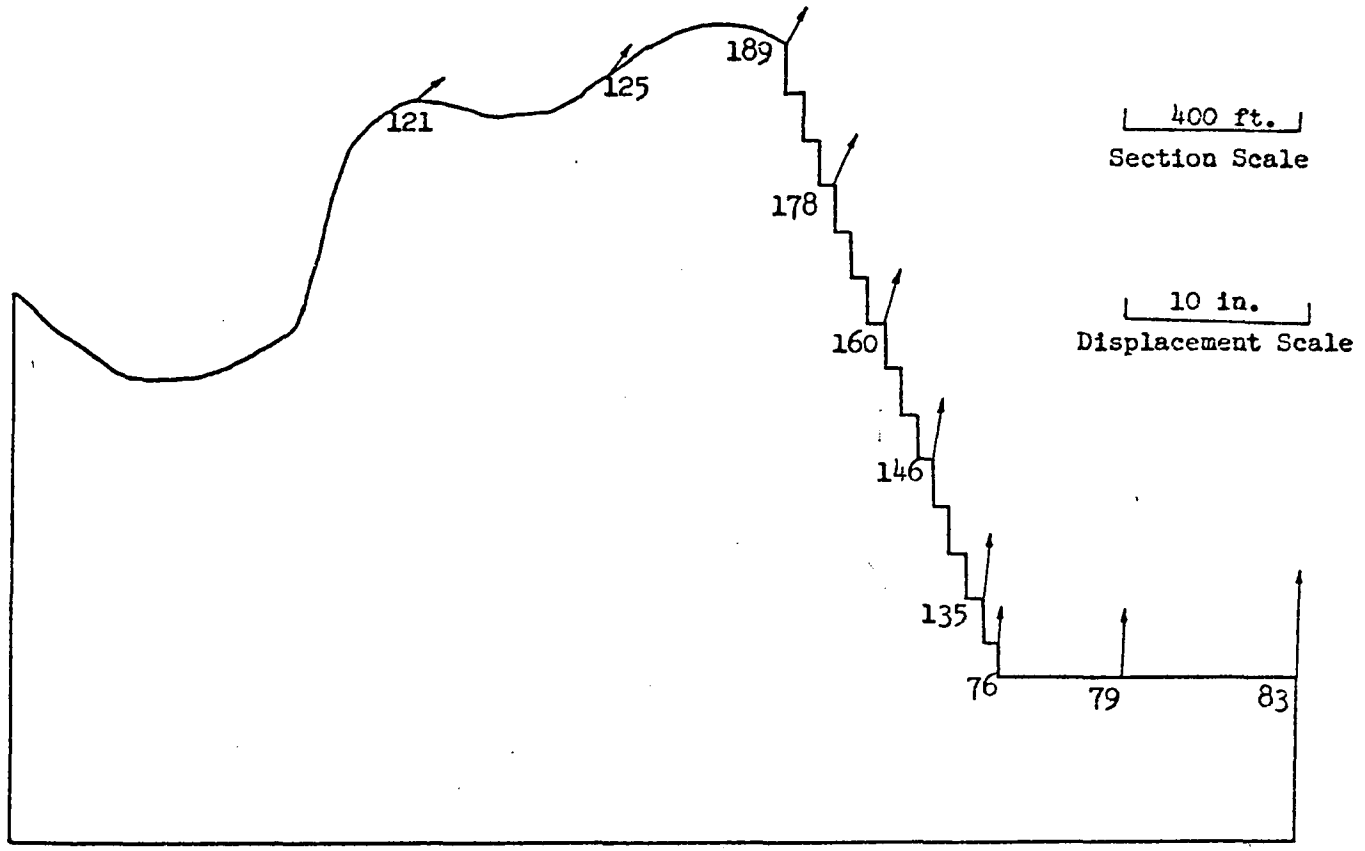

Figure 19. Model 3, Excavation Displacement

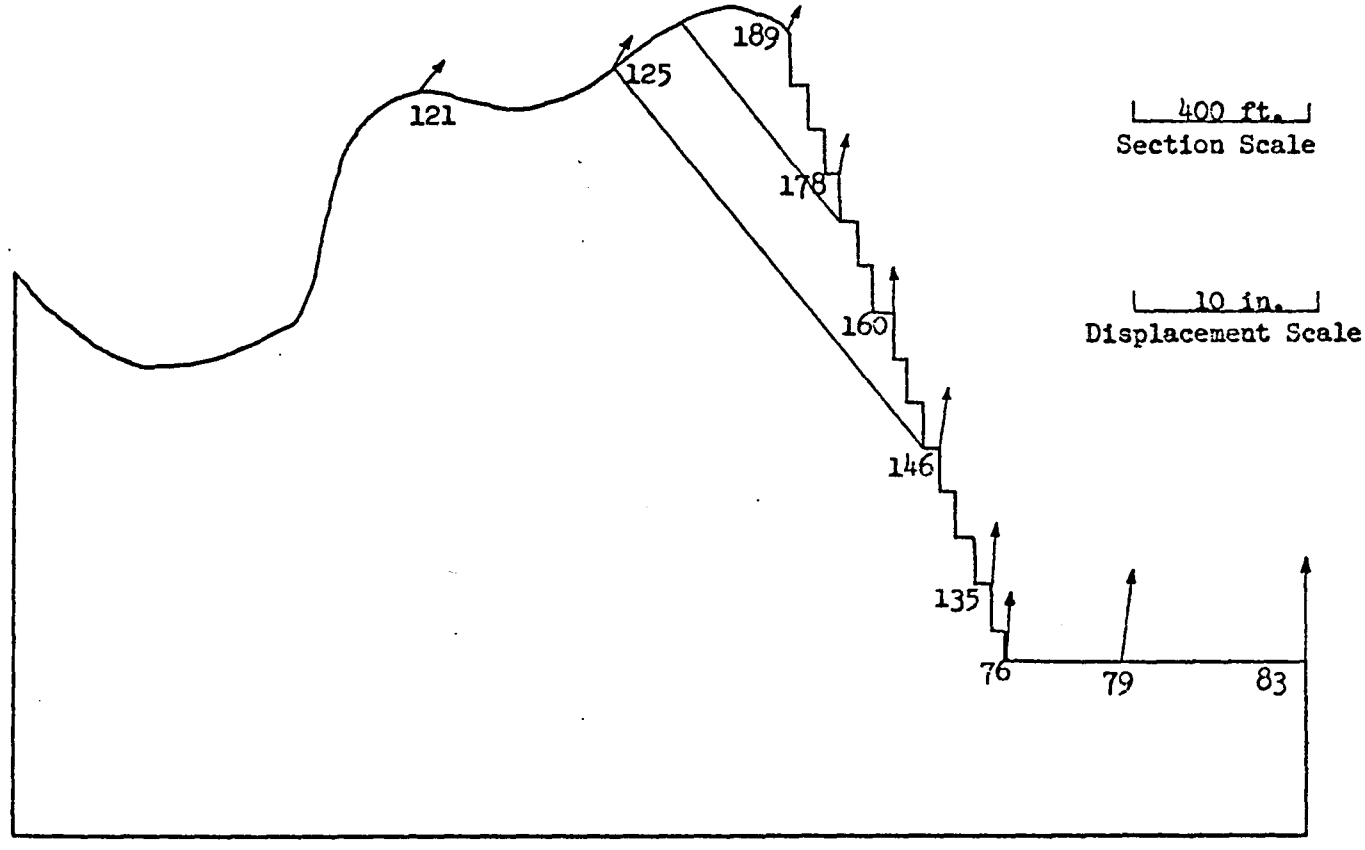

Figure 20. Model 4, Excavation Displacement

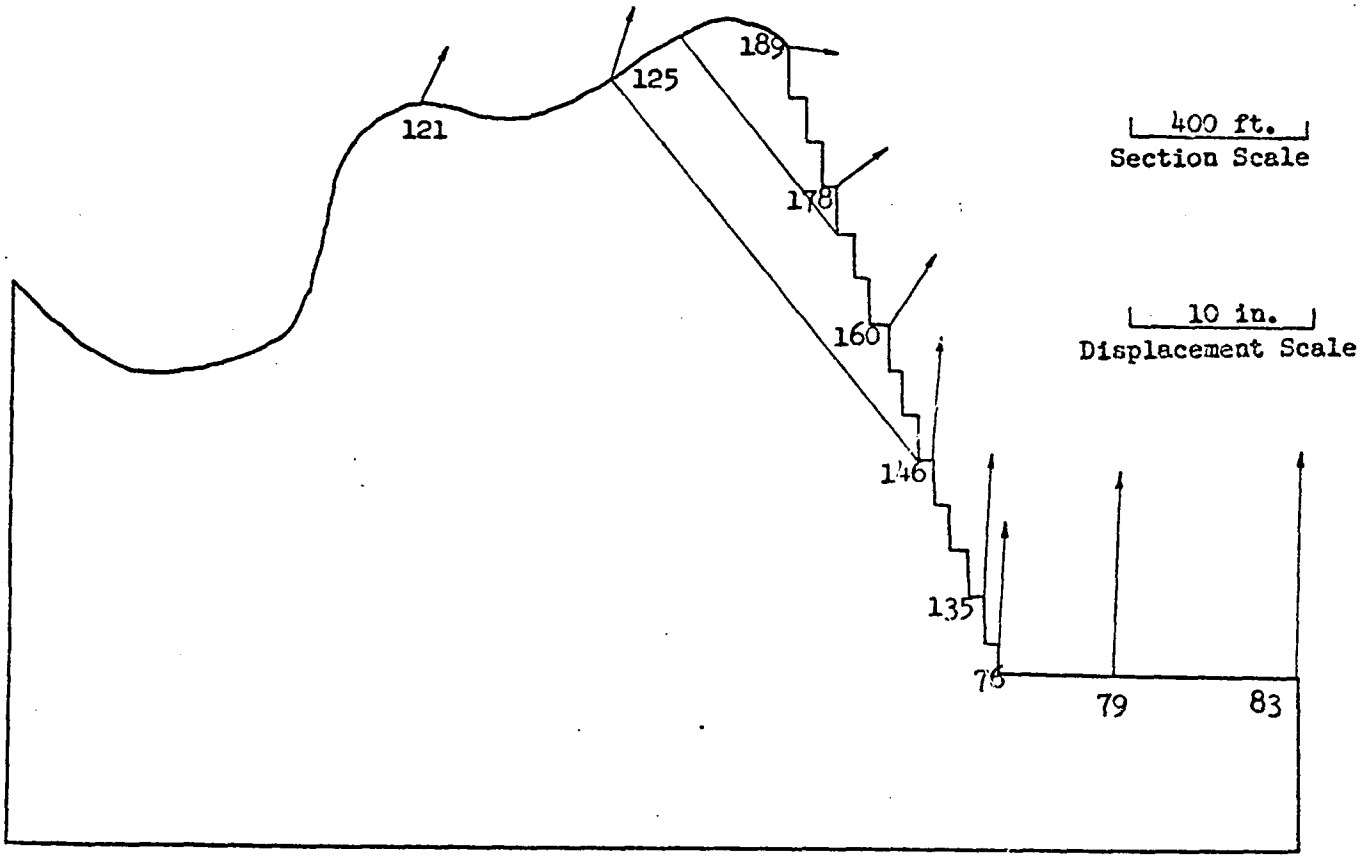

Figure 21. Model 5, Excavation Displacement

Table 7 lists the values of the X and Z components of the resultant excavation displacement vectors. The X component was horizontal and the Z component was vertical.

Excavation displacements were smaller in each model as the analyses progressed from Model 1 to Model 4. It appears that magnitudes of excavation displacement decrease with an increase in modification of model rock properties, which was an attempt to progressively improve the rock mass modeling. This effect was probably due to a decrease in loading and to the modification of elastic parameters. The gravity loads were lower in Models 2, 3 and 4 than they were in Model 1 because the unit weight was reduced in order to model the zone of oxidation and the five different rock types present. Elastic parameters were modified by utilizing the laboratory measured rock substance values of E and μ for Model 2 and by employing modified values of E and μ in Models 3 and 4 which more closely approximated the rock mass properties.

Model 4 utilized the same modified elastic properties in each element as Model 3. However, there was a slight decrease in excavation displacement values. Thirteen joint elements were added to Model 4. Therefore, the small decrease in Model 4 displacement may have been due to a decrease in the average model stiffness as a result of the much smaller E and higher μ of the joint elements. There were minor variations in X and Z displacements in comparison of Model 4 with Models 1, 2 and 3 for nodal points 189, 178 and 160. These variations in displacement were

Table 7. Excavation Displacements

Nodal Point	X-Displacement, inches Model 1	2	3	4	5	Z-Displacement, inches Model 1	2	3	4	5
121	1.57	1.57	1.40	1.20	1.41	1.46	1.44	1.33	1.35	3.17
125	1.58	1.58	1.41	1.16	1.19	2.08	2.06	1.92	1.88	4.11
189	1.20	1.21	1.11	0.59	2.98	2.34	2.35	2.15	1.10	-0.23
178	1.21	1.22	1.11	0.27	2.77	2.84	2.82	2.67	2.08	2.07
160	0.91	0.91	0.73	0.05	2.50	3.15	3.12	3.03	2.47	3.92
146	0.62	0.62	0.41	0.28	0.27	3.44	3.42	3.37	3.19	6.71
135	0.38	0.38	0.15	0.13	0.20	3.80	3.78	3.75	3.70	8.03
76	0.27	0.27	0.10	0.08	0.17	3.90	3.87	3.84	3.81	8.32
79	0.32	0.32	0.21	0.19	0.18	4.99	4.95	4.98	4.99	10.96
83	0	0	0	0	0	5.46	5.42	5.49	5.51	12.21

probably related to the proximity of these nodal points to the joint elements. They were located at and above the joint elements and, therefore, were probably influenced by these geologic discontinuities.

Model 5 had the same modified elastic properties in each element as Model 3 plus the same thirteen joint elements as Model 4. Residual tectonic loads were added to the gravity loads in Model 5, however. There was a two-fold increase in vertical displacement in Model 5, except in the elements above the modeled joints near the top of the pit face at nodal points 189, 178 and 160. This two-fold increase in displacement may have been due to the increase in the magnitude of applied (gravity plus tectonic) loads. Other variations in vertical and horizontal displacement were apparent in the areas above the modeled joints. There was greater horizontal displacement and less vertical displacement in this area in Model 5 than in Models 1, 2, 3 and 4. These effects were probably a result of this area being located within the apparent area of influence of the joint elements and a result of the change in horizontal to vertical stress ratio. In Models 1, 2, 3 and 4, which were subjected to gravity loading only, the mean horizontal to vertical stress ratio was approximately 0.2. In Model 5, which had gravity plus tectonic loading, the horizontal to vertical stress ratio was approximately 1.2 near the top of the pit and 0.4 near the bottom of the pit. Therefore, there was a much higher horizontal to vertical stress ratio in the area above the joint elements in Model 5 than in Models 1, 2, 3 and 4.

Vertical excavation displacement at the pit bottom was calculated to be 5 inches to $5\frac{1}{2}$ inches for Models 1, 2, 3 and 4, and 11 inches to 12 inches for Model 5. At one-half the pit depth at the open-pit mine face, vertical excavation displacement was determined to be $2\frac{1}{2}$ inches to $3\frac{1}{2}$ inches for Models 1, 2, 3 and 4, and 4 inches to $6\frac{1}{2}$ inches for Model 5.

Conclusions

Magnitudes of excavation displacement progressively decrease with the increasing modification (more correct in situ approximation) of model rock properties in Model 1 to Model 4. The areas above the modeled joints in Model 5 have smaller vertical displacements and much larger (250%) horizontal displacements than Models 1, 2, 3 and 4 in the same areas. The remainder of the areas in Model 5 have larger (220%) vertical displacements and smaller horizontal displacements than the previous four models. The larger horizontal displacements in the zone above the modeled joints would appear to be related to two factors: (1) high horizontal to vertical stress ratio in this area and (2) the attitude of the modeled joints and the small strength of the joint elements.

Failure Criteria

In order for the finite element models to be effective for open-pit slope stability analysis, they should yield information about the stability conditions which exist after excavation. The 755 Area pit models were examined for various modes of failure.

Post-excavation models were examined to ascertain if failure was likely to occur in tension, shear or compression. A yield analysis was performed for the joint elements to determine whether non-linear deformation of the joint filling material could be predicted. Joint elements were examined for shear failure which could indicate that sliding on the model joints was likely to occur.

Stress Exceeding Rock Mass Strength

If the stress in a model element exceeds the rock mass strength which was assigned to that element, then that element should fail. Compressive, shear and tensile post-excavation stresses were compared with assigned rock mass strengths for each element in all five finite element models. Table 8 shows the results of this comparison.

There were no predicted rock strength failures, in accordance with this failure criterion, in Models 1, 2, 3 and 4. Model 5 had a small number of elements in the minimum and maximum principal stress directions that had tensile and compressive stresses greater than modeled rock mass strengths. All of these were located within and adjacent to modeled joints near the pit face. The same four joint elements could be predicted to fail in tension in the maximum principal stress direction (Figure 16) as in the minimum principal stress direction. Two elements modeling rock adjacent to the pit face near the joints were predicted to fail in tension in the minimum principal stress direction. The same three joint elements were subject to compressive stress exceeding strength in

Table 8. Stress Exceeding Rock Mass Strength

Model and Stress Plot	Number of Elements with Stress Exceeding Strength		
	Tension	Shear	Compression
1	0	-	0
2	0	-	0
3	0	-	0
4	0	-	0
5 (minimum principal stress)	4 joint elements 2 elements near joint elements	-	3 joint elements
5 (maximum principal stress)	4 joint elements	-	3 joint elements 6 elements near joint elements
5 (maximum shear stress)	-	6 elements near joint elements	-

both the minimum principal stress direction and the maximum principal stress direction. Model 5 had a small zone at the pit face and above the lower modeled joint where shear stresses exceeded the modeled rock mass shear strength of six elements (Figure 35 in Appendix I).

Conclusions. Tensile, shear and compressive stresses are sufficiently high to exceed estimated element strengths in and adjacent to modeled joints located near the pit face in Model 5. Stresses are not high enough to exceed element strengths in Models 1, 2, 3 and 4. Therefore, according to the failure criterion being examined, stress exceeding rock mass strength, several elements in Model 5 are subject to failure and Models 1, 2, 3 and 4 contain no elements subject to failure.

No-Tension Analysis of Rock Mass

A jointed rock mass can not sustain tensile stresses acting on it because joints will open up releasing the tensile stress. Therefore, a stress analysis for jointed rock will be closer to the actual situation when tensile stresses are accounted for. This assumption is particularly applicable for highly jointed rock masses, similar to those at Cananea.

There are several methods of dealing with tensile values in a jointed rock mass. These are two of the most widely used: (1) eliminating the tensile stresses and (2) contouring the tensile zones.

The former method, which involves eliminating tensile stresses, is described by Zienkiewicz, Valliappan and King (1968). The basic steps in this technique are as follows:

1. Eliminate resultant tensile stresses.
2. Since equilibrium must be maintained, restraining forces are introduced and no point in the structure is allowed to be displaced.
3. The effect of the restraining forces is removed, since in fact they do not exist, by superposing equal and opposite forces at appropriate nodal points.
4. The structure is re-analyzed for tensile stresses. Computed stresses are added to those stresses occurring at the end of step 2.
5. If tensile stresses still occur, steps 1-4 are repeated until no tensile values exist or until they are reduced to negligible amounts.

The second method is simply to delineate the tensile zones by contouring or outlining these areas. Studies have shown (Zienkiewicz et al. 1968) that zones of tension which are delineated in this latter manner are approximately equivalent to zones obtained by the more elaborate technique of eliminating tensile stresses and redistributing resultant stress to maintain model equilibrium.

This second technique was used for no-tension analysis of the post-excavation pit walls in the five Cananea models. By outlining zones of tensile stress at the pit face, areas where pre-existing joints can open up were delineated. Joints near the pit face do not open instantaneously, but gradually, as excavation proceeds downward toward the final open-pit floor. These are areas where raveling should be expected on the pit walls.

There were no zones of tension in Models 1, 2 and 3. In Model 4, there were two tensile stress areas for stresses calculated in the minimum principal stress direction. Figure 22 shows the areas, outlined with dashed lines, where pre-existing joints were free to open up due to the presence of tensile stresses. One area was located at the third bench down from the top of the pit. This zone included a portion of the upper modeled joint, the third bench and the area between the two. The second area was located at the ninth bench downward from the top of the pit. This zone included a portion of the lower modeled joint, the ninth bench, the area between the two and an area below the modeled joint. There were no tensile stress areas near the pit walls for stresses calculated in the maximum principal stress direction.

The tensile stress areas for stress in the minimum principal stress direction in Model 5 are shown in Figure 23. Again, dashed lines outline areas of tensile stress where pre-existing joints were free to open up. One area was the first bench at the top of the pit. A second area was located at and between the modeled joints at the pit face. This large zone was composed of the pit wall area from the fifth bench down to and including the tenth bench, incorporating a portion of the lower modeled joint. The third tensile area was located at the top of the south wall of the smaller Colorada Pit.

Conclusions. Models 1, 2 and 3 contain no tensile stress zones. Models 4 and 5 contain isolated tensile stress areas in the

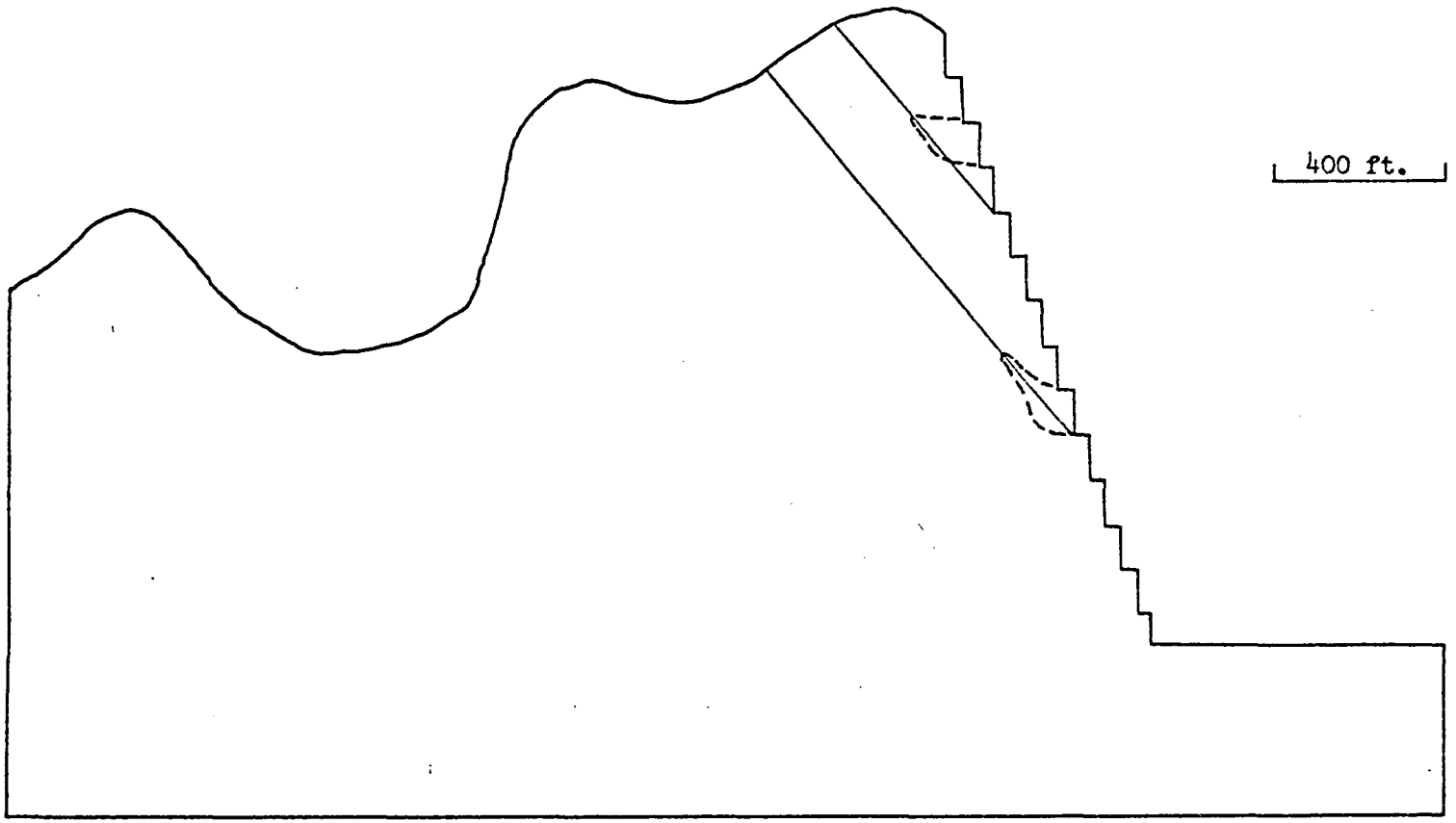

Figure 22. Model 4, Tension Zones Near Pit Face, Minimum Principal Stress Direction

Dashed areas outline tension zones.

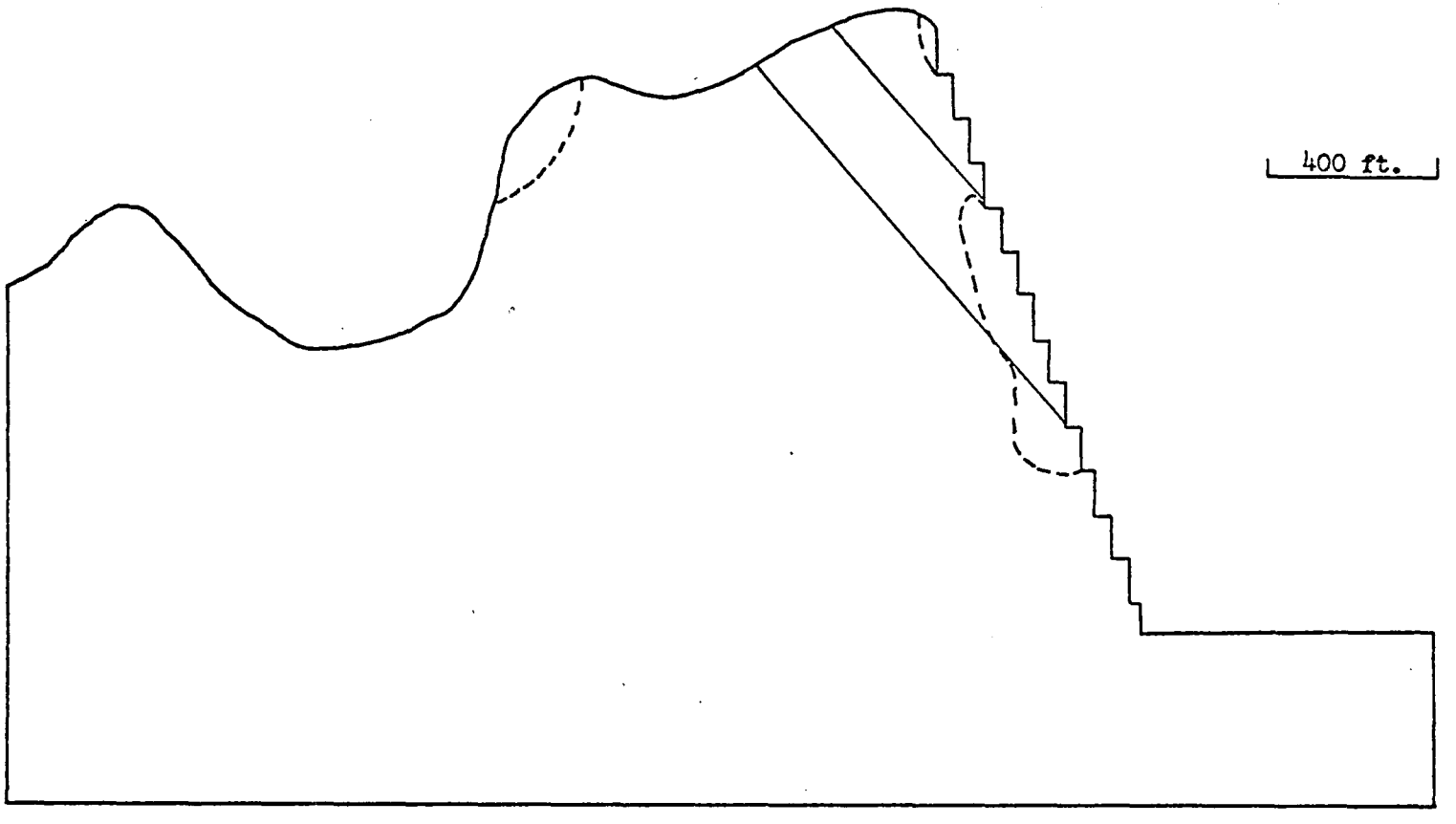

Figure 23. Model 5, Tension Zones Near Pit Face, Minimum Principal Stress Direction

Dashed areas outline tension zones.

minimum principal stress direction. Tensile stress areas at the pit wall are primarily localized near modeled joints in Models 4 and 5. There are, however, other tensile areas in the upper portion of Model 5 that were not located near modeled joints. Also, the tensile zones in Model 5 are somewhat larger than those in Model 4. These effects in Model 5 must be ascribed to the high horizontal to vertical stress ratio which is only present in Model 5, and which acts in the upper model area. The tensile zones in Models 4 and 5 are areas where pre-existing joints would be induced to open up by such stresses.

Yielding of Joint Elements

It was suspected that the stress-strain relationship for the clay gouge filled model joints might be non-linear. Therefore, a yield analysis was performed to determine if the modeled joints could be predicted to yield due to the loading and geometric configuration which would result upon excavation of the open-pit mine model. Mohr's shear strength theory was the criterion utilized for yield determination. Accordingly, yield would occur in a joint element if stress exceeded the assigned strength in shear. Joint elements were assigned values for elastic parameters such that the element stiffness would be low in order to approximate clay gouge material stiffness.

The following non-linear deformation approximation is similar to techniques described in more detail by Clough (1965a), Coates (1969b) and Zienkiewicz and Cheung (1967):

1. Determine if yielding occurs:

According to the Mohr shear strength theory (see Figure 24), at equilibrium:

$$\frac{\sigma_{max} + \sigma}{\sigma_{min} + \sigma} = \tan^2 (45^\circ + \phi/2)$$

where $$\sigma = \frac{c}{\tan \phi}$$

if

$$\frac{\sigma_{max} + \sigma}{\sigma_{min} + \sigma} > \tan^2 (45^\circ + \phi/2),$$

then yielding occurs. If no yield occurs, analysis of this finite element is terminated. If yielding has occurred, proceed to the next step. Figure 25 shows a bi-linear approximation of a curved stress-strain relationship. The dashed line represents the non-linear stress-strain curve. One of the straight line segments represents the pre-yielding state and the other represents the post-yielding state.

2. Calculate yield stress, σ_{yield}:

$$\sigma_{yield} = (\sigma_{min} + \sigma) \tan^2 (45^\circ + \phi/2) - \sigma$$

3. Calculate yield strain, ε_{yield}:

$$\varepsilon_{yield} = \frac{\sigma_{yield} - \mu(\sigma_{min} + \sigma_y)}{E_p}$$

where E_p = the pre-yield modulus

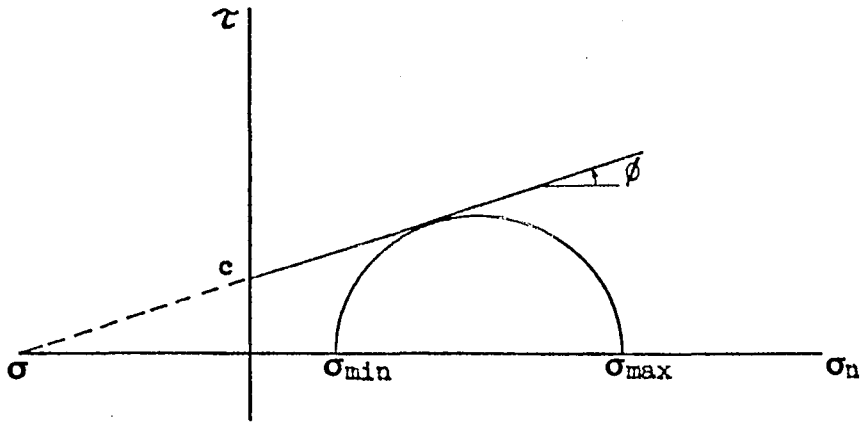

Figure 24. Mohr Diagram

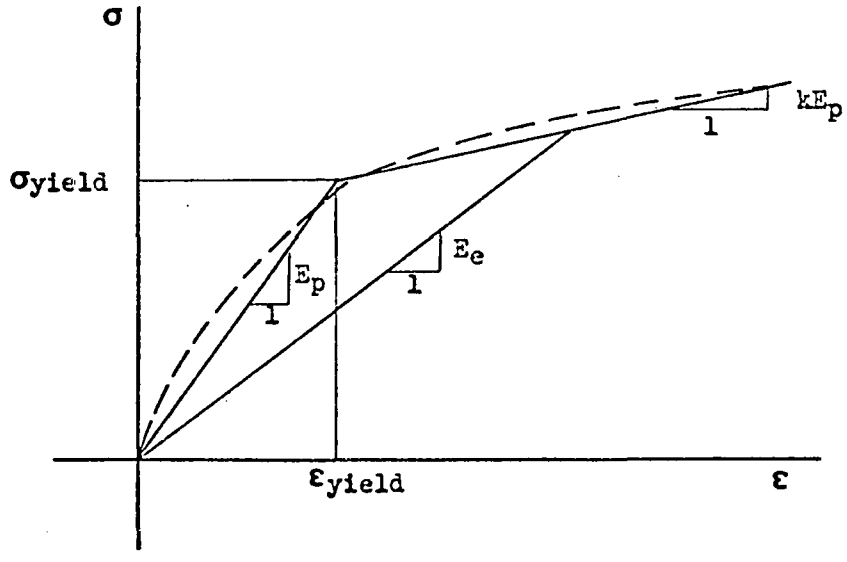

Figure 25. Bi-Linear Approximation of a Curved Stress-Strain Relationship

4. Determine the effective (secant) modulus, E_e:

$$E_e = kE_p + \frac{\sigma_{yield}\ (1-k)}{\varepsilon_{yield}}$$

where kE_p = the post-yield modulus

5. Re-run the finite element analysis using the new modulus, E_e, for the elements which previously yielded.

6. Perform steps 1 to 4. Examine the new effective modulus, E_e. When the new E_e equals the previous $E_e \pm$ an acceptable tolerance, convergence occurs and the final effective modulus, E_e, has been obtained.

The two continuous modeled joints that were introduced into Models 4 and 5 contained thirteen joint elements. Upon applying the above yield analysis, yielding occurred in eleven of the thirteen joint elements. The two elements that did not yield were those that were located at the top of the slope at the uppermost ends of the modeled joints. All joint elements that were located nearer the pit wall yielded. Convergence resulted, an effective modulus for the clay gouge joint filling material was obtained and yielding ceased after four iterations of the non-linear deformation approximation.

Conclusions. Non-linear deformation (yielding) would be anticipated for the modeled joints after excavation for the joint filling material parameters that were assigned. All joint elements near the final pit wall would be expected to undergo non-linear deformation.

Sliding on Joints

An analysis was performed to determine if incipient sliding occurred on the modeled joints. This analysis takes into account the joint attitude, whereas, the yield analysis in the preceding section did not. In this analysis (Duncan and Goodman 1968), the shear stress and the shear strength parallel to the joint plane were compared.

The shear strength along a joint plane was determined in accordance with the Mohr-Coulomb failure criterion:

$$\tau_s = c + \sigma_n \tan \phi$$

where

τ_s = shear strength along the joint plane

σ_n = normal stress on the joint plane

c and ϕ are, respectively, cohesion and internal angle of friction along the joint plane.

The normal stress on the joint, for the plane strain condition, is,

$$\sigma_n = \sigma_x \cos^2 A + \sigma_z \cos^2 B \qquad \text{Eq. 9}$$

where

σ_x, σ_z = stresses in the X- and Z-directions

A, B = angles between the normal to the joint plane and the X- and Z-axes

For the plane strain condition, the shear stress along the joint plane, τ, is,

$$\tau = \left[(\sigma_x \cos A)^2 + (\sigma_z \cos B)^2 - (\sigma_n)^2 \right]^{\frac{1}{2}}$$

The shear strength, τ_s, and the shear stress, τ, along the joint are then compared. If $\tau > \tau_s$, shear occurs within the joint at that point and sliding on the joint plane ensues.

The technique outlined above was used to test for the presence of sliding in each of the joint elements. This examination was performed for the same computer analyses as for the yielding analysis of the preceding section for comparison of results. "Sliding" and "yielding," as determined by these two techniques, should occur in the same joint elements in the same computer run if deformation was occurring.

Upon examination of the results, it was discovered that sliding occurred in the same eleven of thirteen joint elements in the first iteration as in the yield analysis. The only two joint elements that did not undergo sliding were again the two elements nearest the top of the model. The eleven joint elements nearer the pit wall experienced shear failure and, thus, sliding in the first iteration. Sliding occurred in the same joint elements in which yielding occurred in the yield analysis for each succeeding iteration. When the yield analysis converged and yielding ceased, sliding ceased, also.

Conclusions. Sliding occurs in the same eleven of thirteen joint elements, nearest the final pit wall, as in the yield analysis of the previous section. Agreement of results between these two

techniques was achieved. This should probably be expected, however, because both methods are based on Mohr's shear strength theory.

No-Tension Joints

The modeled joints in Models 4 and 5 were examined for the presence of tensile stresses. If natural joint surfaces are uncemented, they can not withstand tensile stresses of any magnitude. Models 4 and 5 modeled joints were assumed to be filled with clay gouge material and uncemented in order to simulate the worst possible joint stability condition.

Stresses normal to the joint plane were calculated and tested for negative values (tension) in all joint elements. Equation 9 was utilized in determining the normal stress, σ_n, on the joint surfaces. Results of this analysis showed that the same four joint elements, from the total thirteen, were in tension in both Models 4 and 5. One of the four elements in the upper modeled joint and three of the nine elements in the lower modeled joint were in tension. These four elements were located near the centers of the modeled joints approximately one-half of the way between the crown area of the slope and the final pit wall.

Conclusions. Four of the thirteen joint elements are subject to tensile stresses in both Model 4 and Model 5. Therefore, the joints should open up in tension in these areas for these two models. This condition must be viewed as a potentially dangerous slope condition and as contributing to potential slope instability.

CHAPTER 6

CONCLUSIONS

The goals of this analysis are, (1) determine the stability conditions of the five slope models in order to utilize those results to estimate the potential stability conditions of a proposed 70^{o} open-pit mine slope and (2) evaluate the finite element method for its applicability in the stability condition determination of open-pit mine slopes.

Stability Conditions of Slope Models

As a result of the various tests performed on the finite element models, it appears that Model 1 (homogeneous and isotropic throughout), Model 2 (rock type varying; homogeneous, isotropic within rock types only), and Model 3 (modified rock mass approximation; non-homogeneous, anisotropic within rock types) are stable in every respect. Model 4 (model joints added to Model 3 rock properties) and Model 5 (tectonic loading added to gravity loading and Model 4 properties) are not stable in particular model areas. Model 4 is unstable within model joint areas. Zones within and adjacent to model joints in proximity to the final open-pit wall are not stable in Model 5.

If the 755 Area pit slope conditions are similar to Model 1, 2 or 3 conditions, the resulting slope should be stable. If the 755 Area slope has conditions similar to either Model 4 or 5, the resulting pit slope is potentially unstable.

Stress Concentration

Results indicate that similar stress magnitudes and stress changes due to excavation occur in homogeneous, isotropic; rock type varying; and rock mass approximation finite element models (Models 1, 2 and 3, respectively). In Model 3, only slightly lower stress magnitudes develop after extensive modification of the finite elements to more closely approximate the in situ rock mass.

Two observations were made in modeling joints in Model 4: (1) post-excavation stresses increase appreciably in areas where modeled joints are contiguous to the final pit wall and (2) contours of stress are extensively altered to conform to model joint orientations and boundaries. As a result of loading Model 5 with tectonic as well as gravity loads, two effects were noted for both pre-excavation and post-excavation conditions: (1) stresses are extremely high near modeled joints and (2) stress magnitudes in other areas of this model are approximately proportional to the loading magnitudes. It appears that joint elements, in conjunction with large loading magnitudes, tend to localize high stresses in jointed areas both prior to and after excavation.

Displacement

Excavation displacement magnitudes decrease somewhat with an increase in modification of model rock mass properties, as is observed in the successive analysis of Model 1 to Model 4. Vertical displacement of approximately 5" to 5½" would be predicted, due to elastic rebound from mining to the proposed pit floor elevation, from the four gravity-loaded models. Small variations in both the horizontal and vertical displacements are indicated between Models 1, 2 and 3 and Model 4 in areas located at and above the model joints.

Larger vertical displacements (100%) and smaller horizontal displacements occur in the tectonic and gravity loaded model (Model 5) than in the four previous models except in the area above the model joints. The area above the joints has smaller vertical, but much greater horizontal, displacements. The larger horizontal displacements in this area may have resulted from (1) the high horizontal to vertical stress ratio in this zone, in conjunction with (2) the small strength of the joint elements and the attitude of the model joints. Vertical displacement at the proposed pit floor, due to elastic rebound after excavation, would be 11" to 12" as determined by this gravity and tectonic loaded model.

Failure Criteria

Models 1, 2 and 3 do not undergo failure for any of the criteria used for the determination of slope instability. Post-excavation tensile, shear and compressive stresses are sufficiently high in several elements to exceed element strengths in and adjacent

to modeled joints located near the pit wall in Model 5. Stresses are not high enough at any location in Model 4 to exceed element strengths.

Upon excavation, tensile stress areas develop near the final pit wall in proximity to the model joints in Models 4 and 5. These tensile zones are areas where pre-existing joints are free to open up. There are more and larger tensile zones in the model with a combination of tectonic and gravity loading (Model 5) than in the model which was only gravity loaded (Model 4). This result may be related to the high horizontal to vertical stress ratio which was present in the upper model area.

Non-linear deformation (yielding) occurs in nearly all of the joint elements in the two modeled joints for the estimated element parameters. All joint elements in proximity to the final pit wall yield. Upon examination for the presence of incipient sliding on the joints, it was determined that sliding results for the same elements as yielding in the yield analysis.

The model joints in Models 4 and 5 were tested for tensile stresses normal to the joint planes. Four of the thirteen joint elements contained high tensile normal stresses and, therefore, during mining, these joint areas should open in tension.

The Finite Element Method and Its Applicability to Stability Condition Determination

By utilizing the basic finite element method, two results, important for stability condition determination of open-pit mine slopes, can be obtained directly: (1) pre-excavation and post-excavation stresses and (2) displacement due to excavation. Resultant total

stress, after pit excavation, can be utilized to examine a variety of failure criteria (appropriate for the given geologic conditions of the slope) in order to evaluate the stability conditions. Calculated excavation displacement is useful as a standard to compare actual measured slope displacement against, if it can be determined that the slope in question responds relatively elastically.

In order to utilize the finite element method for slope design and the determination of stability conditions, two items must be included in the analysis: (1) the pre-excavation in situ stress distribution and (2) geologic discontinuities (joints, faults, seams, bedding) if present. As was shown in the results of this analysis, it is critical to know the in situ stress distribution. The combination of gravity and tectonic loading in Model 5 created very high stresses in several model areas. Geologic discontinuities must be modeled because they affect the stress concentration and, thus, stability. Modeled joints appear to localize areas of stress concentration.

The major limitation of the finite element method, as applied to rock slope stability analysis, is the adequacy of the rock property input data. This information is limited by the present state of knowledge of the physical properties of the rock mass.

NOMENCLATURE

a	Length of rectangular element
$[A]$	Stress-strain matrix defining element properties, plane strain
b	Height of rectangular element
$[B]$	Nodal point coordinate matrix for an element
c	Cohesion of a material
$[C]$	Element internal strain matrix
d	Thickness of an element
E	Young's modulus of elasticity
(G)	Matrix for the summation of gravity forces for the complete assemblage of elements
$[k]$	Element stiffness matrix in local (element) coordinate system
$[K]$	Stiffness matrix of the complete assemblage of elements with respect to local coordinates
$[\chi]$	Stiffness matrix of the complete assemblage of elements in generalized coordinates
(R), (F)	Deflection vector and force vector for the complete assemblage of elements in generalized coordinates
T	Tensile strength
T_B	Brazilian tensile strength
$[T]$	Transformation matrix relating deflections in the local element coordinates and generalized coordinates
$[T_r]$	Matrix for the summation of residual tectonic forces for the complete assemblage of elements

(u), (s)	Deflection vector and force vector for an element in a local coordinate system
(U), (S)	Deflection vector and force vector for the complete assemblage of elements in generalized coordinates
U_c	Unconfined compressive strength
u, w	Displacements of a point in an element and in the continuum in the X and Z directions, respectively
x, y, z	Local coordinates for an element
X, Y, Z	Cartesian coordinates
α	Assumed displacement coefficient for an element
γ	Unit weight
γ_{xy}, γ_{yz}, γ_{xz}	Shear strains in xy, yz, xz planes, respectively
δ	Displacement
ε_x, ε_y, ε_z	Normal strains in the x, y, z directions, respectively
μ	Poisson's ratio
σ_x, σ_y, σ_z	Normal stresses in the x, y, z directions, respectively
σ_n	Normal stress on any plane
τ_{xy}, τ_{yz}, τ_{xz}	Shear stresses in xy, yz, xz planes, respectively
τ	Shear stress on any plane
ϕ	Angle of internal friction of a material (rock, soil)
$[\ ]^T$	Transpose matrix

APPENDIX I

MAXIMUM SHEAR STRESS CONTOURS, MODELS 1-5, PRE-EXCAVATION AND POST-EXCAVATION CONDITIONS

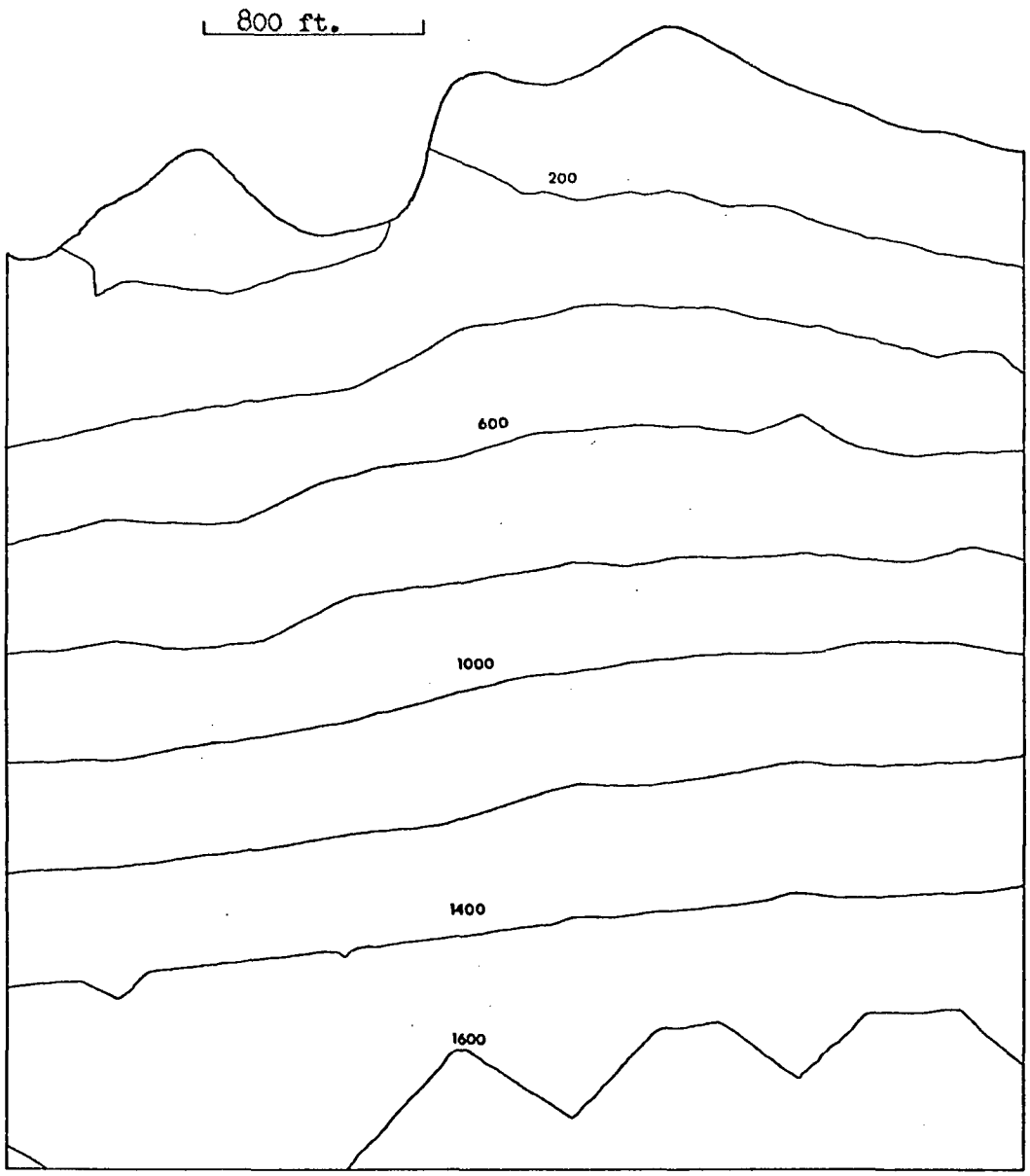

Figure 26. Model 1, Maximum Shear Stress Contours, Pre-Excavation

Contour Interval = 200 psi

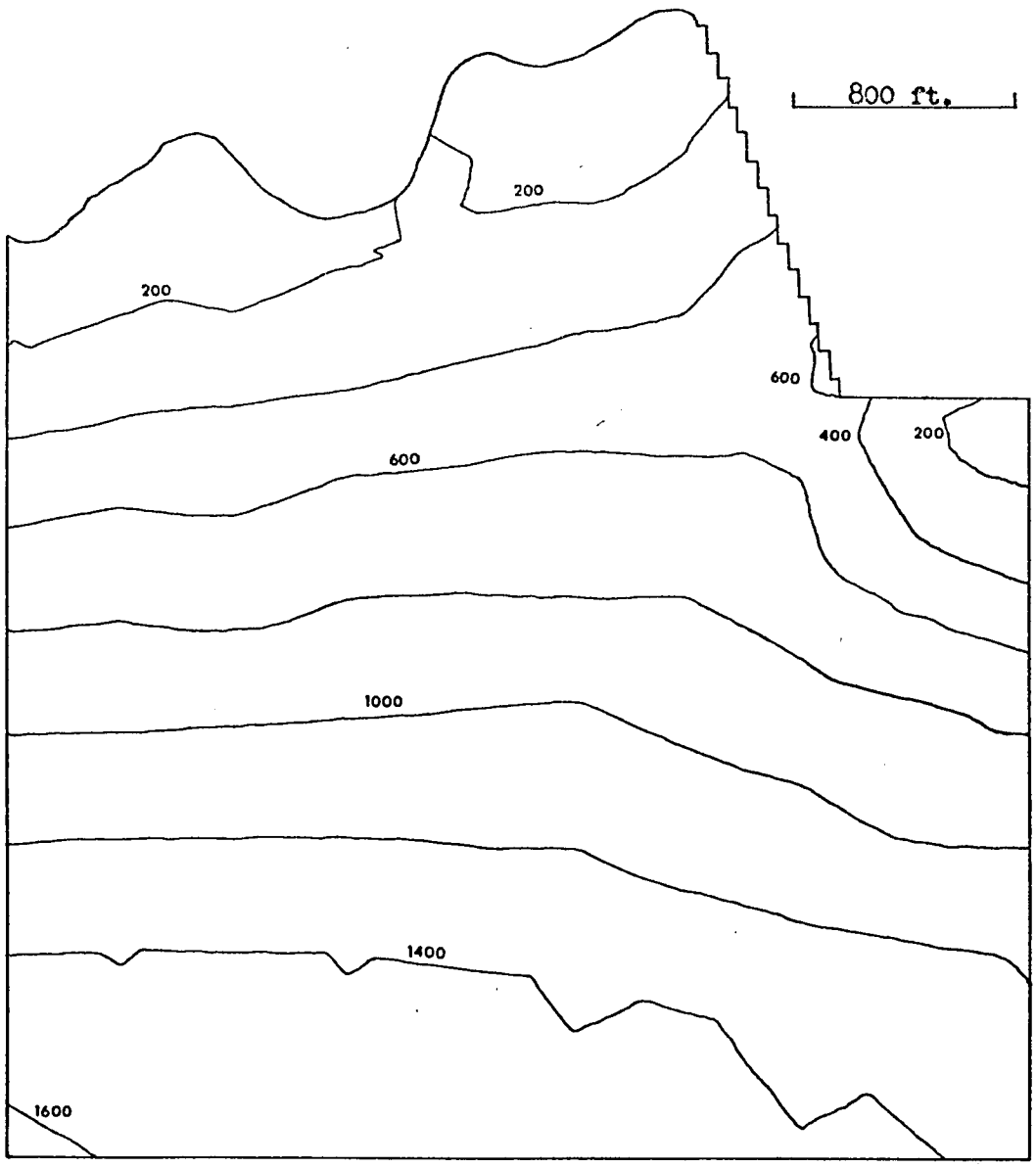

Figure 27. Model 1, Maximum Shear Stress Contours, Post-Excavation

Contour Interval = 200 psi

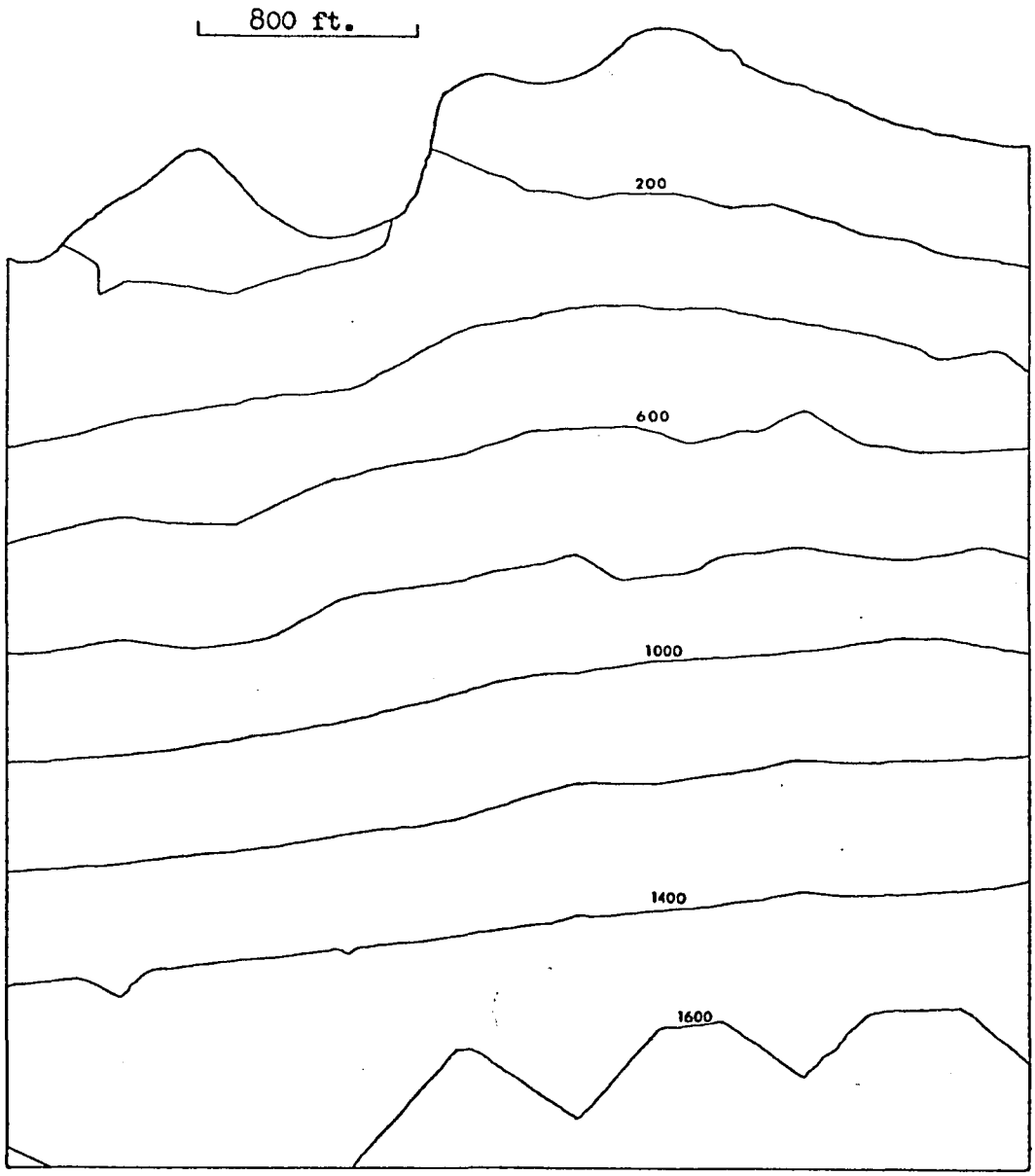

Figure 28. Model 2, Maximum Shear Stress Contours, Pre-Excavation

Contour Interval = 200 psi

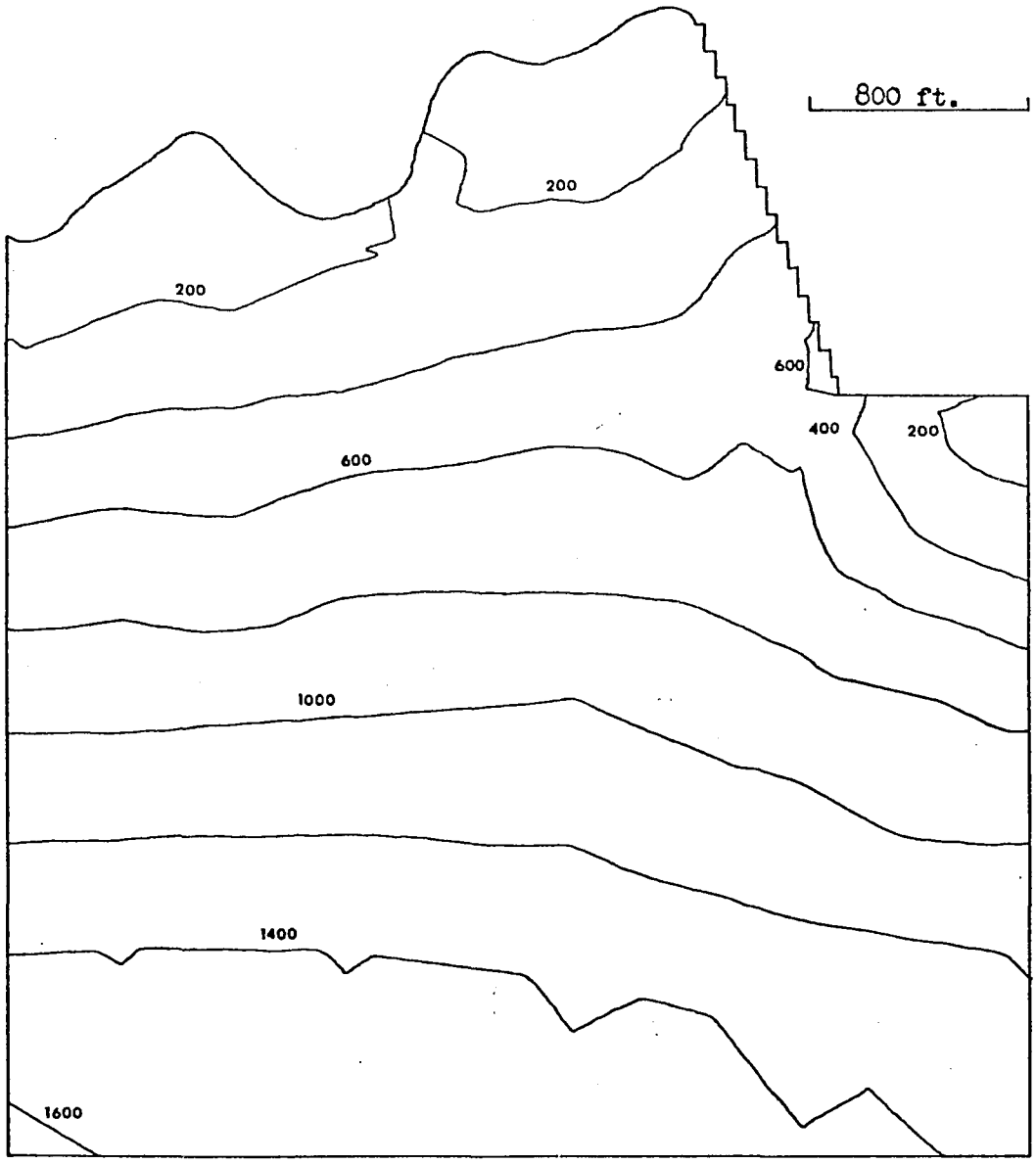

Figure 29. Model 2, Maximum Shear Stress Contours, Post-Excavation

Contour Interval = 200 psi

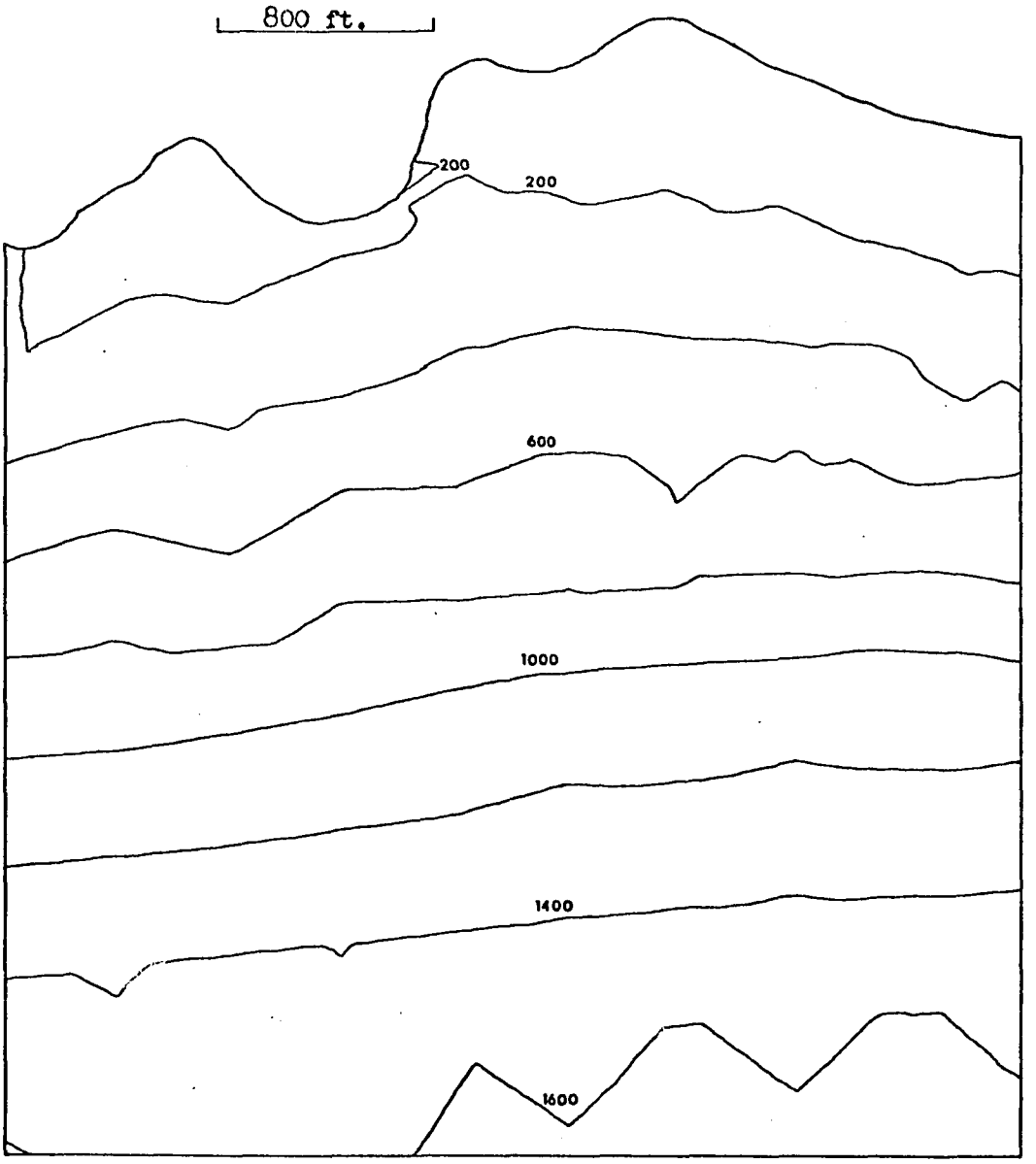

Figure 30. Model 3, Maximum Shear Stress Contours, Pre-Excavation

Contour Interval = 200 psi

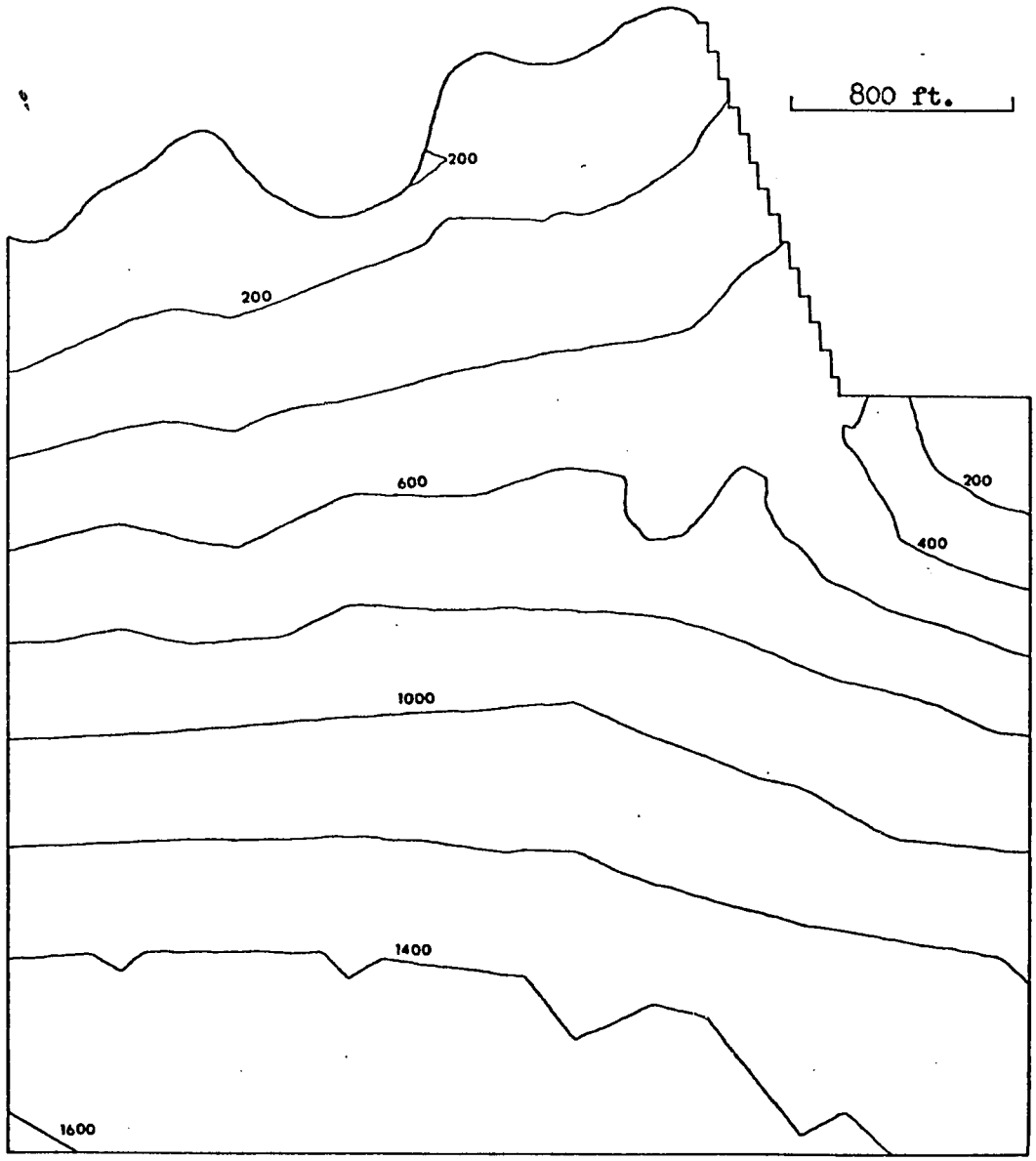

Figure 31. Model 3, Maximum Shear Stress Contours, Post-Excavation

Contour Interval = 200 psi

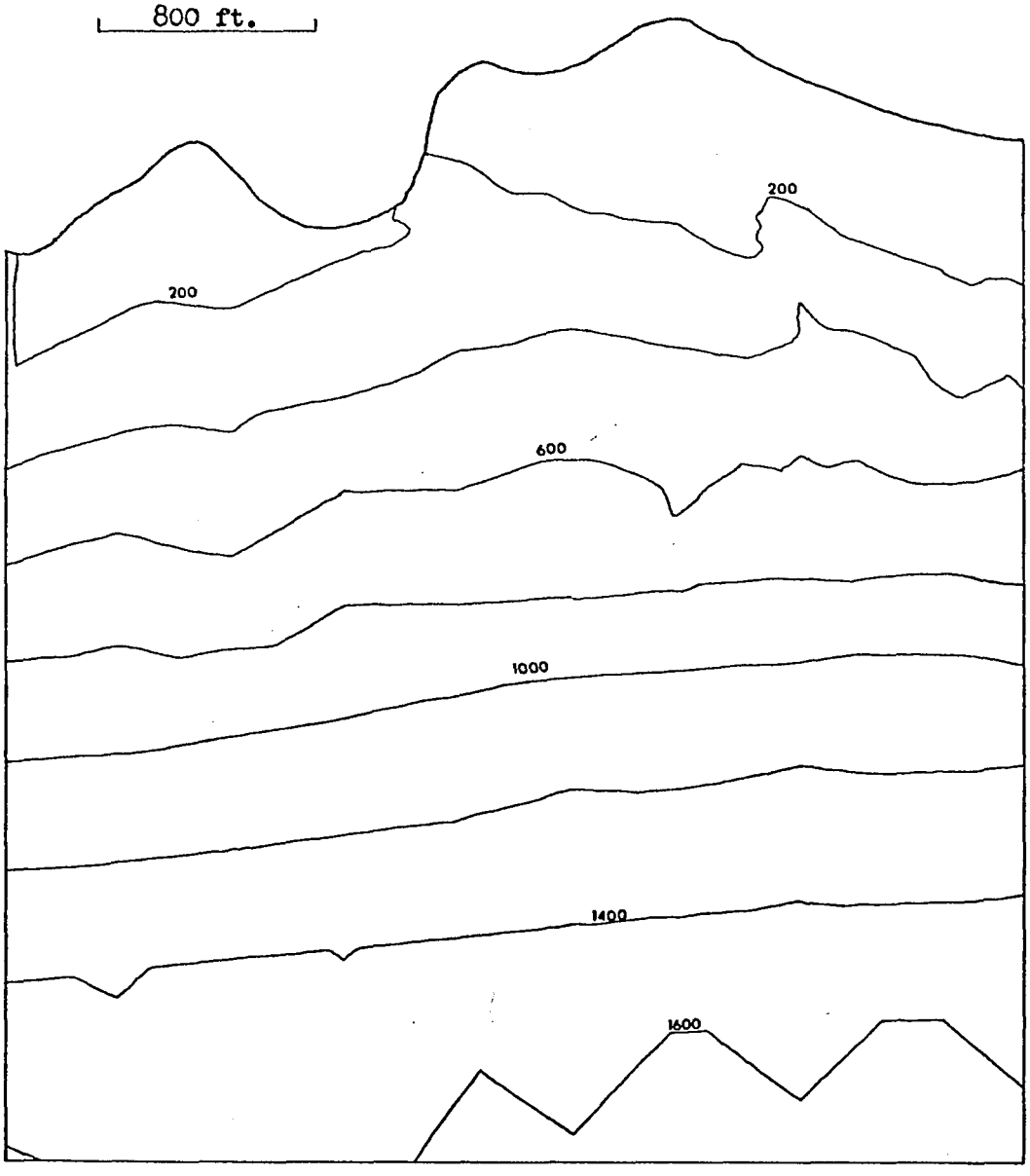

Figure 32. Model 4, Maximum Shear Stress Contours, Pre-Excavation

Contour Interval = 200 psi

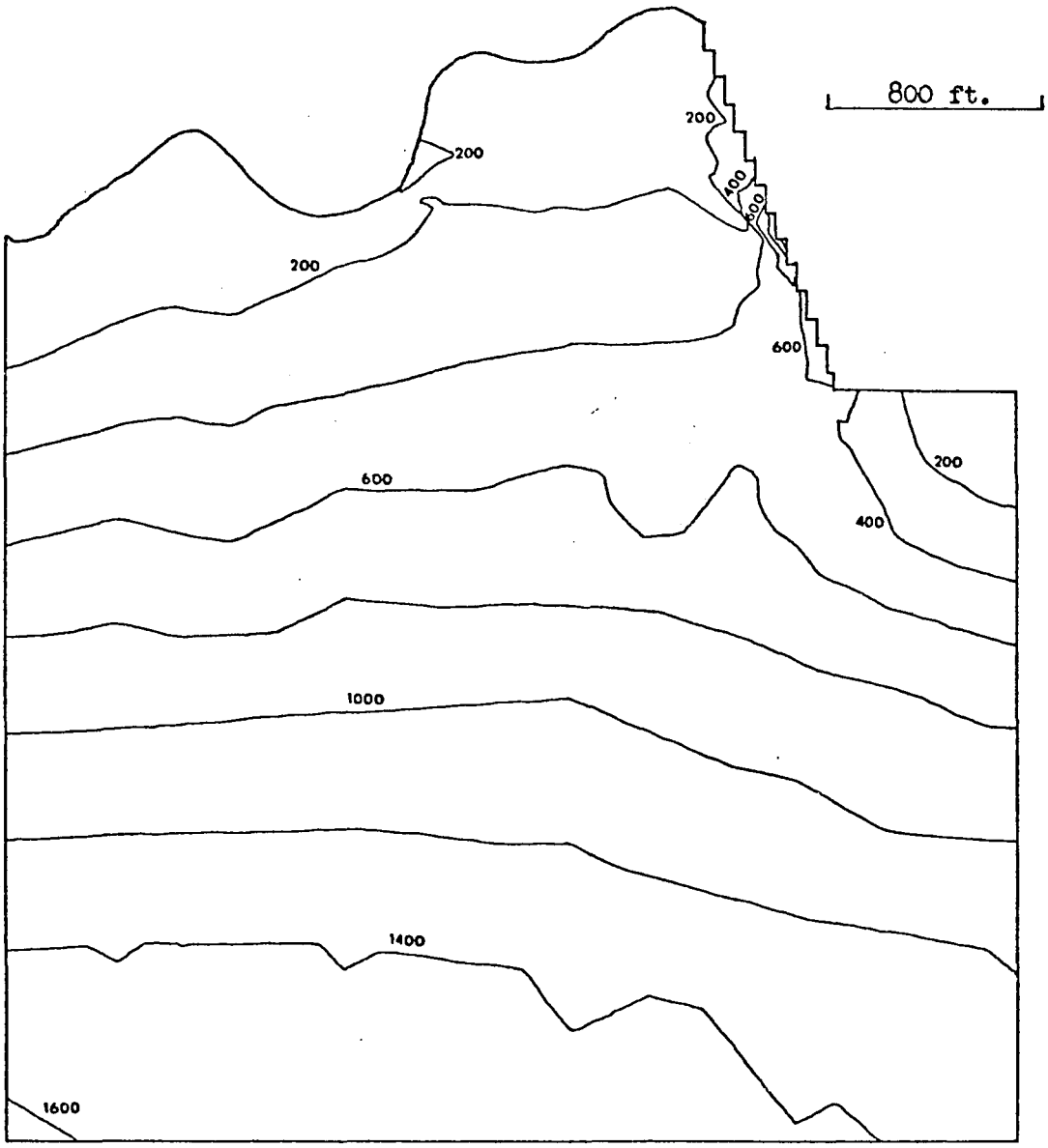

Figure 33. Model 4, Maximum Shear Stress Contours, Post-Excavation

Contour Interval = 200 psi

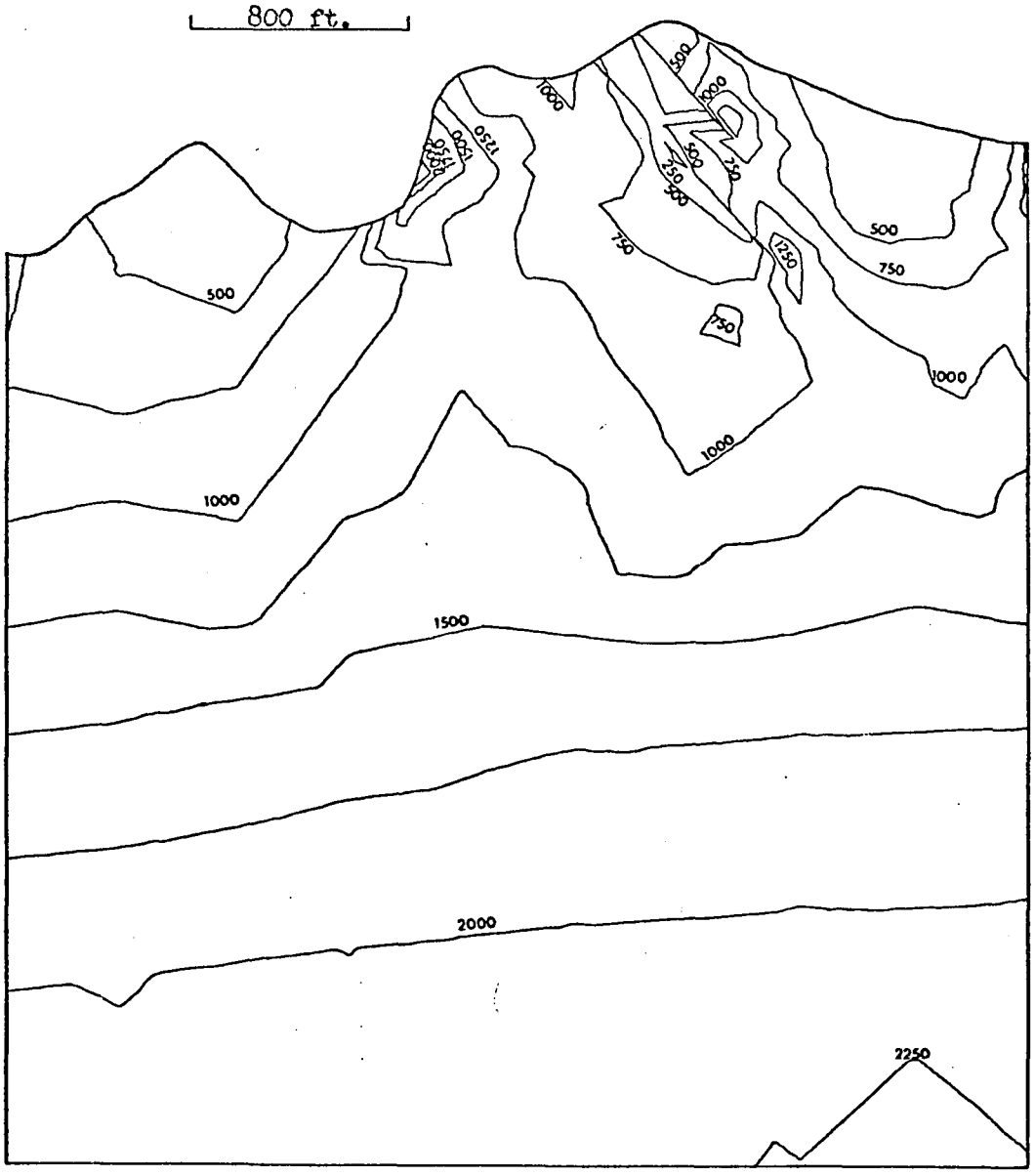

Figure 34. Model 5, Maximum Shear Stress Contours, Pre-Excavation

Contour Interval = 250 psi

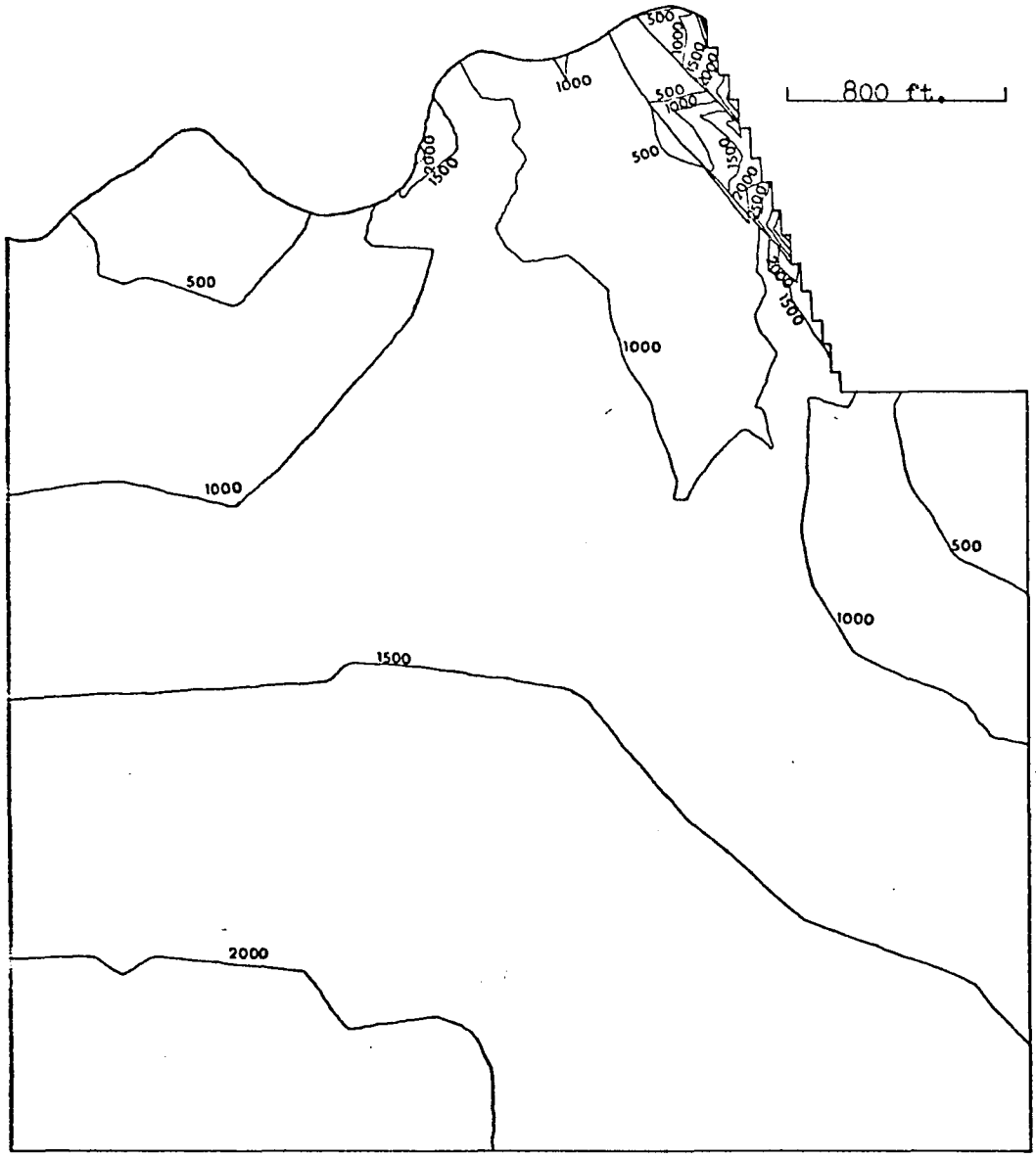

Figure 35. Model 5, Maximum Shear Stress Contours, Post-Excavation

Contour Interval = 500 psi

SELECTED BIBLIOGRAPHY

Blake, Wilson, 1966, Application of the Finite Element Method of Analysis in Solving Boundary Value Problems in Rock Mechanics, International Journal of Rock Mechanics and Mining Sciences, v. 3, no. 3, p. 169-180.

Blake, Wilson, 1967, Stresses and Displacements Surrounding an Open Pit in a Gravity-Loaded Rock, U. S. Bureau of Mines Report of Investigation 7002, Aug. 1967, 20 pp.

Blake, Wilson, 1968, Finite Element Model Study of Slope Modification at the Kimbley Pit, Soc. of Mining Engin. of AIME, Preprint No. 68-AM-63, Feb. 1968, 19 pp.

Brown, C. and Ayala, R., 1966, General Geology of the Cananea Mining District, Cananea, Mexico, Unpublished paper, Compañia Minera de Cananea files, 11 pp.

Call, R. D., 1967, Design of Open Pit Slopes, Fall Meeting AIME, Abstract in Mining Engineering, v. 19, no. 8, 29 pp.

Clough, R. W., 1960, The Finite Element Method in Plane Stress Analysis, Proceedings of the 2nd ASCE Conference on Electronics Computation, Pittsburgh, Sept. 1960.

Clough, R. W., 1965a, The Finite Element Method in Structural Mechanics, Ch. 7 in Stress Analysis, ed. O. C. Zienkiewicz and G. S. Hollister, John Wiley & Sons, London, p. 85-119.

Clough, R. W., 1965b, Finite Element Analysis of Axi-Symmetric Solids, Journal of Engineering Mechanics, ASCE, v. 91, Feb. 1965.

Clough, R. W. and Woodward, R. J., III, 1967, Analysis of Embankment Stresses and Deformations, Journal of Soil Mechanics and Found. Div., ASCE, v. 93, no. SM4, July 1967, p. 529-549.

Coates, D. F., 1967, Rock Mechanics Principles, Mines Branch Monograph 874, Dept. of Mines & Technical Surveys, Ottawa, p. 6-7 and 6-9.

Coates, D. F., 1969a, Geologic Structural Effects in Rock Mechanics, Internal Report MR 69/44-ID, Mining Research Centre, Canadian Dept. of Energy, Mines and Resources, Mines Branch, Ottawa, June 1969, 31 pp.

Coates, D. F., 1969b, The Finite Element Method in Rock Mechanics, Internal Report MR 69/54-ID, Mining Research Centre, Canadian Dept. of Energy, Mines and Resources, Mines Branch, Ottawa, July 1969, 26 pp.

Coates, D. F. and Grant, F., 1966, Stress Measurements at Elliot Lake, Canadian Min. & Met. Bull., v. 59, no. 649, May 1966, p. 603-613.

Deere, D. U., 1969, Geological Considerations, Ch. 1 in Rock Mechanics in Engineering Practice, ed. K. C. Stagg and O. C. Zienkiewicz, John Wiley & Sons.

Deere, D. U., Hendron, A. J., Jr., Patton, F. D., and Cording, E. J., 1967, Design of Surface and Near-Surface Construction in Rock, Ch. 11 in Failure and Breakage of Rock, 8th Symposium on Rock Mechanics, ed. Charles Fairhurst, AIME, p. 237-302.

De Veubeke, F. B., 1965, Displacement and Equilibrium Models in the Finite Element Method, in Stress Analysis, ed. O. C. Zienkiewicz and G. S. Hollister, John Wiley & Sons.

Duncan, J. M. and Dunlop, P., 1969, Slopes in Stiff-Fissured Clays and Shales, Journal of Soil Mechanics and Found. Div., ASCE, v. 95, no. SM2, March 1969, p. 467-492.

Duncan, J. M., and Goodman, R. E., 1968, Finite Element Analysis of Slopes in Jointed Rock, U. S. Corps of Engineers Contract Report S-68-3.

Einstein, H. H., Nelson, R. A., Bruhn, R. W., and Hirschfield, R. C., 1969, Model Studies of Jointed Rock Behavior, Proc. 11th Symposium on Rock Mechanics, Berkeley, California, June 1969.

Gentry, D. W., 1970a, The Measurement of Residual Strains by the Stress-Relief Technique, Unpublished paper, Dept. of Min. and Geol. Eng. files, University of Arizona, Tucson, 22 pp.

Gentry, D. W., 1970b, Elastic Stress Analysis Around Inclusions, Unpublished paper, Dept. of Min. and Geol. Eng. files, University of Arizona, Tucson, 19 pp.

Girijavallabhan, C. V., 1967, Application of the Finite Element Method to Problems in Soil and Rock Mechanics, Ph. D. Dissertation, Univ. of Texas, Univ. Microfilms, Inc., Ann Arbor, Michigan, 111 pp.

Goodman, R. E., 1964, The Resolution of Stresses in Rock Using Stereographic Projection, Intern. Journal of Rock Mechanics and Mining Sciences, v. 1, p. 93-103.

Goodman, R. E. and Taylor, R. L., 1967, Methods of Analysis for Rock Slopes and Abutments - A Review of Recent Developments, Ch. 12 in Failure and Breakage of Rock, ed. C. Fairhurst, AIME, New York, p. 303-320.

Goodman, R. E., Taylor, R. L., and Brekke, T. L., 1968, A Model for the Mechanics of Jointed Rock, Journal of Soil Mechanics and Found. Div., ASCE, v. 94, no. SM3, May 1968, p. 637-659.

Gray, W. M. and Töews, N. A., 1967, Analysis of Accuracy in the Determination of the Ground Stress Tensor by Means of Borehole Devices, Divisional Report FMP 67/28-MRL, Fuels and Mining Practice Division, Can. Dept. of Energy, Mines and Resources, Mines Branch, Ottawa, Feb. 1967, 43 pp.

Hetenyi, M., 1954, Handbook of Experimental Stress Analysis, John Wiley & Sons, Inc., pp. 410-415.

Hooker, V. E. and Johnson, C. F., 1966, In Situ Stresses Along the Appalachian Piedmont, presented at the 4th Canadian Rock Mechanics Symposium in Ottawa, Ontario, Canada, Reprint, 23 pp.

John, K. W., 1968, Graphical Stability Analysis of Slopes in Jointed Rock, Proceedings of ASCE, v. 94, no. SM2, paper no. 5865, March 1968, p. 497-526.

Lacy, W. C., 1963, Quantitizing Geological Parameters for the Prediction of Stable Slopes, SME Transactions, Sept. 1963, p. 1-5.

Leeman, E. R., 1964, The Measurement of Stress in Rock, Journal of the South African Institute of Mining and Metallurgy, Sept. 1964, p. 53-62.

Leeman, E. R., 1968, The Determination of the Complete State of Stress in Rock in a Single Borehole - Laboratory and Underground Measurements, Int. J. of Rock Mechanics and Mining Sciences, vol. 5, no. 1, p. 31-56.

Londe, P., Vigier, G., and Vormeringer, R., 1969, Stability of Rock Slopes, a Three Dimensional Study, Journal of Soil Mechanics and Found. Div., ASCE, v. 95, no. SM1, Jan. 1969, p. 235-262.

Londe, P., Vigier, G., and Vormeringer, R., 1970, Stability of Rock Slopes - Graphical Methods, Journal of Soil Mechanics and Found. Div., ASCE, v. 96, no. SM4, July 1970, p. 1411-1434.

Mahtab, M. A., 1970, Three-Dimensional Finite Element Analysis of Jointed Rock Slopes, Ph. D. Dissertation, Univ. of California, Berkeley, 97 pp.

Malina, H., 1970, The Numerical Determination of Stresses and Deformations in Rock Taking into Account Discontinuities, Journal of the International Society for Rock Mechanics, v. 2, no. 1, May 1970, p. 1-16.

McMahon, B. K., 1968, Indices Related to the Mechanical Properties of Jointed Rock, Ch. 6 in 9th Symposium on Rock Mechanics, ed. N. E. Grosvenor and B. W. Paulding, Jr., AIME, p. 117-128.

McMahon, B. K. and Kendrick, R. F., 1969, Predicting the Block Caving Behavior of Orebodies, Soc. of Mining Engin. of AIME, Preprint no. 69-AU-51, 15 pp.

Melosh, R. J., 1962, Development of the Stiffness Method to Define Bounds on Elastic Behavior of Structures, Ph. D. Thesis, Univ. of Washington.

Merrill, R. H. and Peterson, J. R., 1961, Deformation of a Borehole in Rock, U. S. Bureau of Mines Report of Investigation 5881, 32 pp.

Morgenstern, N. R., 1969, Ultimate Behavior of Rock Structures, Ch. 10 in Rock Mechanics in Engineering Practice, ed. K. C. Stagg and O. C. Zienkiewicz, John Wiley & Sons, p. 321-351.

Nair, K. and Otus, M., 1968, Structural Stability of Large Cavities for Project Payette, Soc. of Mining Engin. of AIME, Preprint no. 68-I-354, 36 pp.

Ngo, D. and Scordelis, A. C., 1967, Finite Element Analysis of Reinforced Concrete Beams, Journal of the American Concrete Institute, v. 64, no. 3, March 1967.

Nichols, T. C., Abel, J. F., and Lee, F. T., 1968, a Solid-Inclusion Borehole Probe to Determine Three-Dimensional Stress Changes at a Point in a Rock Mass, U. S. Geological Survey Bulletin 1258-C, 28 pp.

Nichols, T. C., Lee, F. T., and Abel, J. F., 1969, Some Influences of Geology and Mining upon the Three-Dimensional Stress Field in a Metamorphic Rock Mass, Bull. of the Association of Engineering Geologists, v. 6, no. 2, fall 1969, p. 131-143.

Obert, L., 1964, Triaxial Method for Determining the Elastic Constants of Stress Relief Cores, U. S. Bureau of Mines Report of Investigation 6490, 22 pp.

Obert, L., Merrill, R. H., and Morgan, T. A., 1962, Borehole Deformation Gage for Determining Stress in Mine Rock, U. S. Bureau of Mines Report of Investigation 5978, 11 pp.

Patton, F. D., 1966, Multiple Modes of Shear Failure in Rock and Related Materials, Ph. D. Thesis, Univ. of Illinois.

Perloff, W. H., 1969, Strain Distribution Around Underground Openings, Finite Element Analysis of Underground Openings, Technical Report No. 1, Prepared for Office of the Chief of Engineers, Dept. of the Army, School of Civil Eng., Purdue Univ., June 1969, 233 pp.

Pincus, H., 1951, Statistical Methods Applied to the Study of Rock Fractures, Geol. Soc. of America Bull., v. 62, p. 81-129.

Rashid, Y. R., 1965, Solution of Elasto-Static Boundary Value Problems by the Finite Element Method, Ph. D. Thesis, Univ. of California, Berkeley.

Reyes, S. F., 1966, Elastic Plastic Analysis of Underground Openings by the Finite Element Method, Ph. D. Thesis, Univ. of Illinois, Urbana, Illinois.

Rocha, M., and Silvério, A., 1969, A New Method for the Complete Determination of the State of Stress in Rock Masses, Geotechnique, vol. 19, no. 1, p. 116-132.

Smith, W. K., 1969, A Fortran IV Program for the Determination of Fracture Intersections, Unpublished paper, 17 pp.

Terzaghi, K., 1962, Stability of Steep Slopes on Hard Unweathered Rock, Geotechnique, v. 12, no. 4, p. 251-271.

Timoshenko, S., 1934, Theory of Elasticity, McGraw-Hill Book Co., Inc., New York, 416 pp.

Timoshenko, S. and Goodier, J. N., 1951, Theory of Elasticity, Second Edition, McGraw-Hill Book Co., New York.

Turner, M. J., Clough, R. W., Martin, H. C., and Topp, L. J., 1956, Stiffness and Deflection Analysis of Complex Structures, Journal of Aeronautical Science, v. 23, no. 9.

Velasco, J. R., 1966, Geology of the Cananea District, in Geology of the Porphyry Copper Deposits - Southwestern North America, ed. S. R. Titley and C. L. Hicks, The Univ. of Arizona Press, Tucson, p. 245-249.

Voight, B., 1966, Interpretation of In-Situ Stress Measurements, Proceedings of the 1st Congress of the International Society of Rock Mechanics, v. 3, Sept. 1966, p. 332-348.

Voight, Barry, 1967, On Photoelastic Techniques, In Situ Stress and Strain Measurement, and the Field Geologist, The Journal of Geology, v. 75, no. 1, Jan. 1967, p. 46-58.

Voight, Barry, 1968, Determination of the Virgin State of Stress in the Vicinity of a Borehole from Measurements of a Partial Anelastic Strain Tensor in Drill Cores, Felsmechanik und Ingenieurgeologie, v. 6, p. 201-215.

Wang, F. and Sun, M., 1970a, Slope Stability Analysis by the Finite Element Stress Analysis and Limiting Equilibrium Method, U. S. Bureau of Mines Report of Investigation 7341, Jan. 1970, 16 pp.

Wang, F. and Sun, M., 1970b, A Systematic Analysis of Pit Slope Structures by the Stiffness Matrix Method, U. S. Bureau of Mines Report of Investigation 7343, Feb. 1970, 37 pp.

Wang, Y. J. and Voight, Barry, 1969, A Discrete Element Stress Analysis Model for Discontinuous Materials, International Symposium on Large Permanent Underground Openings, Oslo, Sept. 1969, Article 6, 5 pp.

Wilson, E. L., 1963, Finite Element Analysis of Two-Dimensional Structures, Structural Engineering Laboratory Report 63-2, Univ. of California, Berkeley.

Wilson, E. L., 1965, Structural Analysis of Axisymmetric Solids, American Institute of Aeronautics and Astronautics Journal, v. 3, no. 12, Dec. 1965.

Wisecarver, D. W., 1968, Changes in Stress, Strain and Displacement with Change in Slope Angle at the Kimbley Pit, Paper presented at Annual Meeting of AIME, Feb. 1968.

Wisecarver, D. W., Merrill, R. H., Rausch, D. O., and Hubbard, S. J., 1964, Investigation of In-Situ Rock Stresses, Ruth Mining District, Nevada, With Emphasis on Slope Design Problems in Open-Pit Mines, U. S. Bureau of Mines Report of Investigation 6541, 21 pp.

Woodward, R. J., III, 1967, Analysis of Stresses in Embankments with Non-Linear Material Properties, Ph. D. Thesis, Univ. of California, Berkeley, 110 pp.

Yu, Y. S. and Coates, D. F., 1968, Comparison of Stress Distribution Between Open Pit Mines with Slope Angles of 45° and 60°, Internal Report MR 68/81-ID, Mining Research Centre, Canadian Dept. of Energy, Mines and Resources, Mines Branch, Ottawa, Sept. 1968, 36 pp.

Yu, Y. S. and Coates, D. F., 1969, Development and Use of Computer Programs for Finite Element Analysis, Research Report R-198, Mining Research Centre, Canadian Dept. of Energy, Mines and Resources, Mines Branch, Ottawa, July 1969, 97 pp.

Yu, Y. S., Gyenge, M., and Coates, D. F., 1968, Comparison of Stress and Displacement in a Gravity-Loaded 60 Degree Slope by Photoelasticity and Finite Element Analysis, Internal Report MR 68/24-ID, Mining Research Centre, Canadian Dept. of Energy, Mines and Resources, Mines Branch, March 1968, 34 pp.

Zavodni, Z. M., 1969, Physical Testing Study of Cananea Mine Rock, M. S. Thesis, Univ. of Arizona, May 1969, 93 pp.

Zavodni, Z. M., 1970, Preliminary Geologic Structural Analysis for the 755 Pit, Cananea, Mexico, unpublished report, Dept. of Min. and Geol. Eng. files, Univ. of Arizona, Tucson, 29 pp.

Zienkiewicz, O. C., 1969, Continuum Mechanics as an Approach to Rock Mass Problems, Ch. 8 in Rock Mechanics in Engineering Practice, ed. K. C. Stagg and O. C. Zienkiewicz, John Wiley & Sons, p. 237-273.

Zienkiewicz, O. C. and Cheung, Y. K., 1967, The Finite Element Method in Structural and Continuum Mechanics, McGraw-Hill, New York, 272 pp.

Zienkiewicz, O. C., Irons, B. M., Ergatoudis, J., Admad, S., and Scott, F. C., 1969, Iso-Parametric and Associated Element Families for Two- and Three-Dimensional Analysis, in Finite Element Methods in Stress Analysis, ed. I. Holand and K. Bell, Tapir, Norway.

Zienkiewicz, O. C., Valliappan, S., and King, I., 1968, Stress Analysis of Rock as a 'No-Tension' Material, Geotechnique, v. 18, p. 56-66.